UNIVERSIDAD POLITÉCNICA DE MADRID
Escuela Técnica Superior de Ingenieros Industriales

Control strategy design and installation of a cost-competitive solar concentrating system for industrial processes heat

DOCTORAL THESIS

Submitted for the degree of Doctor by:

Magdalena Barnetche Orensanz
Chemical Engineer

Madrid, 2024

UNIVERSIDAD POLITÉCNICA DE MADRID
Escuela Técnica Superior de Ingenieros Industriales

Doctoral Degree in Sustainable, Nuclear and Renewable Energy

Control strategy design and installation of a cost-competitive solar concentrating system for industrial processes heat

DOCTORAL THESIS

Submitted for the degree of Doctor by:

Magdalena Barnetche Orensanz
Chemical Engineer

Under the supervision of:
Dr. Rubén Abbas Cámara (Supervisor)
Dr. Luis Francisco González Portillo(Supervisor)

Madrid, 2024

Title: Control strategy design and installation of a cost-competitive solar concentrating system for industrial processes heat

Author: Magdalena Barnetche Orensanz

Doctoral Programme: Sustainable, Nuclear and Renewable Energy

Thesis Supervision:

Dr. Rubén Abbas Cámara, Professor (Escuela Técnica Superior de Ingenieros Industriales) (Supervisor)

Dr. Luis Francisco González Portillo, Professor (Escuela Técnica Superior de Ingenieros Industriales) (Supervisor)

External Reviewers:

Thesis Defense Committee:

Thesis Defense Date:

< This thesis has been partially supported by the ASTEP project, which has received funding from European Union's Horizon 2020 research programme under grant agreement N884411. >

"las adas, frente a la esturctura «if... else...», prefiere la estructura «switch... case...» llevada la infinidad de las opciones"- Remedios Zafra

Acknowledgement

Quiero agradecer a mis directores de tesis Rubén Abbas y Luis F. Gonzalez Portillo que me han guiado por el camino de esta tesis doctoral, por su paciencia, apoyo y ayuda en los momentos mas difíciles. Y extender el agradecimiento a las personas nuestro grupo de investigación TE4S y al departamento de Ingeniería Energética, por todos los cafés y mates compartidos junto a Juanjo, Andrés, Antonio, Jesus, Javier, Mariaje y Xuejing. También agradecer a mis compañeros de proyecto ASTEP, en especial, a los compañeros de la UNED, Mercedes, Rubén, Antonio, Imán y David; También a los compañeros de la Universidad Politécnica de Cartagena, Juan Pedro y José, que siempre nos animaban con su ejemplo. Y los compañeros de la FFII, Julio y Javier, por las largas horas de trabajo en Tecnogetafe y las sorpresas que nos llevamos durante la instalación del SunDial desde inundaciones, robos hasta avispas.

Thanks to the Simulation Group of the Institute of Solar Research, Solar High-Temperature Technologies of the German Aerospace Center (DLR) for welcoming me through my research stay, especially to Tobias Hirsch for being my supervisor and the rest of the team: Tim, Alex, and Martin.

Gracias a Madrid por recibirme con los brazos abiertos y a todas las fantásticas personas que conocí en estos 4 años. Especialmente a Diana y a Claudia por estar siempre para las risas y tambien los momentos tristes. Y mis amigas a la distancia, por su compania desde el otro lado del atlantico Agus y Juli.

Gracias a mi familia, mi papá, el Vasco, y mi mamá, Minnie, por su amor incondicional y por siempre ver lo mejor en mí, y mis hermanos, Juan e Iñaki, por estar siempre. A mi abuela Silvia, por animarme todas las mañanas y mandarme su amor. Y a mi abuelo Mariano, que seria el más orgulloso de todos.

Finalmente, a mi confidente y compañero de vida, que siempre me apoya en todas mis decisiones, Alex. Con quien formamos esta pequeña familia, con Willy, estemos en cualquier ciudad del Mundo.

Abstract

The industrial sector consumes one-third of global energy, with 90 % coming from fossil fuels. About 74 % of this energy is used as heat. Solar-concentrating technologies can provide medium-temperature heat, reducing fossil fuel dependence and greenhouse gas emissions. However, solar technology currently accounts for only 0.001 % of industrial heat consumption. The limited number of installations, the variety of industrial processes, and the high capital costs hinder standardization.

This thesis aims to enhance the reliability of solar heat for industrial processes through a simple, cost-effective configuration and control strategy. The system of the present study includes a novel rotary Fresnel collector, SunDial, and latent heat storage to increase system reliability. Two SunDial variants are proposed: one for high latitudes with two tracking axes (SunDial-HL) and another for low latitudes with azimuthal tracking (SunDial-LL). This system, called ASTEP (Application of Solar Thermal Energy to Processes), is part of a European H2020 project. SunDial-HL will be used in a Romanian steel tube factory needing heat at 220 °C for preheating, while SunDial-LL will serve a Greek dairy factory requiring 205 °C for heating and 90 °C for absorption cooling

A dynamic model was used to analyze transient effects in the ASTEP systems, with the thermal energy storage connected in series or parallel, revealing that the in-series configuration provides smooth control during cloudy conditions, while the parallel setup offers quick startups. Both configurations produced similar energy, but the series system required fewer elements and its control was simpler. This model was used to design the controllers and a flexible heat strategy including different power and temperature levels to supply the demand. Significant thermal losses (40 %) were observed in both piping and TES due to the small power of the SunDial. Also, the thermal capacity of the piping was proven to have an impact on the start-up energy calculation. Yearly simulations using a simplified dynamic model demonstrated that implementing a two-level demand strategy improves energy production by 7 %.

An experimental facility was designed to analyze the performance of the SunDial and to replicate the operation in the end-users to test the control strategy. The dynamic model was used to calculate the controller of two air coolers that will replicate the operation of the TES in charge mode and the demand. Three experiments and seven KPIs with a maximum uncertainty of 3 % in the SunDial efficiency were defined.

The construction cost of the SunDial prototypes was higher than market prices due to their small size. An analysis revealed that the collector cost for a larger SunDial-HL version could be reduced to 170-265 €/m², making it more competitive inclusive at low latitudes applications. However, further improvements are needed for the SunDial-LL to reach competitive pricing. A parametric analysis aimed at lowering the levelized cost of heat for the ASTEP system identified an optimal configuration with costs between 23.6 and 36.4 €/kWh, which is below the current natural gas price in Central Europe of 33 €/MWh. Additionally, the SunDial-HL achieves a comparable LCOH to parabolic trough collectors.

Resumen

El sector industrial consume un tercio de la energía global, de la cual el 90 % proviene de combustibles fósiles. Aproximadamente el 74 % de esta energía se utiliza como calor. Las tecnologías de concentración solar pueden proporcionar calor, reduciendo la dependencia de combustibles fósiles. Sin embargo, el número limitado de instalaciones, la variedad de procesos industriales y los altos costos de capital dificultan su implementación que actualmente es menor del 0.001% de la capacidad instalada.

Esta tesis tiene como objetivo mejorar la confiabilidad del calor solar para procesos industriales mediante una configuración y estrategia de control simples y rentables. El sistema del presente estudio incluye un novedoso colector Fresnel rotativo, SunDial, y almacenamiento de calor latente. Se proponen dos variantes del SunDial: una para latitudes altas con dos ejes de seguimiento (SunDial-HL) y otra para latitudes bajas con seguimiento azimutal (SunDial-LL). Este sistema, denominado ASTEP (Application of Solar Thermal Energy to Processes), es parte de un proyecto europeo H2020. El SunDial-HL se utilizará en una fábrica de tubos de acero en Rumanía que necesita calor a 220 °C para el precalentamiento, mientras que el SunDial-LL servirá a una fábrica de productos lácteos en Grecia que requiere 205 °C para calentamiento y 90 °C para enfriamiento por absorción.

Se utilizó un modelo dinámico para analizar los efectos transitorios en los sistemas ASTEP, con el almacenamiento de energía térmica conectado en serie o en paralelo, revelando que la configuración en serie proporciona un control suave durante condiciones nubladas, mientras que la configuración en paralelo ofrece arranques rápidos. Ambas configuraciones produjeron una energía similar, pero el sistema en serie requiere menos elementos y su control fue más sencillo. Este modelo se utilizó para diseñar una estrategia de control que incluye diferentes niveles de potencia y temperatura. Se observaron pérdidas térmicas significativas (40 %) debido a la pequeña potencia del SunDial. Además, se demostró que la capacidad térmica de las tuberías tiene un impacto en el cálculo de la energía de arranque. Simulaciones anuales utilizando un modelo dinámico simplificado demostraron que la implementación de una estrategia de demanda en niveles mejora la producción de energía en un 7 %.

Se diseñó una instalación experimental en Madrid para analizar el rendimiento del SunDial y replicar la operación en las fábricas de manera de poder ensayar la estrategia de control. Se utilizó el modelo dinámico para calcular los controladores de dos enfriadores que replicarán el funcionamiento del TES en modo de carga y la demanda. Se definieron tres experimentos y siete KPIs con una incertidumbre máxima del 3 % en el cálculo de la eficiencia del SunDial.

El costo de construcción de los prototipos fue superior a los precios del mercado debido a su tamaño pequeño. Se halló que el costo del colector para una versión más grande del SunDial-HL podría reducirse a 170-265 €/m², haciéndolo más competitivo inclusive utilizándolo en bajas latitudes. Un análisis paramétrico dirigido a reducir el costo nivelado del calor para el sistema ASTEP identificó una configuración óptima con costos entre 23.6 y 36.4 €/kWh, lo cual está por debajo del precio actual del gas natural en Europa Central de 33 €/MWh. Además, el SunDial-HL logra un LCOH comparable al de los colectores cilindro parabólico.

Scientific Outcomes

During this thesis, numerous scientific achievements were generated, including published papers and conference contributions. The principal results are outlined below along with the research programs that guided this thesis.

Journal Publications

- Barnetche, M., González-Portillo, L.F., Muñoz-Antón, J., Abbas, R., Ibarra, M., Barbero, R. and Rovira, A. (2023) 'Analysis of the thermal inertia of pipelines in SHIP', Results in Engineering 17 (2023) 100908, DOI:10.1016/j.rineng.2023.100908.
- Barnetche, M., González-Portillo, L.F. and Abbas, R. (2023) 'Optimum integration of latent heat storage in a solar thermal system for industrial processes: In series or in parallel?', Applied Thermal Engineering 232 (2023) 121090, DOI:10.1016/j.applthermaleng.2023.
- Abbas, R., Barbero, R., Rovira, A. and Barnetche, M. (2023) 'SunDial, a new collector for solar heat for industrial processes: Optical and thermal design', Thermal Science and Engineering Progress 44 (2023) 102025, DOI:10.1016/j.tsep.2023.102025.

Conferences Publications

- Barnetche, M., González-Portillo, L.F., Abbas, R., Ibarra, M., Barbero, R. and Rovira, A. (2022) 'Defocus Controller for a Rotatory Fresnel Collector', SolarPACES Conference Proceedings, 1 TIB Open Publishing. DOI: 10.52825/SOLARPACES.V1I.733.
- Barnetche, M., González-Portillo, L.F., Ibarra, M., Barbero, R., Rovira, A., Abbas, R. and González-Portillo, L.F. (2023) 'Dynamic analysis of the SunDial, the rotatory Fresnel collector', AIP Conf. Proc, 2815, p. 140002. DOI: 10.1063/5.0149992
- Ibarra, M., Barbero, R., Barnetche, M., Abbas, R. and Rovira, A. (2022) 'Scale-Up Considerations of the Sundial Rotating Fresnel Solar Collector', SolarPACES Conference Proceedings, 1 TIB Open Publishing. DOI: 10.52825/SOLARPACES.V1I.779

Related research project

The ASTEP project has received funding from the European Union's Horizon 2020 research program under grant agreement N°884411.

Contents

List of Figures

List of Tables

Nomenclature

A	Area [m^2]
ASTEP	Application of Solar Thermal Energy to Process
BV	Boiler bypass valve
BOP	Balance of plant
BPV	Bypass valve
C	Heat capacitance [J/K]
c	cost factor
c_p	Specific heat at constant pressure [J/K.kg]
CPC	Compound parabolic collector
CRP	Chiller recirculation pump
CV	Chiller bypass valve
CO_2	Carbon Dioxide
D	Diameter [m]
DNI	Direct normal irradiance
ETC	evacuated tube collector
EU	European Union
F	Force [N]
f_q	Fraction of sensible heat
FC	Flow controller
FPC	Flat plate collector
FHI	Flexible heat integration
G	Thermal conductance [J/K]
Gr	Net radiation conductance [m^2]
GHG	Greenhouse gases
h	Heat transfer coefficient [$W/m^2.K$]
H_{fg}	Phase change specific heat [J/kg.K]
HL	High latitude
HX	Heat exchanger
HTF	Heat transfer fluid
IAM	Incident angle modifier
IEA	International Energy Agency
IRENA	International Renewable Energy Agency

k	Conductivity [W/m.K]
KPI	Key performance indicator
L	Length [m]
LL	Low latitude
LCOH	Levelized cost of heat
LFC	Linear Fresnel collector
LPG	Liquified petroleum gases
m	Mass [kg]
$\dot{m}$	Mass flow rate [kg/s]
MCV	Main Control Valve
MP	Main pump
Nu	Nusselt number
ND	Nominal diameter
ORC	Organic Rankine cycle
PCM	Phase change material
P	Power [W]
p	pressure [kg/m^2] PID
PP	Process pump
Pr	Prandtl number
PTC	Parabolic Trough Collector
$\dot{q}$	Heat flows [J/s]
r	Radius [m]
RP	Recirculation pump
Re	Reynolds number
S	Stress [N/mm^2]
SHC	Solar heating and cooling
SHIP	Solar heat for industrial processes
SM	Solar multiple
SP	SunDial Pump
SV	SunDial bypass valve
TC	Temperature controller
T	Temperature [° C]
t	thikness
TCS	Thermo-chemical storage
TMY	Typical meteorological year
TES	Thermal energy storage
TESP	TES pump
TESV	TES three-way valve
TK	Expansion tank
U	Heat transfer coefficient
UA	Thermal conductance
v	Velocity
x	Liquid fraction

Greek letters

ϵ	Emissivity
η	Efficiency
ρ	Density [kg/m^3]
σ	Stefan Boltzmann constant [W/m^2.K]
θ	incidence angle [rad]
δ	latitude [rad]
μ	viscosity [cp]
ω	time angle [rad]

Subscripts

a	Air
avg	Average
amb	Ambient
c	Capacitance
ext	extended
f	Heat transfer fluid
g	Glass
i	Internal
j	Pipe number
k	Conductance
min	Minimum
mir	mirror
mplt	platform motors
mmir	mirrors motors
mw	Mineral wool
n	Node number
o	External
out	Outlet
p	Phase change material
pl	Phase change material liquid state
pip	piping
ps	Phase change material solid state
r	Radiation
ref	reflective
rec	receiver
rj	rotative joint
s	Steel
str	structure
sun	SunDial
w	Wall
wh	wheels

Chapter 1

Introduction

1.1 Solar heat for industrial processes (SHIP)

To mitigate the impact of climate and avoid reaching the 1.5 °C global temperature rise, nations need to achieve a state of net zero emissions by 2050 [43]. Instead of reducing global energy consumption, between 1971 and 2019 the energy supply increased by 200%, from 210 EJ to 606 EJ [42]. Figure 1.1 shows that the world supply energy matrix is still strongly dependent on fossil fuels, with only a 7% reduction in 46 years. Many countries have adopted renewable sources in the power sector in recent years, but the industry still relies on fossil fuels as the main heat source. Furthermore, 32% of the final energy consumed worldwide corresponds to the industry sector, and 74% of this energy is consumed as heat whereas only 26% as electricity. The primary source of energy for the industry is fossil fuels, with a 90% share. Approximately 37% of the world's greenhouse gas emissions come from industry. The IRENA 2021 report states that, to achieve the 1.5 °C global temperature target, the solar thermal capacity must increase from 4 GW in 2018 to 890 GW in 2030 and 1290 GW in 2050. In 2020, the thermal capacity growth in Europe was only 3%. The main reason why thermal energy capacity is held back is the absence of coordinated and sustained policy support applied to heat decarbonization [47].

In the European Union (EU) the industry accounts for 26 % of greenhouse gas (GHG) emissions, with only a 1.5 % reduction in the past three decades. Furthermore, with the power and transport sector, the industry is responsible for most of the GHG emissions. Figure 1.2 shows industry emissions by subsector in megatons of CO_2 equivalent. These emissions can be produced by the burning of fossil fuels to produce heat (e.g. 100% in food and beverage) or by sub-products of chemical reactions that occurred in the production process (e.g. 50% in the heavy industry sector). Solar thermal energy can only mitigate the emissions produced as a result of the heat demand. As it can be seen in Figure 1.2, mining, oil and gas, and non-metallic minerals are the more emission-intensive sectors. In Europe, Germany is the biggest industrial hub with 22% of the total GHG emissions of the EU [57].

Different temperature levels are required for the consumption of heat in various processes within each industry sector. More than 50% of the heat is consumed at lower (<150 °C)

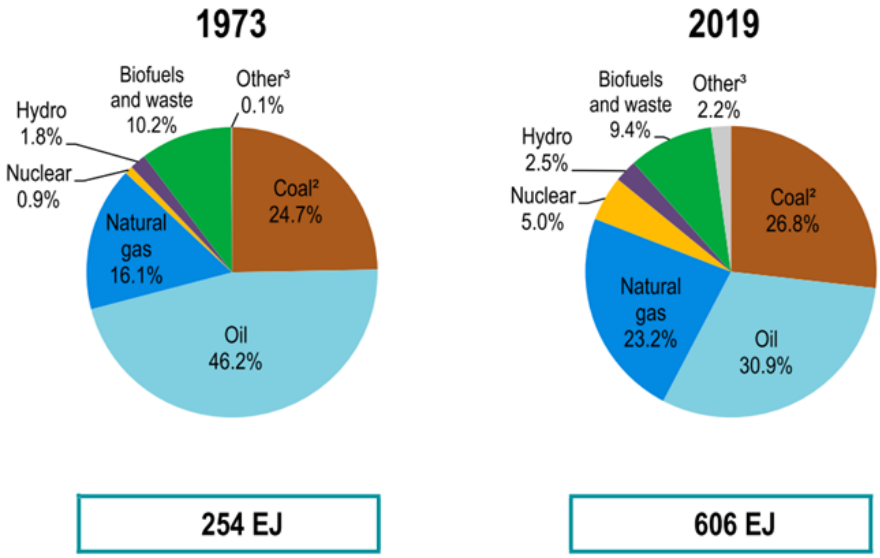

Figure 1.1: Supply world energy matrix in 1973 and 2019.[42].

and medium temperatures (150 to 400 °C), where commercial solar thermal technologies are available. In this temperature range, there are numerous industrial sectors including food and beverage, textiles, chemicals, and more.

Different solar technologies are suitable depending on the temperature level required for industrial processes. For instance, at low temperatures, options include the flat plate collector and the evacuated tubular collector, while at medium temperatures, suitable choices encompass the parabolic trough collector and the linear Fresnel collector. At high temperatures, both tower and dished collectors are not yet in commercial use for SHIP application. Figure 1.3 depicts the temperature range pertinent to each technology and industrial process branch but only for low and medium temperature levels.

By 2023, there were 1089 SHIP projects installed with a collector area of 1.23 million square meters and a capacity of 987 MW [77]. However, this capacity only represents 0.001% of the total consumed heat by the industry. Figure 1.4 shows the solar industrial outlook for the next years within an expected growth in the sector due to the next driving factors: a gas shortage in Europe and gas prices peak in 2022, funding available in some European countries, and the United States, the commitment of some producers to reduce their carbon footprint, emission trading system within Europe, carbon pricing mechanisms and European supply chain due diligence law in 2023.

The world's largest SHIP plant has a thermal capacity of 300 MW and is powered by parabolic trough collectors (PTC) in Oman. Secondly, a SHIP plant for a greenhouse in Australia of 36.6 MW, and thirdly a SHIP plant for a copper mine in Chile of 27.5 MW. However, most of the projects installed are of small capacity less than 0.35 MW (<300 m^2). The countries with the largest installed capacity after Oman are China, Chile, Australia, and Mexico (which represent the major number of projects, 89) [78]. Figure 1.5 shows the capacity installed by collector type, where the technology that accounts for more installed MW is the PTC because

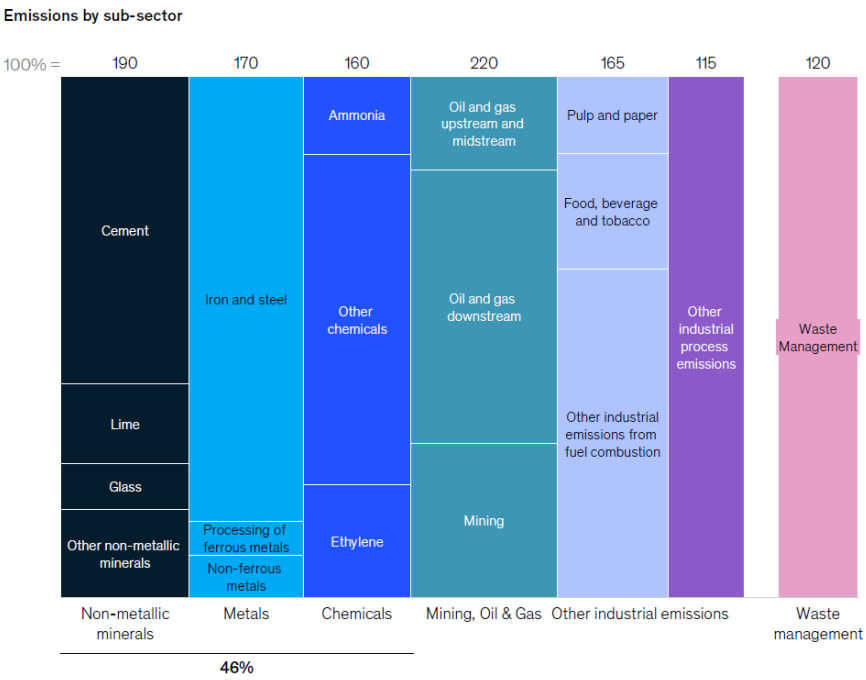

Figure 1.2: European Union industry greenhouse gas emissions by sector [57].

of the Oman project. However, when referring to the number of projects, flat plate collector is the first technology with 219 systems, followed by PTC with 65, and finally linear Fresnel collector (LFC) with 24 projects, which is the least commercially developed technology [78].

The prevailing trend in collector technology is shifting towards concentrative collectors because of their reduced land needs and wider temperature range. For 2023, 70 % of new additions are expected to be concentrating collectors. A change of tendency in the type of contract is also appreciated towards the heat delivery contracts opposite to the EPC (Engineering, Procurement, and Commissioning) system contracts predominantly until 2022.

Analyzing the tendency of the type of industries that were more receptive to applying solar thermal energy solutions, the larger number of installations correspond to the food and beverage sector, whereas in terms of capacity, the first is the mining sector due to the Oman project [78]. Researchers have carried out studies on SHIP integration and found that the sectors of food, fabric and apparel, paper, chemical, and medicines are attractive due to the low-temperature levels required and the high levels of energy consumed in heating [51]. Kumar et al. [65] reviewed the scientific literature and found that most SHIP studies focus on analyzing a particular solar technology applied to a particular industrial process. This study concludes that the integration of solar technologies within the process industry is highly dependent on local solar irradiance, land availability, fossil fuel prices, the quality of the steam required, and the process demand flexibility [65].

One of the major challenges of SHIP is the huge capital investment for large-scale systems. However, the average installed cost has decreased in the last 6 years by 68%, from 1679 USD/kW in 2014 to 531 USD/kW in 2020. The economies of scale of larger plants (more than

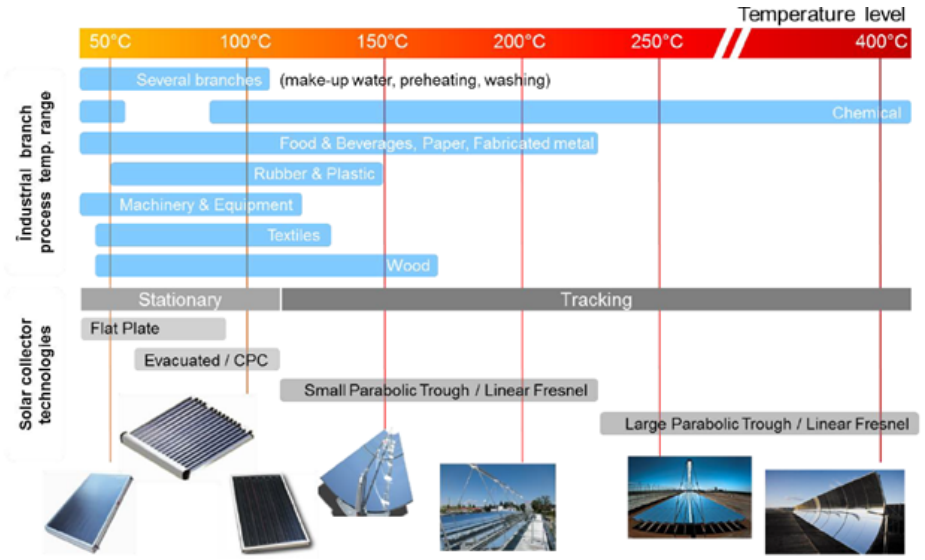

Figure 1.3: Solar collector technologies and industrial process branches for different temperatures level [38].

35 kW) were responsible for the cost reduction, mainly due to the lower cost of materials, the improvement of manufacturing efficiency, and the lower fixed cost (permission, design, engineering) [77]. The lower price of 3.9 USD-cent/kWh can be found in Asia because of the lower cost of materials and labor., followed by Mexico with an LCOH of 4.4 USD-cent/kWh, due to the high levels of irradiance and production optimization due to the competitive market. In contrast, in Europe, the average cost is higher due to the higher labor cost, 6.4 USD-cent/kWh for Southern Europe, and 9.2 USD-cent/kWh for Central Europe due to the lower irradiance.

A recent study carried out by the German Industry Association of Concentrating Power [61] concludes that the combination of solar thermal, storage, and electric heating is economically viable in the short term to replace fossil fuels from the industry sector. They estimated an installation cost of 400 €/m^2 for large fields (>10.000 m^2). Furthermore, the LCOH calculations give a result of 3-4 c€/kWh and a 3-year payback period, considering a price of gas of 140 €/MWh and 50% of federal subsidy.

1.1.1 Solar concentrating technologies

Solar concentrating technologies can achieve higher temperatures than non-concentrating technologies, by concentrating the solar flux in a smaller area. The two principal elements of a concentrator are the reflector and the receiver. The reflector is composed of a mirror that reflects and concentrates the irradiance. The receiver is an absorber surface where the irradiance is collected: typically, a tube with a heat transfer fluid circulating through it. Concentrators can be classified by a concentrated factor that is related to the mirror's geometry and as a result with the maximum temperature reached. Figure 1.6 shows the existent technologies that are divided by the type of focus: linear or point. Linear collectors,

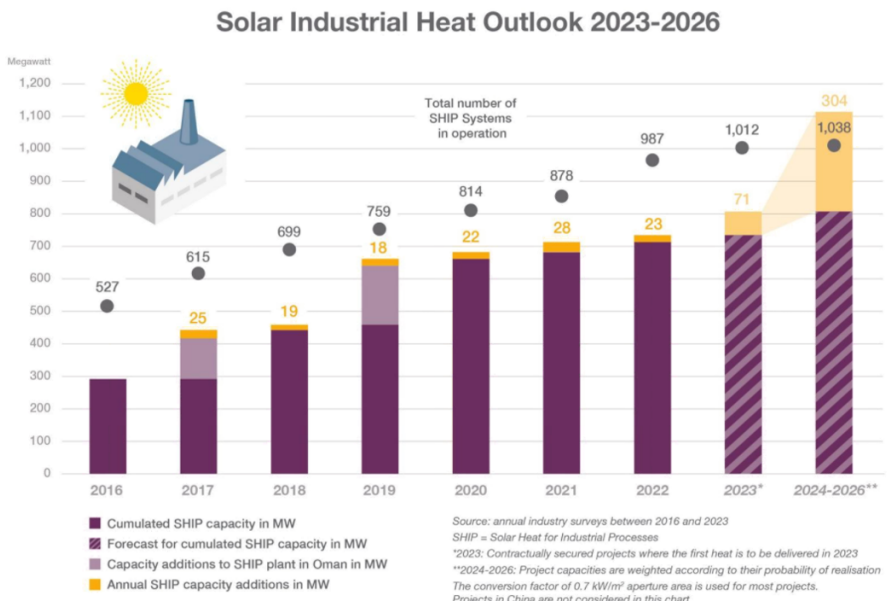

Figure 1.4: Solar industrial heat installed capacity and outlook for 2026 [77].

which are parabolic trough collectors and linear Fresnel reflectors, have a lower concentration ratio, between 30-80, so they achieve lower temperatures with a maximum of 500 °C and they require one-axis tracking. Point collectors, which are towers and dish collectors, can achieve higher temperatures with a maximum of 1500 °C, due to their higher concentrating ratio (maximum of 3000), but they require two-axis tracking.

The most applied technology for solar heat for industrial processes is the parabolic trough collector (PTC). PTC is built from a parabolic-shaped receiver that concentrates the irradiance in the focus line of the parabola (Figure 1.7a). In the focus line of the parabola, an evacuated tube is placed, which absorbs the irradiance and heats a fluid. The heat transfer fluids most used are thermal oils, steam, and molten salts. It is worthing to notice, that the type of PTC used for SHIP are different from the ones used for power generation, principally in size. For example, a Eurotrough collector used for electric power has an aperture area of 12 m^2 per module (Figure 1.7a), in contrast, the Inventive power collector used for SHIP has an aperture area of 3.36 m^2 (Figure 1.7b).

Linear Fresnel collectors (LFC) are less exploited than PTC which is a mature technology. However, this technology can be particularly suitable for heating and cooling because of its flexibility and modularity [86]. They are also more cost-effective in comparison to parabolic trough collectors (PTC), although their efficiency is lower [1]. LFC consists of an array of flat or curved mirrors, that together form a parabolic shape and a static receiver placed in the focus of the parabola (Figure 1.8).

The main disadvantages of LFC are the variation of energy production during the day, the reduction of energy production for higher latitudes, and the problems of blocking and shading among the mirrors [62]. Thus, there is significant interest in the optical and thermal design of solar concentrators applied to supply heat for industrial processes, aiming to overcome these principal challenges of the technology.

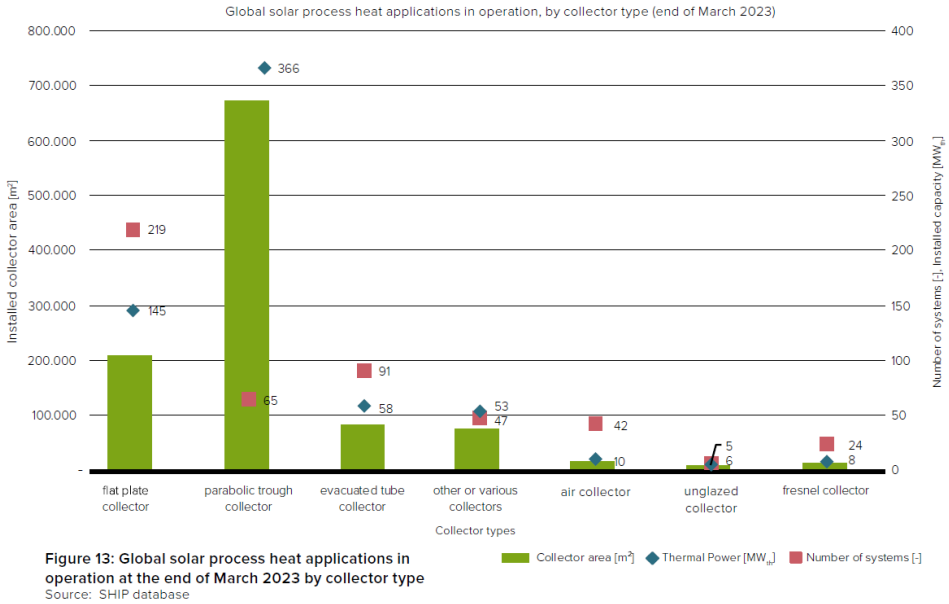

Figure 1.5: Solar process heat applications in operation by the end of March 2023 by collector types (only systems larger than 50 m2 are included) [78].

In this framework, several research projects emerge with innovative solutions such as ASTEP, "Application of Solar Thermal Energy to Process", which includes the design, construction, and testing of a new rotatory solar Fresnel collector. This collector, called SunDial, seeks the reduction of installation, maintenance, and operation requirements [3]. One of the main topics of this thesis is the characterization of the SunDial, by a theoretical analysis including dynamic simulation and the design of an experimental installation to carry out the testing of the SunDial.

Furthermore, there has been an interest in the industry of linear Fresnel collectors applied to SHIP. For example, six companies around the world produce in-house or in-site LFC such as the Spanish company Solatom which has modular Fresnel collectors that can be easily shipped in a container (Figure 1.8a). Additionally, 25% of the new installations of concentrated collectors for SHIP in 2022 are LFC [77].

1.1.2 Thermal energy storage

Solar irradiance exhibits dynamic characteristics, unlike fossil fuels that can be managed as needed. To ensure a reliable solution for the process industry, the solar system must incorporate thermal energy storage (TES). TES is a key element in the integration of the solar field with an industrial process due to the mismatch between the solar irradiance and the energy of the process demand. Furthermore, industrial processes have distinct demand time profiles depending on whether they are continuous or batch. Hence, TES increases the reliability of the solar system, by mitigating the effects of daily solar cycles and random variations caused by the clouds. Therefore, the TES can be classified into three different

Lineal Focus		Point Focus	
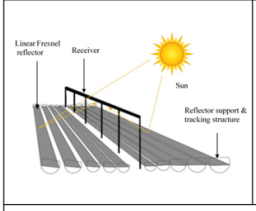	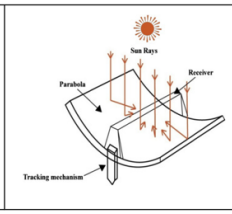	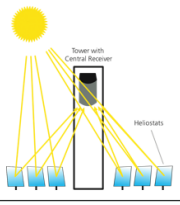	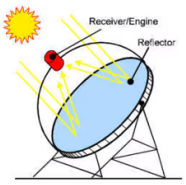
Operational Temperature Range			
150 - 550 ºC	250 – 550 ºC	500 – 1200 ºC	600 – 1500 ºC
Concentration Ratio			
30 - 80	30 - 80	200 - 1000	1000 - 3000
Relative Cost			
Very low	Low	High	Very High
Annual Efficiency			
13 – 18 %	14 – 22 %	15 – 23 %	18 – 25 %

Figure 1.6: Solar concentrate technologies by type of concentration [79].

(a) **(b)**

Figure 1.7: Parabolic trough collector for power production in Plataforma Solar de Almeria (a) and solar field of PTC from Inventive power for industrial heat applications (b) [44].

categories depending on the energy dispatched strategy, which are: buffering power delivery, extending the delivery period, or displaying the delivery period. The buffering tank's objective is to smooth the output variations of the solar plant due to clouds. Then extending or displacing the period of production could be useful to match a particular time demand of the industry [31]. TES can also be classified by type of energy storage mechanism: sensible heat storage, latent heat storage using phase change materials (PCM), and thermo-chemical storage (TCS). Sensible heat storage is at present the cheapest way to store heat. The most used materials to store heat are water, molten salts, and rocks. Thermal energy can be stored up to 1200 °C in sensible heat storage solid materials. However, it requires larger volumes than the other types due to its low energy density. TCS and PCM - based storage systems are at present in the development and demonstration stage. The cost of sensible heat storage ranges between 0.1 and 10 €/kWh, for latent storage between 10 and 50 €/kWh, and for TCS between 8 and 100 €/kWh [45].

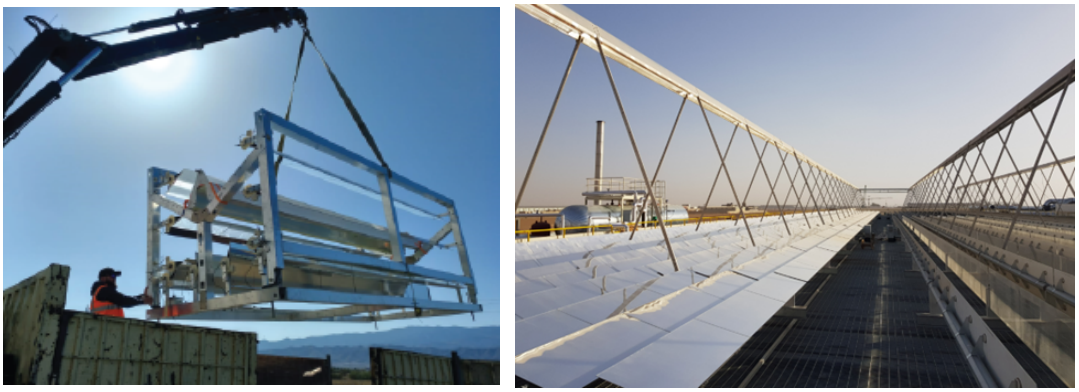

(a) **(b)**

Figure 1.8: (a) Installation of Solatom Fresnel collector and (b) Fresnel collector from Industrial Solar GmbH in a Tobacco factory [44].

Figure 1.9 shows the percentage of number type of storage used in the 552 solar plants for industrial processes installed worldwide that are registered in SHIP plants data-based [44], created in the framework of IEA Task 49/IV. It can be seen that the larger percentage of installations do not specify to have thermal storage, which probably means that they do not count with thermal storage. The second most applied storage type with a 40% share is the water storage tank. Finally, all the thermal storage systems installed on commercial SHIP plants are of the sensible heat type, no plants have been reported with latent or thermochemical storage.

In the research area, there is an interest in developing higher thermal density technologies in the medium-high temperature (150-400 °C), a range that represents 22% of the industry energy consumption [21]. Latent thermal storage can store between 3-4 times more energy than sensible thermal storage, which implies a smaller tank volume. This is particularly interesting to SHIP due to the lack of space in the process industry. The ASTEP project includes latent storage built from a storage tank filled with a phase-change material with a phase-change temperature applicable to the medium-high range.

1.1.3 Integration alternatives for SHIP

One of the major challenges is the integration of solar energy into processes due to the variety of industries, different heat profile demands, and availability of space for the collectors. Industries consume a lot of energy in the form of heat that is typically supplied by: boilers, co-generation systems, burners, and heat pumps. These systems, except for the heat pump that uses electricity and electric heaters, are fed with fossil fuels such as gas, LPG, oil, and coal or with biofuels such as biogas or biomass. Regarding the heat transfer fluid, the most applied in the industry are steam or pressurized hot water [48].

It is difficult to find a standardized solution for the industry, because each industry's best solution may be different depending on the heat transfer fluid used, the demand profile, and the level of temperatures required. However, the production process of each industry can be

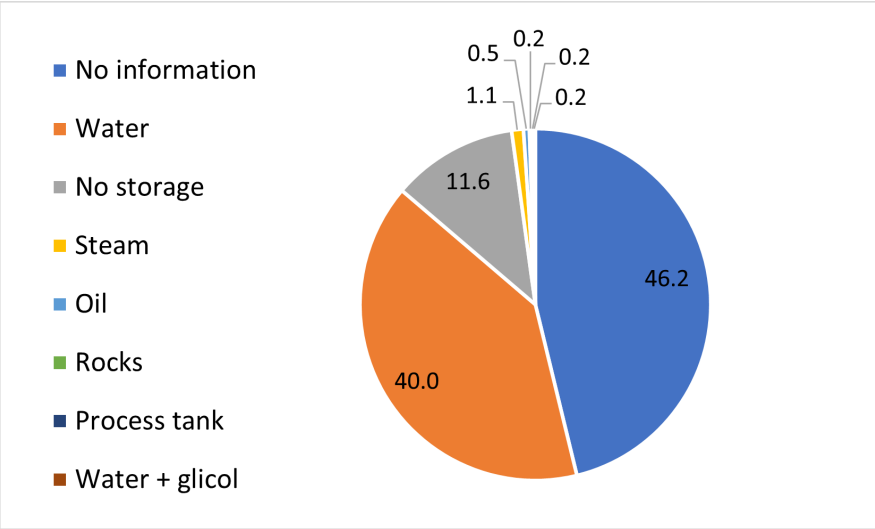

Figure 1.9: Percentage of number of type of thermal energy storage in SHIP installations worldwide (elaborated with SHIP database [44]).

divided into different thermal processes that are common in different industry sectors, e.g., distillation, drying, sterilization, etc. These specific thermal processes are called operation units and can be characterized by the industrial sector they appeared, the temperature range applied, and the medium they used. For example, the sterilization process which is applied in the food and beverage sector involves a temperature range of 100-140 °C and uses steam as HTF.

Having characterized the different thermal processes involved in each industry sector is easy to identify which solar thermal technology will better fit. But, how to integrate the solar field into the industry process is something that requires a deeper analysis. The solar field can be directly integrated into the process level by heating the process medium or a process vessel. Also, can be integrated at a supply level by heating make-up water of the conventional source, or directly heating in the supply network. The integration at the supply level is usually easier to carry out the the process level. The best technique to define the point of integration is the Pitch analysis, which allows the optimization of the heat exchanger's network of the industrial process [64].

Another important aspect is the integration of the thermal energy storage, which can be integrated into the supply network, the process level, or the solar field. For example, in the industry is common to find the storage installed at the supply level when the heating system is a biomass or coal boiler because these systems require some time to achieve the peak load. The process heat storage is usually done with the process medium. Finally, solar thermal energy requires thermal energy storage (TES) to ensure the heat supply when there is no solar radiation [49]. Moreover, the solar field storage systems can be integrated in different ways depending on the type of connection with the solar collector and the industrial process, discerning between series and parallel configurations. These two possible configurations are illustrated with a simple box diagram in Figure 1.10.

The solar field can be directly integrated or indirectly, this will depend on the fluid that is

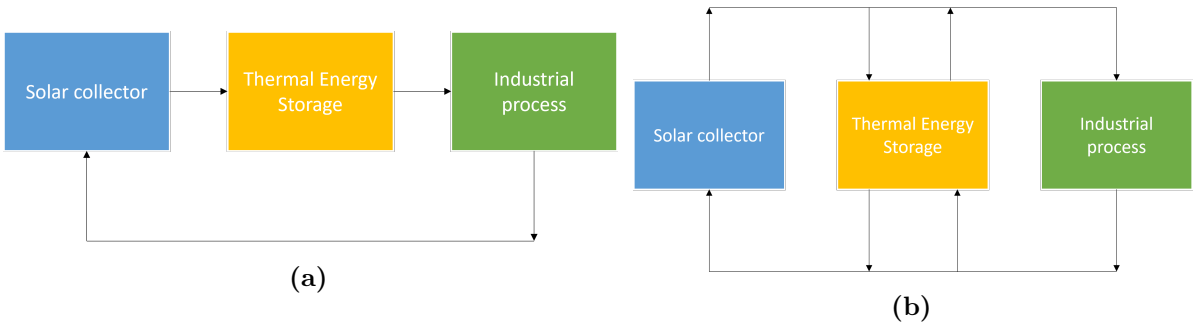

Figure 1.10: Series configuration (a) vs Parallel configuration (b)

used in the solar collectors. Medium-temperature solar collector's most used working fluids are synthetic oil, pressurized water, or steam. Synthetic oil can be used in a wide range of temperatures without changing phase, avoiding the freezing and boiling problems of water. Pressurized water is used in lower-temperature applications to limit the pressure required and reduce the pumping energy. Most of the process that operates at medium temperature uses steam as a heating medium. However, the direct steam application on solar collectors presents several technical drawbacks such as thermohydraulic instabilities and the complexity of control system design [72].

1.1.4 State of art dynamic modelling in SHIP

Computational models of SHIP plants are required in the design stage of feasibility studies or development phases of projects to size and predict the performance of the system. They can also be used to evaluate different possible arrangements of the system components and different control strategies. Stationary models are used to compare and estimate the annual performance of the systems. However, for control system design and transient phenomenon evaluation, dynamic simulations are required.

A recent study carried out from the IEA SHC Task 64/SolarPACES Task IV— Subtask C, which aims to address the lack of standard simulation tools for Solar Heating of Industrial Processes (SHIP) plants, concluded that there is a lack of sustainable guidelines and design tools to aid the design process and also to deliver reliable information to the final sector [64]. They compared several simulation tools available (commercial, open source, or in-house developed) and found differences of 10% in the annual energy yield between the results of the different tools. Furthermore, on a monthly or daily basis, the error was higher between 15 and 20%. They conclude that the source of error could be related to the next causes: applying different time shifting in the solar angles because of the hourly data of the TMY (typical meteorological year), ignoring the thermal capacitance of the system, ignoring the piping thermal losses in the system, considering constant effectiveness in the heat exchanger modeling, simplifying the model of TES and making rough approximations in the load profile.

A comprehensive literature review was conducted to delve into the subject of SHIP (Solar Heat for Industrial Processes) modeling. Various aspects were carefully analyzed, including system configuration, control strategies, solar collector types, heat transfer fluids, thermal

energy storage methodologies, process temperature ranges, and the software employed for modeling purposes. A concise summary of the reviewed papers can be found in Table 1.1, which encapsulates the essence of the findings. The main objective of this review is to analyze the state-of-the-art dynamic modeling for solar concentrated collectors applied to solar heat for industrial processes with a special focus on system modeling and control strategies. Within this review, the scope was further refined to encompass systems incorporating thermal energy storage, categorizing the type of thermal energy storage as either sensible or latent and discerning between the type of connection with the process in series or parallel.

This literature review specifically focuses on solar heat applications within the industrial sector, excluding any papers that treated alternative applications like district heating, organic Rankine cycles, or power generation. The attention has been predominantly directed toward systems employing solar-concentrated collectors due to the main topic of this thesis involving the modeling of a novel rotatory Fresnel collector. Nevertheless, it is noteworthy that papers featuring non-concentrated collectors with latent thermal storage [55] have been incorporated, due to the limited cases of latent storage used in SHIP found in the literature. Non-concentrating collector models developed using the Modelica language were also encompassed for the same reason.

Analyzing the information resumed in Table 1.1, it can be noticed that the majority of the studies employ more mature technologies, specifically sensible thermal storage, and parabolic trough collector, with only two instances of latent storage application [55], [14]. However, in a paper review of latent heat thermal storage, this technology has been identified as a promising alternative to SHIP, although the state of the art is far away from a commercialization stage [21]. In this review several studies that include modeling of latent thermal storage were identified, the most simulated configuration was the tube and shell tank whereas the enthalpy method was the most used for modeling. But, all of these studies were applied to concentrated power generation. Notably, the parallel configuration for thermal energy storage accounts for 60% of the utilized designs. However, no papers analyzing what is the best configuration of the TES were found.

Additionally, only one study incorporates a linear Fresnel collector [15], which is a small-scale collector specially designed to be applied in SHIP (shown in Figure 1.11). The innovation on the LFC involves a 10° tilt of the mirrors and the receiver in the North-South direction, and the receiver is shifted to the north direction, these modifications are meant to improve the optical performance of a common LFC. The main objective of this work was to predict the performance of the new collector applied to different industries demands. Hence, they developed a quasi-dynamic simulation in TRNSYS software for two different industries and compared it with the results obtained for a PTC. They found that the performance in terms of MWh per m^2 of land was better for the LFC.

The prevalent heat transfer fluids employed in these studies are pressurized water and synthetic oil. These are the mediums most used in solar collectors because are easier to control than steam which involves a change of phase. However, some authors study direct steam generation but only apply it to concentrated power generation.

Table 1.1: Literature review of modeling for solar heat for industrial process

Author	Collector	HTF	Thermal energy storage	Layout	Temp.	Software
Cruz-Robles et al. 2023 [23]	Tower	molten salts	molten salts (sensible)	series	600 °C	Solar Pilot
Ktitis et al. 2022 [50]	PTC	thermal oil	concrete (sensible)	parallel	188 °C	TRNSYS
Yilmaz et al. 2022 [85]	PTC	thermal oil	water (sensible)	parallel	200 °C	Visual Basic
Immonem et al. 2022 [46]	PTC	thermal oil	thermal oil(sensible)	parallel	380°C	Simulink
Biencinto et al. 2021 [14]	PTC	water	pentaglycerine (latent)	parallel	80 °C	TRNSYS
Biencinto et al. 2021 [15]	LFC	water	water (sensible)	parallel	165 °C	TRNSYS
Crespo et al. 2021 [22]	PTC	water	water (sensible)	series	90 °C	TRNSYS
Oliveira et al. 2021 [59]	FPC	water	water (sensible)	series	95 °C	Modelica
Bolognese et al. 2020 [16]	PTC	thermal oil	thermal oil (sensible)	series	220 °C	Dymola
Lamari et al. 2020 [55]	FPC	air	paraffin (latent)	series	80 °C	TRNSYS
Kurup et al. 2020 [53]	PTC	water	water (sensible)	parallel	80 °C	SAM
El Gazzani et al. 2017 [30]	PTC	thermal oil	thermal oil (sensible)	parallel	150 °C	TRNSYS
Suresh et al. 2017 [80]	Dish	water	water (sensible)	parallel	250 °C	SAM
Guisado et al. 2016 [39]	PTC	thermal oil	thermal oil (sensible)	parallel	250 °C	Dymola
Silva et al. 2013 [75]	PTC	thermal oil	thermal oil (sensible)	series	150 °C	TRNSYS/Modelica

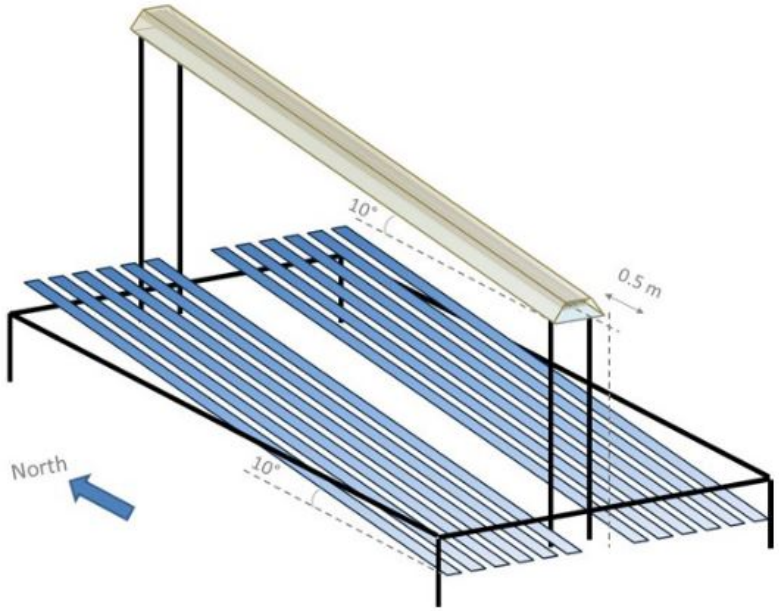

Figure 1.11: Innovative Fresnel collector for a SHIP [15].

Simulations are predominantly conducted using TRNSYS probably because it provides a large standard library with validated models called Types that can be used to model solar thermal systems. TRNSYS is characterized by using a procedural language and a discrete-time integration algorithm. Modelica, in contrast, is an object-oriented language and equation-based and also counts with a standard library of common components. Hence, in Modelica is easier to build new components which reduces the development time of a larger simulation system between five to ten times [84]. The library includes an implicit integration algorithm of variable step size which is interesting to simulated control systems.

One of the common objectives of several researchers implementing dynamic simulations is to test the performance of a new integration system for a solar concentrator in a particular industry. Therefore, the dynamic simulation is used to evaluate the control strategy, the modes of operation, and the results in terms of energy, power, and temperature profiles of the novel systems. This is extremely useful for optimizing new systems and evaluating their results before the construction of the prototypes or installation in the final users which are the industrial factories.

For instance, Biencinto et al. [14] developed a novel system to provide heat to a dairy factory at two different temperature levels (40 and 80°C) using pentaglycerine latent storage and a parabolic trough collector (PTC). Their focus was on analyzing the control strategy of the thermal energy storage (TES) system connected in parallel and different operational modes. They were able to increase the industry's heat demand coverage from 40% to 52% with a thermal storage duration of 3 hours. Similarly, Bolognese et al. [16] conducted a similar analysis for a pasta factory located in a complex topographical area. To simulate the system, they used Dymola and implemented a Proportional Integrative Derivative (PID) controller to manage the mass flow of the solar system, a critical parameter for maintaining high efficiency. Guisado et al. [39] took advantage of Dymola's dynamic capabilities to

assess the impact of a thermocline sensible storage tank used to store heat generated by a PTC solar field applied to a drying process in the agricultural sector. They achieved heat coverage between 87% and 100% for various scenarios during the summer season. Immonen et al. [46] applied a technique called flexible heat integration, enabling the system to provide heat at different levels and temperatures for the industrial process. They found that this approach increased solar efficiency by 7.5% compared to a conventional control system with a fixed high-temperature setpoint. Lamati et al. [55] optimized the design of a latent heat storage system applied to a wood drying process that required a temperature of 80°C. Finally, Cruz-Robles et al. [23] conducted a feasibility analysis for implementing a tower system to supply heat to a high-temperature mining process operating at 600°C, achieving a coverage rate of 22%.

Furthermore, several studies have enhanced the credibility of dynamic simulations applied to Solar Heat for Industrial Processes (SHIP) by validating their models with experimental data. For example, Ktistis et al. [50] validated their TRNSYS model by comparing it with real data obtained from an installation in a beverage factory. They achieved an average weekly error in the system's contribution to the process of 6.45%. Crespo et al. [22] conducted an enhanced scenario analysis by increasing the operating temperature of a solar system that was operating below its capacity in a beverage factory. Yilmaz et al. [85] conducted multiple experiments involving solar systems applied to the food industry and developed a dynamic model to predict annual operation. Their model demonstrated a maximum difference of 2% in the outlet temperature of the solar field when temperatures were high, likely due to thermal losses not accounted for in the model. Silva et al. [75] validated their parabolic trough collector model, developed in Modelica, by comparing it with experimental results. They achieved a root mean square error of 1.2%. The rest of the system was co-simulated with TRNSYS to enable the performance of annual simulations.

Moreover, additional research efforts have delved into the economic advantages of applying solar thermal technology to industrial heat processes. For example, Biencinto et al. [15] conducted a comparative study of three solar technologies: Parabolic Trough Collectors (PTC), Flat Plate Collectors (FPC), and a novel Linear Fresnel Collector (LFC) using dynamic simulations in TRNSYS. They discovered that the LFC, while yielding less total energy, offers significantly higher energy production per unit of occupied land, making it an intriguing option for Solar Heat for Industrial Processes (SHIP) applications. Suresh et al. [80] also performed a comparative analysis of three different solar technologies - Flat Plate Collectors (FPC), Evacuated Tube Collectors (ETC), and Dish collectors - for the Indian industrial sector. They employed SAM, a performance and financial analysis tool developed by the National Renewable Energy Laboratory (NREL). However, it's worth noting that this analysis did not consider control and technical issues related to resource intermittency. Their findings emphasized the strong dependency of achieving low payback periods on fossil fuel prices. Oliveira et al. [59] utilized Modelica to simulate a solar plant designed to provide heat to a ceramic manufacturing facility. Their simulation yielded a promising 3-year payback period, which holds significant appeal for the industrial sector, highlighting the economic viability of such solar thermal applications.

1.2 Framework project

Application of Solar Thermal Energy to Process (ASTEP) is a Horizon 2020 European project [8] whose objective is to find a low-cost, easy-to-install and operate, and lower maintenance solution to the solar thermal for industrial process sector. The ASTEP is a system specially designed to provide heat between the temperature range of 150 °C and 240 °C. The system's principal novelties are the solar concentrator, called SunDial, and the latent thermal storage.

Two SunDial prototypes are being built by the Universidad Politécnica de Madrid. Each version counts with a different objective: the former looks for a cost reduction while the other seeks higher performance than regular LFC. The first prototype is a linear Fresnel concentrator mounted above a rotary platform that follows the sun's trajectory azimuthally. The mirrors which are placed above the platform, different from a regular LFC, are fixed. The second prototype is designed to be used at high latitudes, where commercial collectors' efficiency will be compromised. This SunDial has a double tracking system, so the mirrors above the rotary platform follow the sun's elevation.

The thermal energy storage is based on the latent heat transfer mechanism by a phase change material salt. The system is of the type tube and shell and the main novelty is the metal inserts of the tubes that improve the thermal transference between the heat transfer fluid and the storage media. This TES is being built and tested at the Universidad Politecnica de Cartagena.

The objective of the ASTEP project is to achieve a Technology Readiness Level five (TRL-5), implying the solar system has been validated in an industrial environment. Therefore, this project intends to integrate the prototypes into two industrial sites: a dairy factory located in Corinth, Greece (latitude 37.93° N), and a tube steel factory at Iasi, Rumania (latitude 47.1° N). The dairy factory requires a temperature of 205 °C for the pasteurization process and 90 °C for an absorber chiller, which is used for milk cooling. The factory opens between 9 and 17 hs when the pasteurization is carried out, but the cooling is required 24/7. The tube steel company operates 24/7 and the required temperature is 220 °C in a preheating process.

The author of this thesis was involved in the combined design of ASTEP components and the construction at a laboratory scale. The process diagram and control strategy for the complete ASTEP system were determined in the first task. Including the selection of equipment, sensors, and connections (piping and accessories) that best adjust to the construction of the ASTEP system in each end-user. A dynamic model was developed to analyze the performance of the designed system in the two different factories. Then, the second task was to build a testing facility to characterize the performance of the two SunDial prototypes and to test the control strategy applied by each end-user.

1.3 Thesis scope

The main objective of this thesis is to **design the integration and control strategy for cost-competitive, novel solar concentrating systems for industrial processes.**

To achieve this objective, the following tasks were defined:

1. Design a system configuration comprising the SunDial and the latent storage, along with a control strategy capable of meeting the energy demand of two different industrial processes (referred to as ASTEP system).
2. Develop a dynamic model for ASTEP system to test the control strategy and asses the transient effects.
3. Design and build a testing facility for SunDials capable of replicating the end-user control strategy.
4. Demonstrate the ASTEP system cost-competitiveness through a techno-economic study.

1.4 Methodology

A brief description of the topic covered in each chapter is presented in this section. As presented in the introduction, the industry is responsible for 37% of global greenhouse gas emissions and utilizes 74% of energy for heat production, with 90% coming from fossil fuels. While solar thermal energy is a feasible solution, obstacles such as high capital costs, space limitations, and solar intermittency need to be addressed. The primary aim of the ASTEP concept is to identify an affordable, easy-to-install, and operate solution with reduced maintenance requirements through a modular system comprising the SunDial collector and latent thermal storage.

The ASTEP system is developed in Chapter 2 concerning system configuration and control strategy. It encompasses an explanation of the main components and design criteria. Subsequently, two distinct system setups, differing in how thermal energy storage is connected either in series or parallel, are implemented for use at a dairy factory and a tube steel factory. The control approach for these four configurations is formulated and detailed within this chapter.

Due to the lack of simulation tools for solar thermal energy used in industrial processes and the innovative nature of the SunDial and TES, a model for the ASTEP system is developed and detailed in Chapter 3. This model can perform dynamic simulations that are utilized to explore control strategies and assess the controller's design for the ASTEP system, including the defocus controller of the SunDial. Additionally, this model is employed to analyze the thermal inertia of the system and its response to cloud cover. A simplified version of this original model is applied to conduct annual simulations aimed at examining different configurations' performance and selecting a final configuration for ASTEP.

The information gathered from the simulations is used to design a testing facility for investigating the performance of the SunDial. This facility is equipped to replicate operations in the factories where the ASTEP system will be tested. Consequently, a series of experiments are designed to test both the control strategy and the SunDials. Chapter 4 includes a comprehensive description of the experimental installation built in Madrid.

A techno-economic evaluation of the SunDial and ASTEP system is presented in Chapter 5. Initially, the prototypes' expenses are determined based on the procurement of all construction materials. However, since the prototype cost exceeds that of a commercial collector, a cost estimate is derived using available literature and market prices. An analysis correlating cost with size was conducted to identify the optimal dimensions for the SunDial. Subsequently, LCOH for the ASTEP system is computed and through parametric assessment, a configuration with lower LCOH is identified. This configuration was then contrasted against its market competitor PTC.

Finally, Chapter 6 present the conclusions obtained from the work carried out in this thesis and discuss future work and recommended actions to further follow this line of investigation.

Chapter 2

System design

Solar heat applied for industrial processes is still in the developing phase. As it was introduced in Chapter 1 only 1089 installations were operative worldwide by 2023 [77]. In the case of solar heat plants different from photovoltaic, each installation is custom-designed for a project. No standardization is available, which implies a high capital cost. The standardization and modularization of solar heat plants not only can reduce the cost but also increase the reliability of the technology.

This chapter aims to formulate a modular and flexible system configuration and control strategy that can be applied in two different industries in two different locations. The goal is to integrate the SunDial and TES systems with the underlying process, with a focus on reducing costs, ensuring operational simplicity, and optimizing heat production while minimizing energy waste.

Therefore, first the design basis, which delineates the boundary conditions for the ASTEP system are presented. Subsequently, two distinct configurations for the system, with the promise of simplifying the integration with the process and the cost reduction are described. The analysis of these configurations pertains specifically to the dairy factory and the tube steel factory. Lastly, the control strategy is developed across both factory settings.

2.1 ASTEP system

ASTEP's concept starts from the necessity of bringing a cost-effective and modular solution to the heat demand of the process industry. Two main features of ASTEP are the solar collector, the SunDial, and the thermal energy storage, which are specially designed for heat applications. The TES is required to unbound the solar irradiance from the heat production and to provide reliability to the solar system.

The SunDial is the result of four Spanish patents ES2578804B2, ES1138715U, ES2537607B2, and ES2713799A1, and two international patents WO/2016/166388A1 and WO/2016/166390A1 developed by the Universidad Politécnica de Madrid (UPM) and Universidad Nacional de

Educación a Distancia (UNED). There are two versions of the SunDial, the first only can be applied in low-latitude locations and focuses on cost reduction. The second is for high latitudes and aims to achieve high efficiency in latitudes where a Fresnel collector would not perform well. The principal characteristics of the two SunDial prototypes are:

- SunDial low latitude (SunDial-LL) (Figure 2.1a) [69]: the collector is mounted above a rotary platform, while the mirrors remain fixed. This setup reduces the number of tracking motors required for the system and facilitates easy and quick installation and maintenance. Furthermore, to improve the geometrical efficiency, the field is tilted longitudinally, and the receiver has a longitudinal offset.
- SunDial high latitude (SunDial-HL) (Figure 2.1b) [68]: the platform rotates to maintain the sun in the cross-section, and each mirror tracks the sun's elevation. Additionally, the mirrors' field is tilted in the cross-section. These improvements enable the SunDial to achieve the same energy production at a latitude of 47.1° N as it does at 37.9° N.

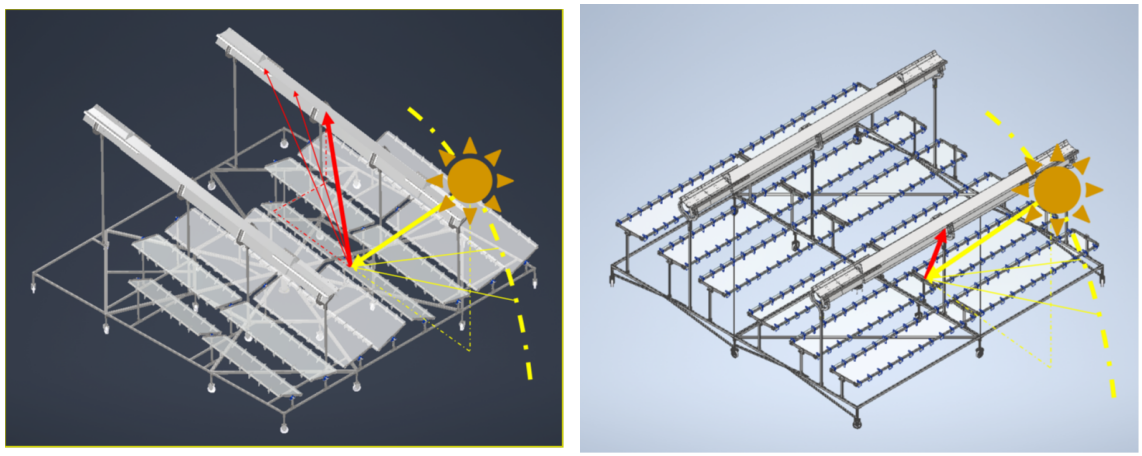

(a) **(b)**

Figure 2.1: SunDial for low latitudes (a) vs SunDial for high latitudes (b)

Another key element of the ASTEP system is thermal energy storage. The technology selected is solid-liquid latent heat storage, which has the potential to store 3-4 times more energy than conventional sensible storage, making it particularly interesting for industrial applications with a lack of space. The thermal storage tank (Figure 2.2) is a tubular heat exchanger with metal inserts to increase the heat transfer between the salts (the storage media) and the thermal oil that flows inside the tubes (the heat transfer fluid). The phase change material is a mixture of potassium nitrate and sodium nitrate with a melting temperature of 222 °C [76].

The ASTEP system will be installed in two different locations, with different latitudes, weather conditions and industrial processes. The SunDial-LL will be set in a dairy factory in Greece and the SunDial-HL will be installed in a steel factory in Rumania. The selected industrial processes are different so the heat demand profiles will differ in temperature levels and other requirements which are briefly described.

The Greek dairy factory specializes in the production of yogurt and milk desserts. The

production requires heat for the pasteurization process and also cooling for product storage. The heat required for the pasteurization is provided by a steam boiler powered by liquefied petroleum gas, which produces steam at 175 °C and 8 bar. The boiler operates continuously from Monday to Friday and between 9:00 am and 17:00 producing 960 kg/h at base load. A second steam generator, capable of producing 600 kg/h, is available for peak loads [11]. However, the annual yield of the ASTEP system will be lower than the plant requirements (less than 1 %), so the process steam boiler will continue to be used. The ASTEP system will be integrated at the heat supply level but only will cover 8 kW of steam at 175 °C and 8 bar. For the milk cooling, the plant has two refrigerant systems: a direct expansion system for the cold rooms and a distribution line of refrigerant for the cooling coils for the pasteurized milk. The cooling systems operate 24 hours 7 days a week. In this case, the ASTEP will cover 6 kW of the heat source of the absorption chiller with a second heat exchanger that heats water at 80 °C.

The Rumanian steel factory facilities include hot stretched reduction mills annealing furnaces for normalizing, colour coating lines, and machines for threading. The ASTEP system will be integrated into colour powder-based coating line. The colour coating uses a thin layer of coloured protective/decorative material covering the whole tube's external surface. To apply this coating on the tubes, they need to be pre-heat using an inductor heater to a temperature between 180-200 °C. The ASTEP system will be integrated parallel to the line of production and will only deliver 14 kW to pre-heat the tubes at the required temperature.

2.1.1 System requirements

As was previously seen in Section 1.1.3, there are several possibilities to integrate a solar field with the process. However, the scope of this study will be limited to the point of integration heat exchanger and will not analyze the optimum way to integrate the ASTEP system with the process. The ASTEP system objective is to achieve a stage of TRL-5, this means that the prototype will be applied in an industrial environment. However, the heat production of the ASTEP will be far smaller than the energy demand of the industrial sites. The next targets have been defined for ASTEP [8]:

- Heat supply over 190 °C in latitudes where commercial technologies are not able to supply it.
- Yearly energy production of 25 MWh.
- Daily energy production of 135 kWh in summer for at least 30 days.
- Daily energy production of 50 kWh in winter.

The first conditions to determine are those required at the connection point with the industry. In this case, a flexible heat integration (FHI) is implemented using two heat exchangers. The flexible heat integration is constituted by different temperature and power levels, this control is more efficient than the most common application of keeping the setpoint fixed at the maximum temperature. For example, Immonen et al. [46] achieved an increase of 7.5 % from the common control scheme by using FHI. To implement this at the dairy factory,

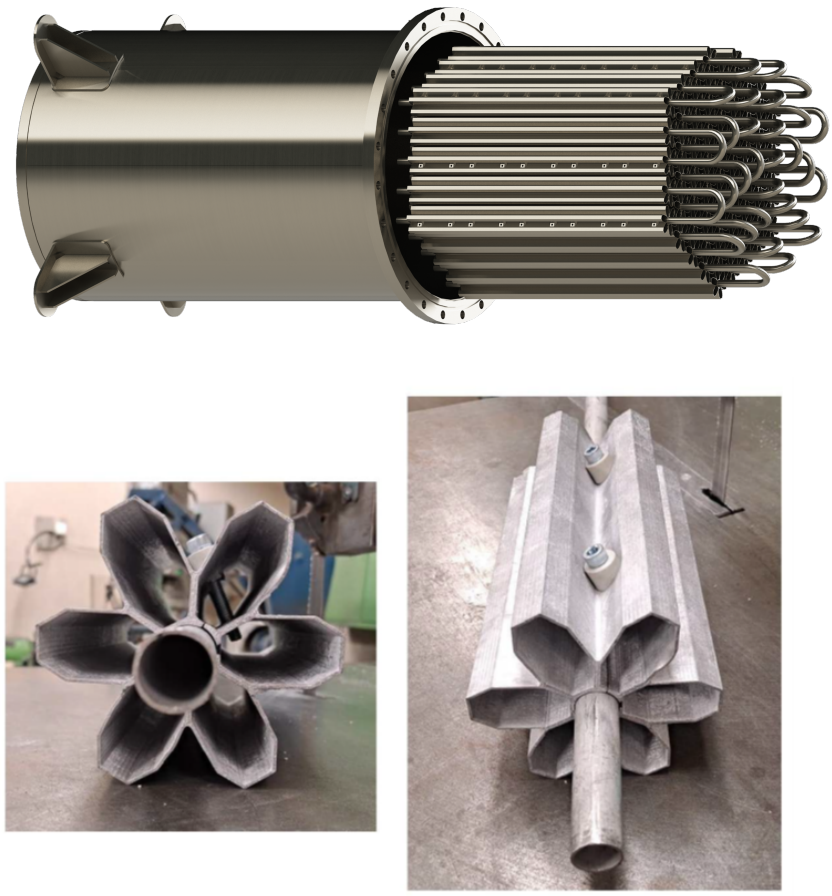

Figure 2.2: Storage tank heat exchanger and metal tubes with inserts [76].

two heat exchangers will be utilized, the first for the heating demand and the second for the cooling. Three levels were defined, 6 kW and 195 °C using only the cooling HX, 8 kW and 205 °C with the heating HX, and 14 kW and 220 °C with both HX. The parameters for these heat exchangers (HXs), shown in Table 2.1, were previously defined in the ASTEP project, and are boundary conditions for this study. Here it can be seen the power of demand, the required inlet temperature and mass flow rate, and the difference of temperature between the outlet and the inlet of the HTF in the HXs. In the case of the tube steel company, the requirements are only for heating. However, two heat exchangers are connected in series, which can supply energy to the process at two different levels of power and temperature: only one HX working at 7 kW and 205 °C and two HXs working at 14 kW and 220 °C. The parameters for the tube steel factory, are shown in Table 2.2.

Table 2.1: Heat Exchanger parameters for dairy factory

Heat Exchanger	Heating	Cooling
Power [kW]	8	6
Inlet temperature [°C]	205	95
ΔT [°C]	15	5
Mass flow rate [kg/s]	0.23	0.59

Table 2.2: Heat Exchanger parameters for the tube steel factory

Heat Exchanger	High	Low
Power [kW]	7	7
Inlet temperature [°C]	220	207
ΔT [°C]	13	13
Mass flow rate [kg/s]	0.23	0.23

The first step in defining the system's configuration involves analyzing the characteristics of the SunDial. The SunDial dimensions were optimized using a thermal model for the receiver, an analytic model for predicting mirror shape, an analytical model for reducing the number of optical design variables, and a Monte Carlo Ray Tracing model for the final field [3]. The results of this analysis define the dimensions of the SunDials that are shown in Table 2.3 .

The SunDial is a linear Fresnel collector mounted above a square platform. The platform has wheels to allow the SunDial to rotate. An important parameter for the layout is the land factor, which represents the relation between the reflecting surface and the total area occupied by the collector (for the SunDial the circle is formed by the rotation of the external wheels). The SunDial receiver is a standard evacuated tube like the one used by parabolic trough collectors (Figure 2.4). This type of receiver has been selected because it is standardized which implies a lower cost and a faster procurement than a specially-made receiver. The HTF flows inside the absorber tube which has an internal diameter of 0.066 m. It is important to maintain a minimum fluid velocity to prevent thermal oil fouling and to ensure a high heat

transference coefficient. Therefore, the SunDial will operate at a minimum velocity of 1 m/s, this implies a minimum mass flow of 4 kg/s.

The main difference between the two prototypes is the higher efficiency of the SunDial-HL. This higher efficiency is a result of the two-axis tracking system that increased the value of the incident angle modifier (IAM) in contrast to the SunDial-LL as seen in Figure 2.3. The values of the IAM angles illustrated in the Figure were calculated with a Monte Carlo Ray tracing model [4].

An improvement in the efficiency of the two-axis tracking of the SunDial-HL is noticed by comparing the IAM plots for the two SunDials. In the SunDial-HL the maximum IAM value corresponds to 0.6281 and this value is maintained constant until the zenith angle surpasses 60°. In contrast, in the SunDial-LL the IAM starts to decrease at a zenith angle of 33°, and when the zenith angle is 60° the value of the IAM is 0.35. This impacts directly on the impinging power.

The mirror fields of the SunDials are tilted to increase the direct component of the irradiance. The increase of the tilt implies a more favorable cosine factor which is included inside the IAM, but also a higher receptor height. So the tilt was defined to limit the height of the receiver at 1.5 m for a cost consideration. The tilt result was 10° in the SunDial-LL and 5° in the SuDial-HL [3].

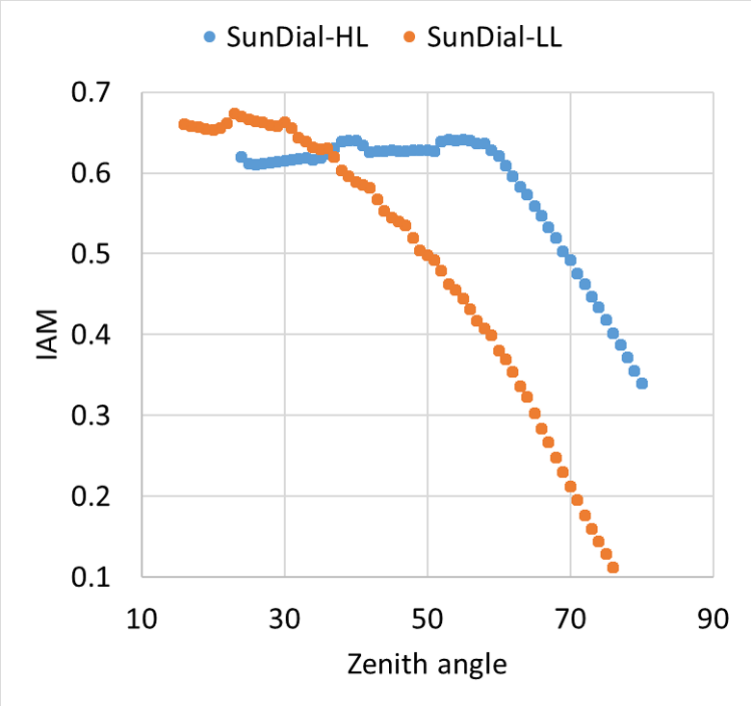

Figure 2.3: Incidence angle modifiers for the SunDials

The second main component in ASTEP is the thermal storage system (TES). This TES has been designed by Universidad Politécnica de Cartagena and Politechnika Wroclawska [76]. The principal mechanical characteristics of the TES tank are in Table 2.4. The ASTEP will include two tanks of around 1 tonne of salts, and each tank has inside a serpentine of 60 tubes

of a nominal diameter of 25.4 mm. The two tanks will be connected in parallel to reduce the pressure losses. Similar to the SunDial, the TES requires a minimum velocity of 1 m/s to prevent fouling and to achieve a high heat transference coefficient, which implies a minimum flow mass of 0.5 kg/s.

Table 2.3: SunDial principal parameters.

Parameters	SunDial-LL	SunDial-HL
Reflecting surface [m^2]	47.50	44.00
Platform area [m^2]	116.17	103.08
Land factor	2.45	2.34
Receiver height [m]	3.40	2.55
Radius external wheel [m]	6.08	5.73
Mirrors length [m]	6.3 & 5.3	8
Width mirrors [m]	1.03	0.94
Mirrors per receiver	4	3
Receiver length [m]	8	8
Internal diameter of absorber [m]	0.066	0.066
External diameter of absorber [m]	0.07	0.07
External diameter of glass [m]	0.115	0.115
Receivers per platform	2	2
Mirrors per platform	8	6

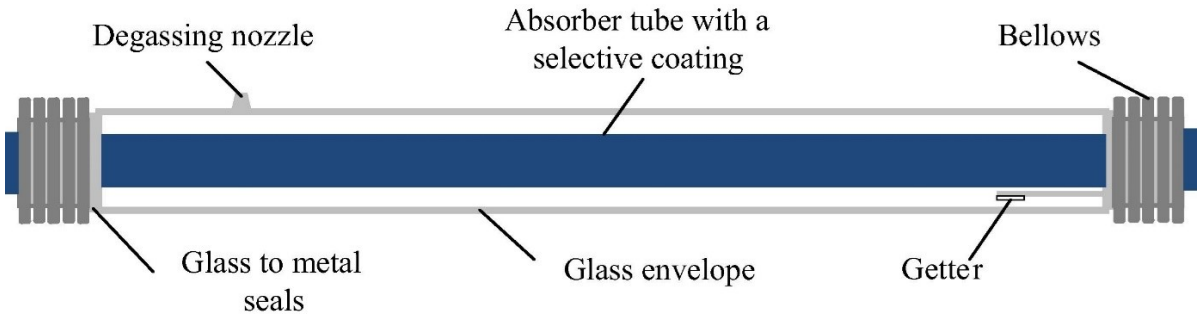

Figure 2.4: Standard evacuated tube receiver [33].

The heat transfer fluid selected for the ASTEP system was a thermal oil, called Therminol 59, which has a temperature application range between -49 and 315 °C. The selection of the fluid was based on the low temperatures achieved in Rumania in winter, -18 °C, so using water was dismissed to avoid freezing. Furthermore, using thermal oil implies a lower pressure of the system than required if steam was used due to the high-temperature requirements. The maximum temperature admitted by the system will be 240 °C to reduce the thermal losses in the storage tank and the thickness of the thermal insulation for the pipes.

However, the system can overheat if thermal energy storage is full and the energy production in the SunDial is higher than required by the process. Therefore, the maximum allowed

temperature could be exceeded. This would lead to degradation of the components of the system, which would have to be replaced, leading to economic losses and the solar system being out of service. To avoid this, the tracker system requires a control that partially defocuses the SunDial mirrors to reduce the heat generation and, thus, to maintain the maximum temperature of the system to a safe value.

Table 2.4: Thermal storage tank characteristics

Tubes length [mm]	1400
Tube inner diameter [mm]	22.1
Number of tubes	61
Shell inner diameter [mm]	909.5
Shell height [mm]	1907
PCM weight [kg]	1109
Tank empty [kg]	1061

Solar tracking systems can be categorized by different characteristics such as control strategy, degrees of free motion, drives, or tracking strategy (Figure 2.5). The solar industry has a long history of solar tracking systems. Solar concentrators such as PTC and LFC use a single axis. The drives most used are the actives, such as slew drives. The closed-loop strategy is more precise than the open-loop but requires a sensor to monitor the radiation. For the tracking strategy, there are two options: the photodiodes or the solar algorithms that calculate the position of the sun.

The SunDial is mounted above a rotary platform that precisely tracks the azimuthal trajectory of the sun. One of the key safety mechanisms integrated into the SunDial system is the partial defocusing of the mirror achieved by rotating the platform. This defocusing action is implemented to cap the maximum temperature that the SunDial can reach. Therefore, for the SunDial a closed-loop strategy based on an algorithm and with active drives was selected.

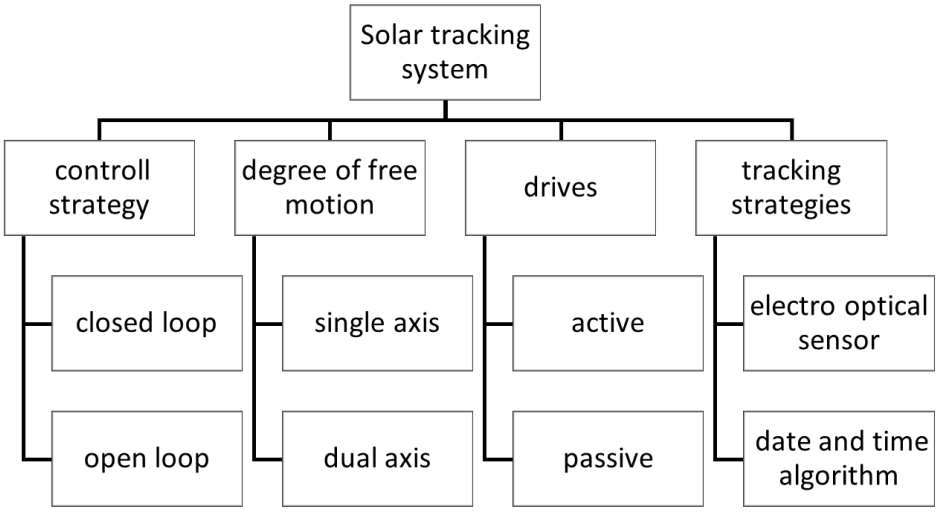

Figure 2.5: Types of solar tracking technologies.

2.1.2 Weather conditions for the industrial sites

The weather conditions for a solar plant are a determining parameter, especially the direct normal irradiance (DNI), which is the useful irradiance for solar concentrators. Figure 2.6 presents the typical meteorological year (TMY) principal parameters that impact heat production: the DNI, the wind velocity, and the ambient temperature, for the two locations: Iasi, Rumania, and Corinth, Greece.

As can be seen in Figure 2.6, the mean DNI value is somehow higher for Corinth than IASI (464 W/m2 versus 417 W/m2). Also in summer, a higher concentration of points is noticed over the average DNI line in Corinth. Regarding the ambient temperature, a higher difference can be noticed for the two locations. The annual mean temperature in Corinth is 18.3 °C (with a range from -0.9 °C to 40.6 °C) and in Iasi is 10 °C (from -17.5 °C to 36.9 °C). Finally, the wind speed is moderated in both locations, the mean wind speed is 2.9 m/s for Corinth and 3.1 m/s for IASI. This is an acceptable value for concentrating solar energy.

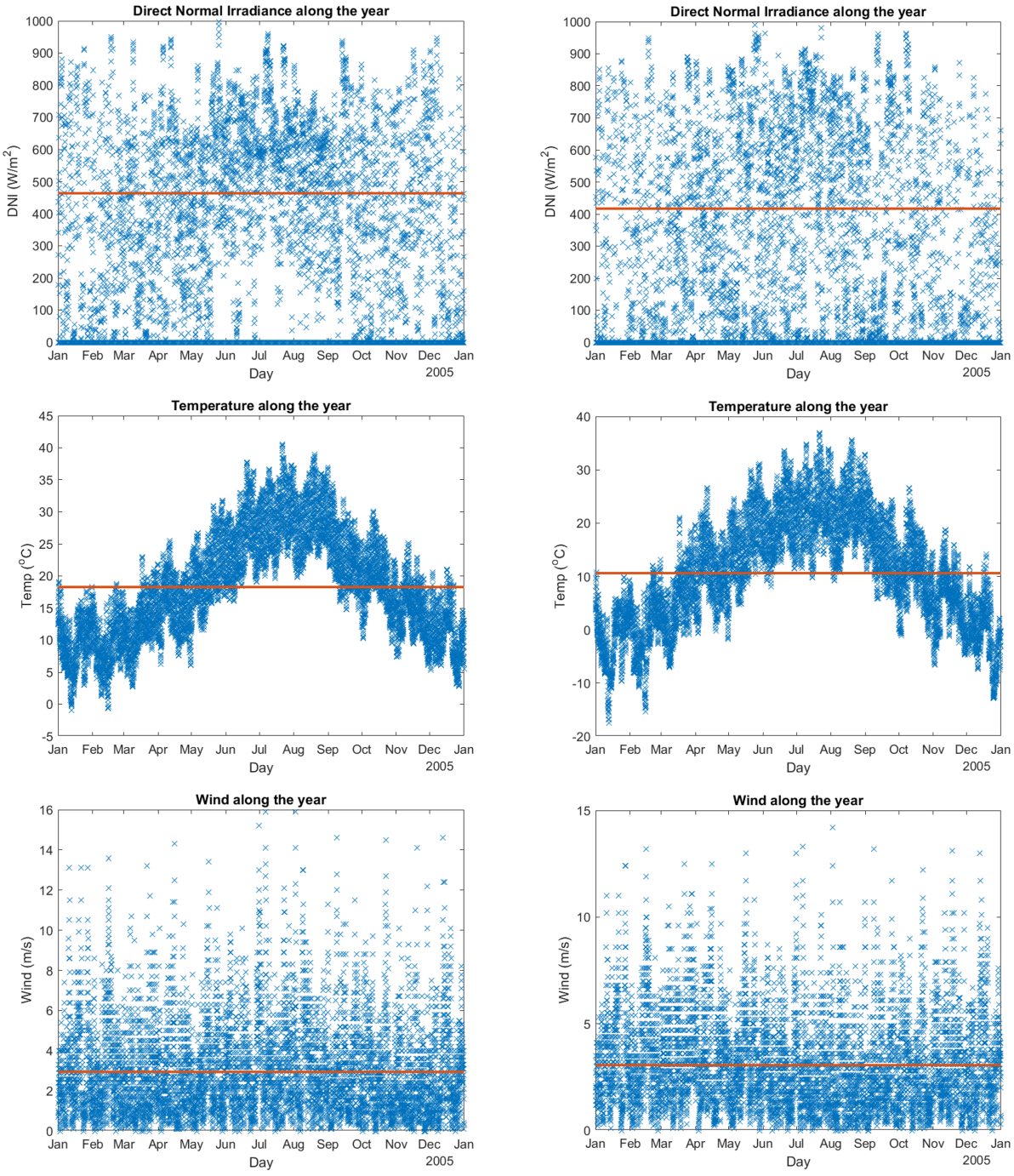

Figure 2.6: Typical meteorological year data for Corinth (a) and IASI (b) [6].

To carry out a detailed analysis of the system's performance, three characteristic days of each location were chosen based on the DNI level: high, medium, and low. The high DNI day corresponds to the highest DNI day, which was interesting to analyze to avoid the defocus of the SunDial. The medium DNI day was selected as an average summer day. The low DNI day

was chosen as a representative day of winter. The DNI, temperature, and wind values along these representative days are represented in Figure 2.7. These days are later implemented in the dynamic model to obtain different system operation modes. The average DNI of each day is shown in Table 2.5.

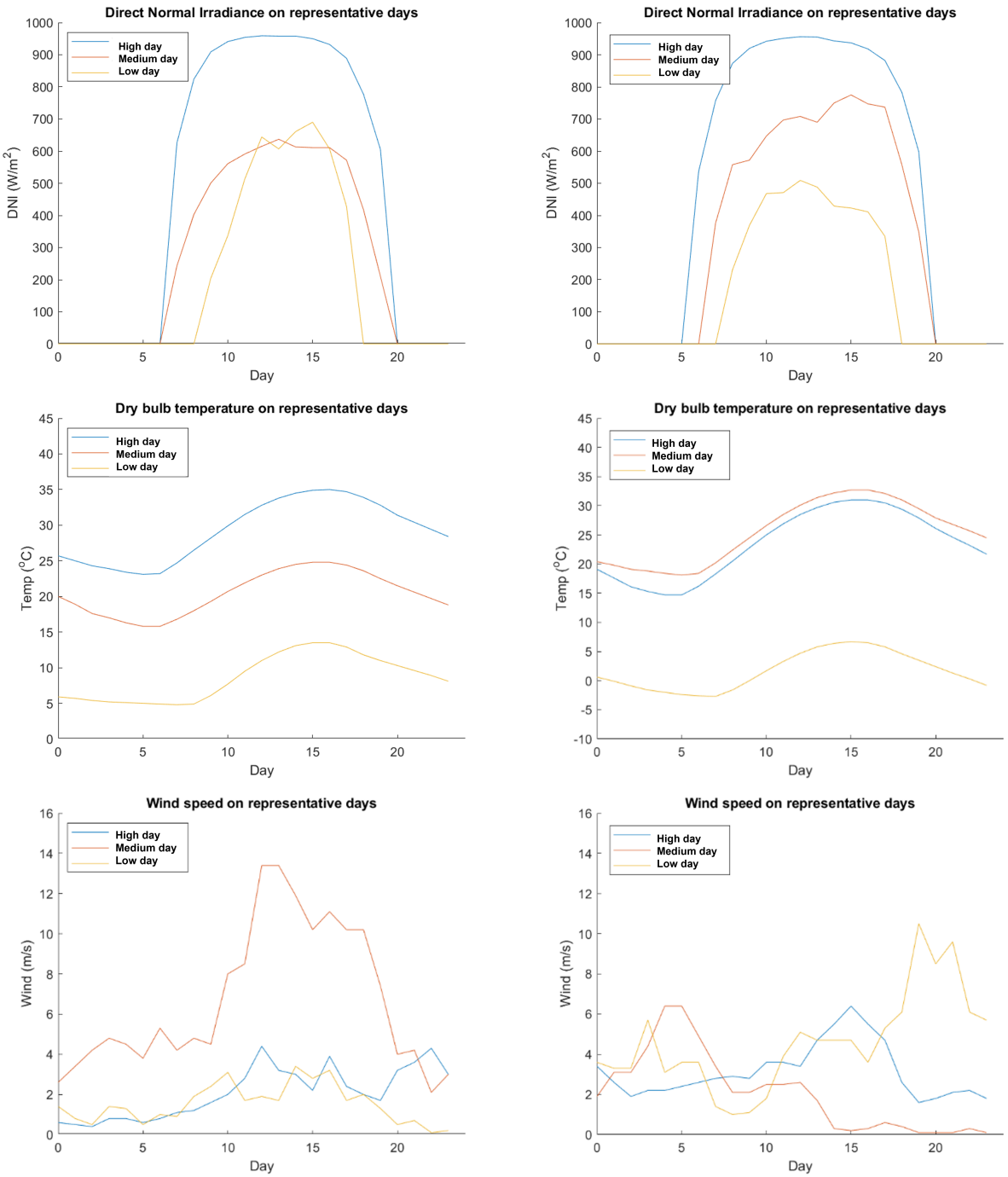

Figure 2.7: Weather conditions for the selected days in Corinth (a) and Iasi (b) [6].

Table 2.5: Selected days based on DNI levels

	Corinth			Iasi		
	high	medium	low	high	medium	low
day	8-07	16-05	7-02	27-05	17-08	7-03
DNI [kWh/m^2]	11.3	6.6	4.7	12.0	8.2	4.1

2.2 System Configuration and control strategy.

In solar heat plants control strategy is an important factor due to the intermittency of the solar irradiation. In a review paper about control systems for solar heat plants [37], the authors enumerated the next advantages of control systems:

- Provided the process energy at desirable conditions of temperature improving the efficiency of the system.
- Balance the amount of energy produced by the solar system and the demand, minimizing the dumping of energy.
- Operating the installations near the design conditions, guarantees the maximum efficiency of the system and durability.

In Section 2.1.1, the desired conditions for the key components of the ASTEP, the SunDial, the TES, and the demand heat exchangers, have been defined. These conditions are called operation conditions and can automatically be controlled to their desired values (called setpoints) by a control system.

Control techniques for CSP have been deeply studied in the literature, for example, Camacho et al. [17] have surveyed the different control techniques applied in solar plants to control the outlet temperature. They found that most of the solar plants are controlled by traditional PID controllers. Although solar plants are nonlinear systems in which advanced control systems can be used, the PID controllers reported in the literature achieve good results in terms of setpoint tanking and disturbance when restricting the bandwidth of the controllers.

Advanced controllers have been also applied to solar heat plants, as Gil et al. [37] remark in their review on control strategies. However, they conclude that these controllers have their drawbacks such as the requirement of accurate prediction of the model process and adequate irradiance forecasting methods. Because the SunDial and the TES are new prototypes with no experimental results available nor adequate irradiation forecast data, the traditional approach of PID controlling has been selected for the ASTEP system. The design of the controllers will be explained in further detail in the Chapter 3.1 .

Table 2.6 shows the control variables of the system. The inlet temperature at the heat exchangers has been set according to the industrial process requirements. The heat exchanger mass flow rate is defined by the temperature difference and the power required by the heat exchangers. The TES and the SunDial require a minimum flow velocity of 1 m/s to avoid

thermal oil fouling. The minimum flow through the TES is higher than the demand flow. Therefore, the TES flow will be fixed to its minimum value and a control valve will bypass the excess flow. The SunDial minimum mass flow is higher than the one that can admit the TES. Hence, the SunDial will count with a recirculation pump to guarantee this flow. The maximum temperature of the system was limited to 240 °C to reduce the cost of the materials in the system.

Table 2.6: Defined control variables and setpoint of ASTEP.

Variable	Dairy factory	Tube steel factory
SunDial flow	4 kg/s	4 kg/s
SunDial maximum temperature	240 °C	240 °C
TES flow	0.5 kg/s	0.5 kg/s
Heat exchanger flow	Heating 0.23 kg/s Cooling 0.59 kg/s	0.23 kg/s
HX inlet temperature	Heating 205 °C Cooling 95 °C	220 °C

Two possible configurations were analyzed for the thermal energy storage connection with the SunDial and the heat exchanger (HX). The first configuration connects the TES in series with the solar collector and the process. This implies that the solar collector outlet stream always goes through the TES before reaching the process. The second configuration connects the TES in parallel with the solar collector and the process. This implies that the solar collector outlet stream can be connected to the TES or the process. These two configurations will be explained in detail in the next sections.

2.2.1 Series configuration

In this section, the series configuration which consists of connecting the TES in series with the SunDial and the heat exchangers is explained for each factory. The system of both factories is intended to be as similar as possible to follow a modular and standardized concept. The benefit of standardization is that scale production can be applied, which drives down the cost the solar systems [77]. Therefore, the only difference between the systems is in the process integration arrangement of the heat exchangers.

Dairy factory

Figure 2.8 shows the ASTEP system, which is composed of the solar collector (the SunDial), the TES (latent heat storage) connected in series, and two heat exchangers to provide heating (boiler) and cooling (chiller) to the process. The chiller heat exchanger is connected in series, so the temperature of the oil stream that exits the boiler is reduced from 190 °C to 95 °C before entering the chiller heat exchanger to avoid thermal stresses. An expansion tank (TK) is required to equalize the pressure of the closed system due to the thermal expansion of the thermal oil. Several controllers were implemented using valves and pumps with frequency

drivers. The controlled variable is represented in a circle (where the letters TC are for temperature control) and connected with a dashed line to the actuator. Table 2.7 shows a list of the actuators of the system. Also, the sensors of the system are represented to measure the principal operative variables: temperatures (T), pressure (P), and flow (F).

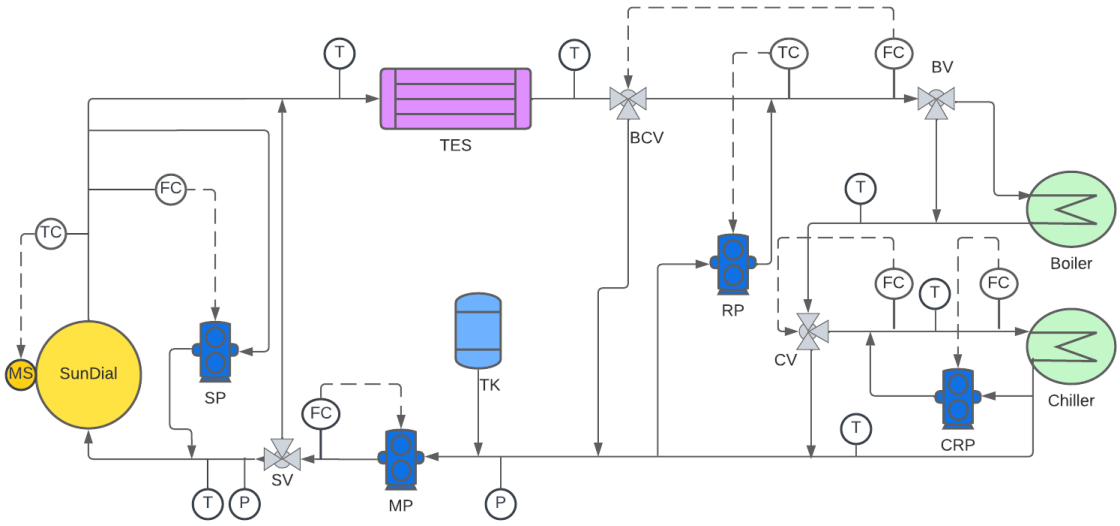

Figure 2.8: ASTEP diagram with the TES connected in series of the dairy factory.

Table 2.7: Actuators in the series configuration of the dairy factory system.

Name	Tag	Task
Sundial tracking motors	MS	Move Sundial platform to locate the mirrors in the right position and defocus in the case the max. temp. is achieved
SunDial pump	SP	Drive a constant flow through the SunDial
Main pump	MP	Drive a constant flow through the TES
Recirculation pump	RP	Keep a specific temperature in the HX inlet
Chiller pump	CRP	Drive a constant flow through the chiller HX
SunDial bypass valve	SV	Drive the fluid through the Sundial or bypass it
Boiler bypass valve	BV	Drive the fluid through the boiler HX or bypass it
Chiller bypass valve	CV	Keep a specific temperature in the HX chiller inlet
Bypass control valve	BCV	Keep a constant mass flow rate at HX inlet
Expansion tank	TK	Keep a constant pressure in the MP inlet

Regarding flow control for the minimum velocity to prevent fowling in the TES and the SunDial, a main pump (MP) sets the TES flow to a constant value of 0.5 kg/s. The SunDial

counts with a recirculation pump (SP) that sets the mass flow to a constant value of 4 kg/s. The mass flow of the boiler is controlled by bypassing the excess flow to the inlet of the main pump (MP) with a bypass valve (BPV). This PI controller is represented as a white circle with the letter FC in Figure 2.8. The inlet temperature of the demand is controlled with a recirculation pump (RP), which mixes the cold stream from the chiller outlet with the hot stream from the TES outlet. A recirculation pump (CRP) and a three-way valve (CV) adjust the inlet flow and temperature of the chiller, which was set to a lower value to avoid thermal stress.

Regarding the operation of the solar plant, the boiler heat exchanger will work only when the factory is open. The chiller would be operational 24/7 but prioritizing the boiler when the energy is insufficient for both. When the factory is closed, the chiller will work until the storage is empty. Therefore, the ASTEP system could operate in different modes depending on the SunDial heat production and the TES state of charge, described below.

- **Mode 1 - Preheating (M1)**: When irradiance reaches the minimum value to overcome the heat losses, the SunDial will re-circulate to preheat the HTF. This mode will end when the outlet temperature of the SunDial reaches the demand setpoint or is higher than the TES salt average temperature.
- **Mode 2 - SunDial and TES Charging (M2):** This mode will occur if the SunDial outlet temperature is higher than the TES salt average temperature, but there is insufficient temperature to supply to the process.
- **Mode 3 - SunDial and TES Charging and Process (M3):** This mode will be active when the SunDial is producing more power than the process demand, and the excess will be stored. This happens when the outlet temperature of the TES is higher than the process setpoint and the temperature of the PCM is lower than the outlet of the SunDial.
- **Mode 4 - SunDial and TES discharging and Process (M4):** This mode will occur when the SunDial power is lower than the process demand requirements, but the TES could supply the missing energy. This happens when the outlet temperature of the TES is higher than the process setpoint and the outlet temperature of the SunDial is lower than the PCM.
- **Mode 5 - TES and Process (M5):** This mode will occur when the SunDial is shut down and the TES has enough energy stored to supply the process demand. This means that the outlet temperature of the TES is higher than the process setpoint.
- **Mode 6 - SunDial and Process (M6):** If the TES is full, the SunDial will partially defocus to feed the exact amount of power that the process demand requires. The outlet temperature of the SunDial will be limited to 240 °C. This implies that the maximum temperature of the TES will be also 240 °C.

In the series configuration, the different operational modes will be selected by measuring the value of the HTF at the TES outlet temperature ($T_{out,TES}$) and comparing it with a defined setpoint. These start and shutdown temperature setpoints for the boiler and chiller are shown in Table 2.8. A 5 °C difference is considered between startup and shutdown to

avoid chattering, that is, to avoid the shutdown a short time after start-up due to transient oscillations in the TES outlet temperature. The operation of the boiler is prioritized over the operation of the chiller. Therefore, when the factory is opened, the chiller setpoint is set at a higher value to ensure sufficient energy for both. Different chiller start temperatures were tested in a dynamic simulation for different levels of irradiance to define the adequate setpoint the results are explained in Chapter 3.1.

Regarding the SunDial start-up, it depends on several facts: first, the measure of direct normal irradiance (DNI), has to be higher than the minimum to overcome the thermal losses (DNI_{min}); second, the SunDial outlet temperature ($T_{out,Sun}$) has to be higher than the chiller setpoint, or higher than the TES average salt temperature ($T_{TES,avg}$). Finally, the SunDial shutdown occurs when the DNI is lower than the minimum (DNI_{min}) or the SunDial outlet temperature ($T_{out,Sun}$) is lower than the process minimum setpoint and the TES sats average temperature.

Table 2.8: Start-up and Shutdown conditions for the series layout of the dairy factory .

Mode	Start-up	Shutdown
Sundial	($T_{out,Sun} > T_{TES,avg} + 5$ or $T_{out,Sun} > 195$ °C) and $DNI > DNI_{min}$	$DNI < DNI_{min}$ or $T_{out,Sun} < 190$ °C and $T_{out,Sun} < T_{TES,avg}$
Boiler	factory open and $T_{out,TES} > 210$ °C	factory closed or $T_{out,TES} < 205$ °C
Chiller	when factory closed $T_{out,TES} > 195$ °C when factory open $T_{out,TES} > 215$ °C	when factory closed $T_{out,TES} < 190$ °C when factory open $T_{out,TES} < 210$ °C

The operation strategy for SunDial differs from the typically implemented in SHIP, where the outlet temperature of the collector is controlled by the variation of the mass flow with a PID control scheme [37] and the temperature difference on the solar field is fixed. This strategy is used mainly in larger solar plants than our prototype with sensible storage or no storage. In these configurations the inlet temperature of the solar field is constant.

In the ASTEP system, the inlet temperature of the SunDial is variable and will increase as the TES is charged until the maximum temperature is achieved. In consequence, the outlet temperature of the SunDial will also increase. Therefore, the outlet temperature difference will be variable and dependent on the incident power and the state of charge of TES, this will be further explained in the Chapter 3.1.

Tube steel factory

As depicted in Figure 2.9, the process diagram for the steel tube factory is presented, wherein the unique difference from the preceding diagram (the dairy factory) lies in the process integration. In this particular scenario, two heat exchangers (HX) are arranged in a series configuration, affording the flexibility to either bypass one of them or concurrently engage both. A comprehensive list of system actuators is outlined in Table 2.10.

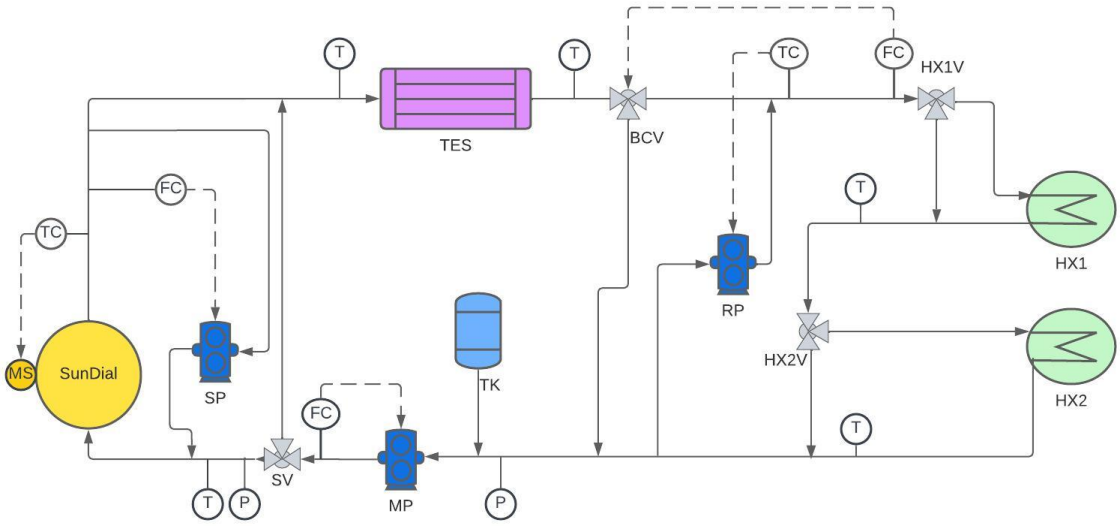

Figure 2.9: ASTEP diagram with the TES connected in series of the tube steel factory.

Table 2.10: Actuators for the series configuration of the tube steel factory.

Name	Tag	Task
Sundial tracking motors	MS	Move Sundial platform to locate the mirrors in the right position and defocus in the case the max. temp. is achieved
SunDial pump	SP	Drive a constant flow through the SunDial
Main pump	MP	Drive a constant flow through the TES
Recirculation pump	RP	Keep a specific temperature in the HX inlet
SunDial bypass valve	SV	Drive the fluid through the Sundial or bypass it
HX1 bypass valve	HX1V	Drive the fluid through the HX1 or bypass it
HX2 bypass valve	HX2V	Drive the fluid through the HX2 or bypass it
Bypass control valve	BCV	Keep a constant mass flow rate at HX inlet
Expansion tank	TK	Keep a constant pressure in the MP inlet

This operational arrangement facilitates a dual-tiered heat supply, capable of delivering either 7 kW (involving a single HX) or 14 kW (involving both HX units). This strategic approach aims to enhance system efficiency, particularly during the winter season or on low solar irradiance days, instances in which only one HX unit would remain operational. Notably, it is discernible that the system for the steel tube factory necessitates one less pump in comparison to the dairy system, attributed to the exclusion of HX2 temperature control.

Concerning the operational strategy, it is important to note that the plant operates continuously the 24 hours of the day and the 7 days of the week, thereby the operation of the heat exchangers (HXs) is independent of the time of day. The first HX will start working when

the outlet temperature of the TES is higher than 205 °C. However, is important to emphasize that a temperature controller will govern the inlet temperature of HX1. This controller will maintain the inlet temperature at 220 °C once the threshold is achieved, meaning that until this threshold is reached, the inlet temperature will remain uncontrolled. Subsequently, both HXs will operate in tandem when the TES outlet temperature surpasses 225 °C. This operational arrangement aims to optimize the efficiency of heat exchange during different irradiance periods.

Paralleling the approach undertaken in the dairy factory scenario, a range of 5 degrees has been designated between the start-up and shutdown setpoints. This provision is implemented to avert undesirable chattering phenomena, as outlined in Table 2.11. The operational modes mirror those of the series layout configuration of the dairy factory expounded previously.

Table 2.11: Start-up and Shutdown conditions for the series layout of the tube steel factory.

Mode	Start-up	Shutdown
SunDial	($T_{\text{out,Sun}} > T_{\text{TES,avg}} + 5$ or $T_{\text{out,Sun}} > 210$ °C) and $P_{\text{hit}} > P_{\text{min}}$	$P_{\text{hit}} < P_{\text{min}}$ or $T_{\text{out,Sun}} < 204$ °C and $T_{\text{out,Sun}} < T_{\text{TES,avg}}$
HX1	$T_{\text{out,TES}} > 210$ °C	$T_{\text{out,TES}} < 205$ °C
HX1 &HX2	$T_{\text{out,TES}} > 220$ °C	$T_{\text{out,TES}} < 215$ °C

Control strategy for the series configuration

Having established the configurations for both factories, as well as the controller's setpoint and operational range, the control strategy can be formulated. The ASTEP system is designed to operate autonomously, eliminating the necessity for operator intervention. Figure 2.10 depicts a flow diagram outlining the general control strategy.

The initial set of parameters subject to information sent by the sensor's measurement covers the power supply to the process, the DNI, wind velocity, the temperature of the TES salts, and the operational state of the Main Pump (MP) (on or off). Serving as the primary stage, the startup routine is elaborated in greater detail in Figure 2.11.

The start-up routine comprises two distinct phases: firstly, the initiation of the SunDial, which concludes when the SunDial attains the temperature required for TES charging or process supply. Secondly, the beginning of TES operations, culminated in the connection of the TES to the process heat exchangers.

In the context of SunDial's start-up, the initial step involves an assessment of the weather conditions, specifically wind velocity and DNI. If the wind velocity remains below the designated maximum threshold, the SunDial is enabled to operate; but, if the wind velocity exceeds this threshold, the SunDial is conducted into a stow position. This protective stance serves to prevent wind-induced damage to the SunDial's structure.

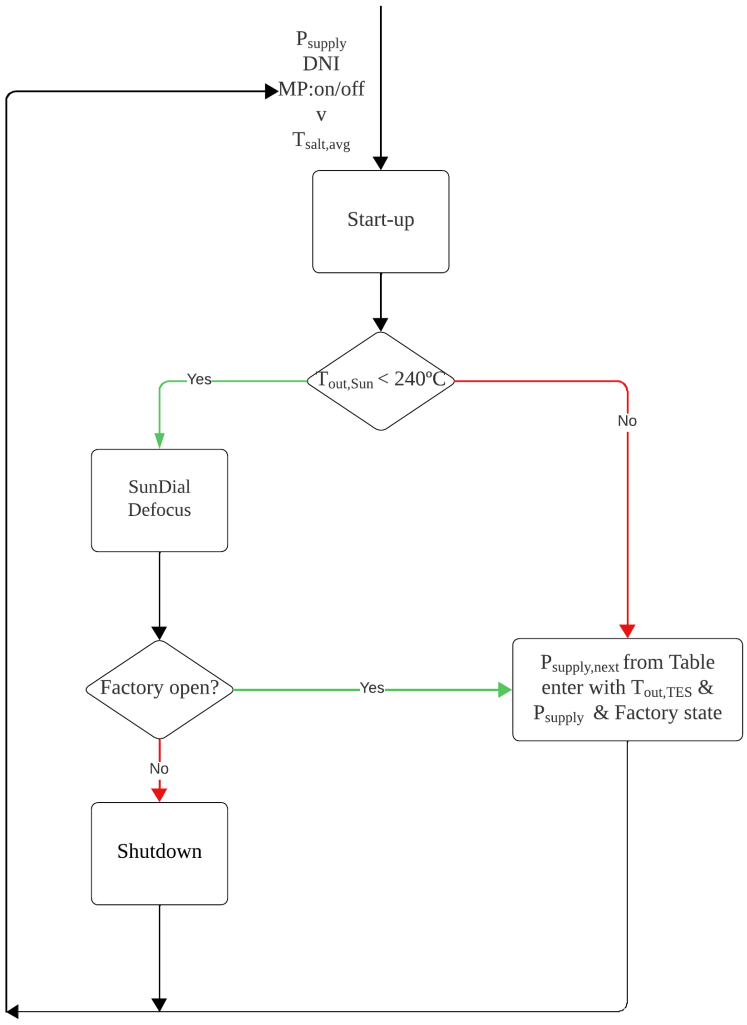

Figure 2.10: General flow diagram for series configuration.

Subsequently, the DNI is measured to verify if it surpasses the minimum requirement necessary to offset heat losses. In the affirmative case, the SunDial is activated, starting the SunDial motors to align the mirrors into the focus position. Additionally, the SunDial Pump (SP) is activated, initiating the recirculation of the HTF for preheating purposes. Eventually, the SunDial's start-up sequence concludes when the SunDial's temperature reaches the level requisite for either supplying the process or charging the TES system.

Upon the completion of the SunDial start-up phase, the TES system is automatically engaged, triggering the activation of the Main Pump (MP), as the flow exiting the SunDial invariably passes through the TES. Nonetheless, in cases where the SunDial is not operational, the TES may either be operational or not. This distinction can be discerned through the state of the MP: an active MP denotes the TES is operative. The MP can be triggered when the TES's salt temperature is above the process setpoint independent of the SunDial's temperature.

Finally, the TES start-up process culminates when either the outlet temperature of the TES (if the SunDial is online) or the average temperature of the salts (if the SunDial is offline) surpasses the designated process start-up setpoint.

Referring to the overall control flow diagram (Figure 2.10), once the start-up of the thermal energy storage system is completed, the outlet temperature of the SunDial solar collector is compared to a maximum allowable value. If this maximum threshold is reached, activation of the defocus controller takes place and the outlet temperature of SunDial is regulated to maintain at 240 °C. If a defocusing situation occurs and the factory is closed, the shutdown sequence will be initiated.

Alternatively, once the facility is operational, the flow control proceeds to a decision table that determines the next power supply. In this table, the conditions for connecting the process heat exchangers depend on factors such as the outlet temperature of the thermal energy storage system and previous power supplies to ensure the efficient operation of the plant.

In the case of the dairy factory, the conditions depend on the state of the factory (open or closed), so there are two tables: Table 2.13 is used when the factory is open and Table 2.15 is when the factory is closed. For the tube steel factory only Table 2.16 is required.

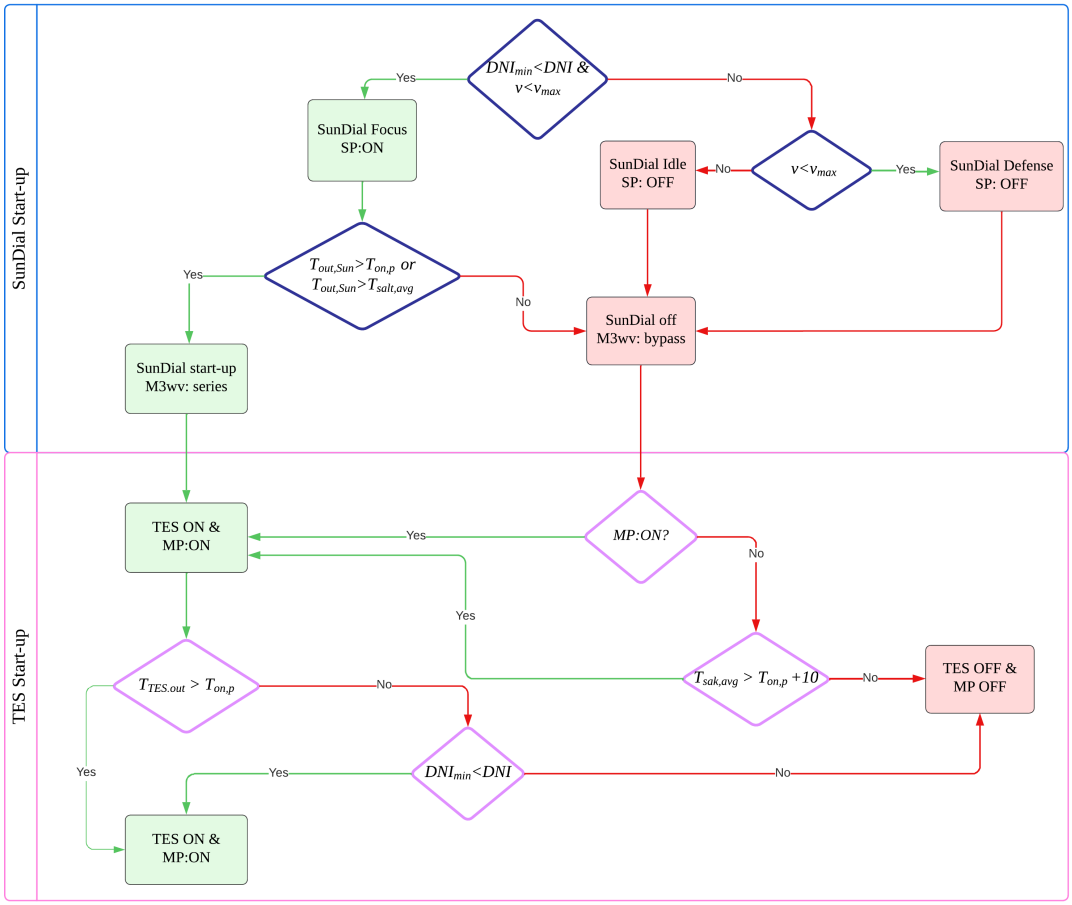

Figure 2.11: Start-up flow diagram for series configuration.

Table 2.13: "Next Power" associated with a TES outlet temperature when the dairy factory is open.

Power Supply	TES outlet temperature				
	<205 °C	205 °C - 210 °C	210 °C - 220 °C	220 °C - 225 °C	>225 °C
0	None	None	Boiler	Boiler	Bo+Ch
Boiler	None	Boiler	Boiler	Boiler	Bo+Ch
Chiller	None	None	Boiler	Boiler	Bo+Ch
Bo+Ch	None	Boiler	Boiler	Bo+Ch	Bo+Ch

Table 2.15: "Next Power" associated with a TES outlet temperature when the dairy factory is closed.

Power Supply	TES outlet temperature		
	<190 °C	190 °C - 200 °C	>200 °C
0	None	None	Chiller
Chiller	None	Chiller	Chiller

Table 2.16: "Next Power" associated to TES outlet temperature for the tube steel factory.

Power Supply	TES outlet temperature				
	<205 °C	205 °C - 210 °C	210 °C - 220 °C	220 °C - 225 °C	>225 °C
0	0	0	HX1	HX1	HX1+HX2
HX1	0	HX1	HX1	HX1	HX1+HX2
HX1+HX2	0	HX1	HX1	HX1+HX2	HX1+HX2

Finally, the shutdown sequence is represented in Figure 2.12. It should be noted that all pumps, except for the SuDial Pump, are deactivated. The SP continues to operate to recirculate the flow and dissipate heat until the outlet temperature of the SunDial reaches 150 °C.

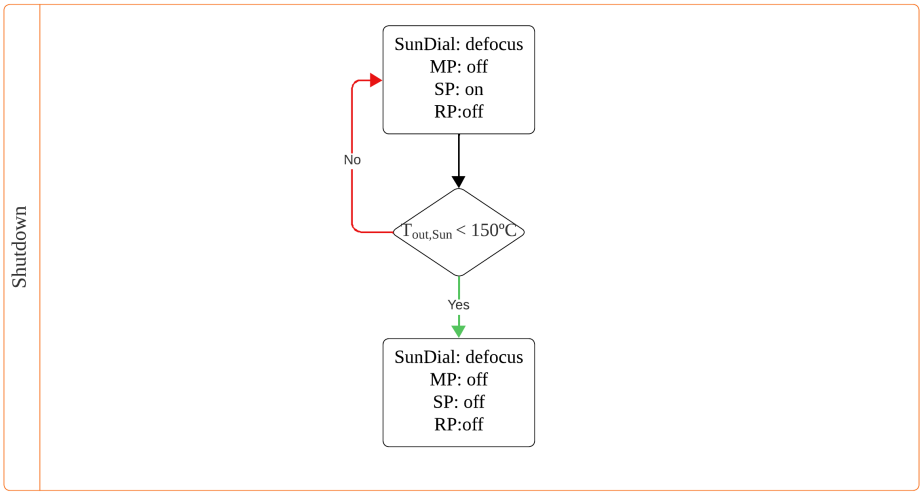

Figure 2.12: Shutdown flow diagram for series configuration.

2.2.2 Parallel configuration

The second configuration analyzed compromised the parallel connection with the SunDial and the heat exchangers. This was the most implemented configuration in the literature review accounting the 60% of the cases. Like in the series connection, the systems for the dairy factory and the tube steel factory are equal between them except for the recirculation of the second HX.

Figure 2.13 shows the TES connected in parallel to the SunDial and the process for the dairy factory in (a) and the tube steel factory in (b). Table 2.18 illustrates a list with the extra actuators that are different from the series configuration, where it can be noticed that parallel configuration requires a higher number of controllers. Identical to the series configuration, the SunDial flow is maintained constant by the SunDial recirculation pump (SP) in both factories.

In the dairy factory system, the variables at the chiller inlet were adjusted analogously to the series configuration with a bypass valve (CV) and a recirculation pump (CRP). But in this case, the bypass valve needs a PI controller, while in series it is in a fixed position. This controller is required because the pressure profile of the system is variable depending on whether the TES is in charge, discharged, or idle.

In both factories, the TES flow is fixed by an independent recirculation pump (TESP). Then the inlet flow to the boiler or HX1 is controlled by the process pump (PP). The biggest difference from the series configuration is in the boiler or HX1 inlet and Sundial outlet temperature controllers, which vary depending on the mode of operation. These temperature controllers are described in operating modes 2,3,4 and 5 below.

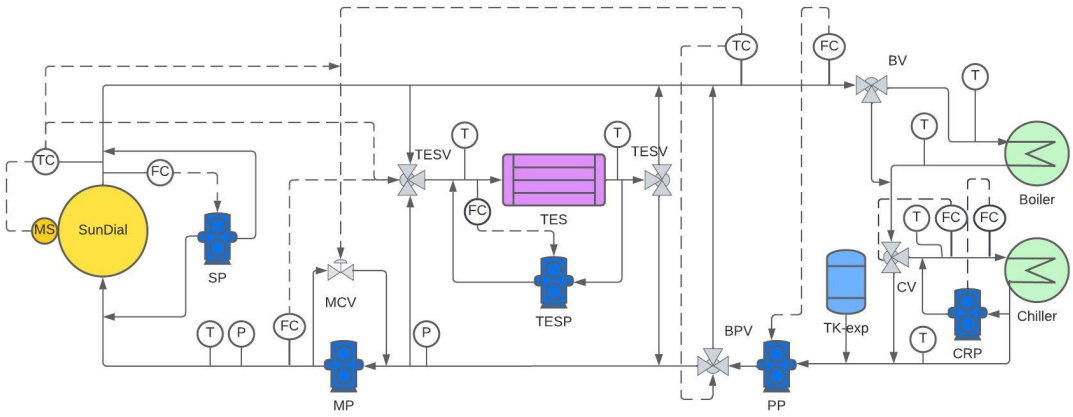

(a)

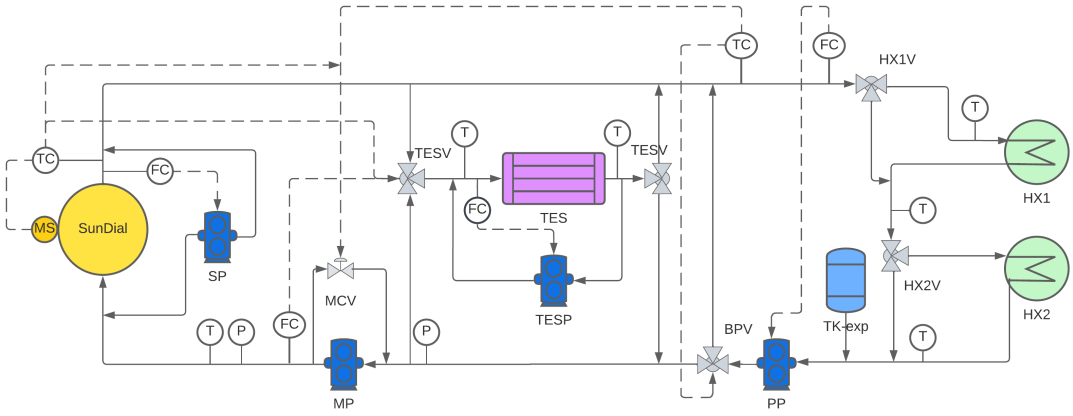

(b)

Figure 2.13: ASTEP diagram with the TES connected in parallel of the dairy factory (a) and of the tube steel factory (b).

Table 2.18: New actuator for the parallel configuration.

Name	Tag	Task
Main pump	MP	Keep a specific temperature in the SunDial outlet with MCV valve for low flows
Process pump	PP	Keep a constant flow at through the boiler HX
TES recirculation pump	TESP	Drive a constant flow through the TES
Main control valve	MCV	Keep a specific temperature in the SunDial outlet with MP at low flows
TES valves	TESV	Drive TES mode into charge or discharge
Chiller control valve	CV	Keep a specific temperature in the HX chiller inlet

- **Mode 1 - Preheating (M1)**: When irradiance reaches the minimum value to overcome the heat losses, the SunDial will re-circulate to preheat the HTF. This mode will end when the outlet temperature of the SunDial reaches the demand setpoint or is higher than the TES salt average temperature.
- **Mode 2 - SunDial and TES Charging(M2):** the SunDial outlet temperature is controlled to 3 °C over the TES average salt temperature. This PI control activates the main control valve (MCV), which recirculates part of the main pump flow (MP), reducing the flow sent to the SunDial. However, the MP is fixed to 0.5 kg/s, so when the radiation is high the MCV valve will be closed, the flow to the SunDial will be 0.5 kg/s and the outlet temperature of the SunDial will be above the set point.
- **Mode 3- SunDial and TES Charging and Process (M3)**: the HX1 or the boiler inlet temperature is controlled by the three-way bypass valve (BPV). This valve reduces the outlet temperature of the SunDial by mixing it with the cold stream from the outlet. Then, the SunDial outlet temperature is controlled with the main control valve (MCV) to 3 °C over the TES salt average or to the process setpoint when the TES average temperature is lower than the process temperature.
- **Mode 4- SunDial and TES Discharging and Process (M4):** the HX1 or the boiler inlet temperature is controlled with the main control valve (MCV). This controller splits the flow between the TES and the SunDial to achieve the temperature setpoint.
- **Mode 5- TES discharging and process(M5):** the boiler inlet temperature is controlled with the bypass valve (BPV).
- **Mode 6 - SunDial and Process (M6):** If the TES is full, the SunDial will partially defocus to feed the exact amount of power that the process demand requires. The outlet temperature of the SunDial will be limited to 240 °C. This implies that the maximum temperature of the TES will be also 240 °C.

The flow fed to the SunDial previous to the SunDial recirculation is variable and will be adjusted by a valve (MCV) that recirculates the flow from the outlet to the inlet of the main pump (MP). The flow variation is overseen by a PI controller whose objective is to achieve a temperature setpoint at the outlet of the SunDial equal to 3 °C above the TES salt average when this temperature is above the demand setpoint or equal to the demand setpoint when it is below. However, the MP flow is fixed to 0.5 kg/s so the flow rate fed to the SunDial is limited to a maximum of 0.5 kg/s. When this limit is achieved the SunDial temperature is not controlled to a specific value but will always be above the average temperature of the salts in the TES and the demand setpoint. The SunDial will be shutdown when the minimum hit power is reached or the flow direct to the SunDial is zero.

The TES mode will depend on the conditions in the SunDial: the inlet flow and the outlet temperature. Therefore, if the flow directed to the SunDial is higher than the process flow (0.23 kg/s) and the outlet temperature of the SunDial is higher or equal to the TES average salt the TES mode will be set to charge. In contrast, if the SunDial inlet flow (before the SunDial recirculation) decreases below the process flow, the system will be in discharge mode. A third option can occur when the sundial flow is higher than the process flow but

the temperature is lower than the salt's average temperature, in this case, the TES will be discharged because the exceeding flow will be sent to the TES, but the positions of the valves will be on the charge mode. In this configuration, we need to relate the process operation to the average salt temperature instead of the outlet temperature of the HTF stream exiting the TES, because there is no flow always going through the TES. Then, if either the Sundial or the TES salts' average temperature is higher than the setpoint, the process will be connected. And for the shutdown, both temperatures must be lower than the setpoint. To avoid chattering in the boiler, a temperature of 10 °C is implemented (5 degrees higher than in the series layout). Table 2.19 and 2.21 show the start-up and shutdown conditions of the demand and the SunDial, and the selection of the TES mode (charge or discharge) for each factory.

Table 2.19: Start-up and Shutdown conditions for the parallel layout of the dairy factory .

Mode	Start-up	Shutdown
Sundial	($T_{out,Sun} > T_{TES\_avg} + 7$ or $T_{out,Sun} > 210$ °C) and $DNI > DNI_{min}$	$DNI < DNI_{min}$ or $\dot{m}_{Sun} < 0.02$ kg/s
Boiler	factory open and $T_{out,Sun} > 215$ °C or $T_{TES,avg} > 215$ °C	factory closed or $T_{out,Sun} < 205$ °C and $T_{TES,avg} < 205$ °C
Chiller	when factory closed $T_{out,Sun} > 195$ °C or $T_{TES,avg} > 195$ °C when factory open $T_{out,Sun} > 215$ °C or $T_{TES,avg} > 215$ °C	when factory closed $T_{out,Sun} < 190$ °C and $T_{TES,avg} < 190$ °C when factory open $T_{out,Sun} < 210$ °C and $T_{TES,avg} < 210$ °C
TES	Charge	Discharge
	($\dot{m}_{MP} > 0.23$ kg/s and $T_{out,sun} > T_{setpoint}$)	$\dot{m}_{MP} < 0.225$ kg/s or ($\dot{m}_{MP} > 0.23$ kg/s and $T_{out,sun} < T_{setpoint}$)

Table 2.21: Start-up and Shutdown conditions for the parallel layout of the tube steel factory

Mode	Start-up	Shutdown
Sundial	($T_{out,Sun} > T_{TES\_avg} + 7$ or $T_{out,Sun} > 195$ °C) and $DNI > DNI_{min}$	$DNI < DNI_{min}$ or $\dot{m}_{Sun} < 0.02$ kg/s
HX1	$T_{out,Sun} > 210$ °C or $T_{TES,avg} > 210$ °C	$T_{out,Sun} < 205$ °C and $T_{TES,avg} < 205$ °C
HX2	$T_{out,Sun} > 225$ °C or $T_{TES,avg} > 225$ °C	$T_{out,Sun} < 220$ °C and $T_{TES,avg} < 220$ °C
TES	Charge	Discharge
	($\dot{m}_{MP} > 0.23$ kg/s and $T_{out,sun} > T_{setpoint}$)	$\dot{m}_{MP} < 0.225$ kg/s or ($\dot{m}_{MP} > 0.23$ kg/s and $T_{out,sun} < T_{setpoint}$)

Control strategy for the parallel configuration

The main diagram flow for the parallel configuration is depicted in Figure 2.14 and is practically the same as the series layout. The main differences are in the start-up and the demand operation which are detailed next. The shutdown flow which is shown in Figure 2.17 is identically but with the addition of the TES pump shutdown.

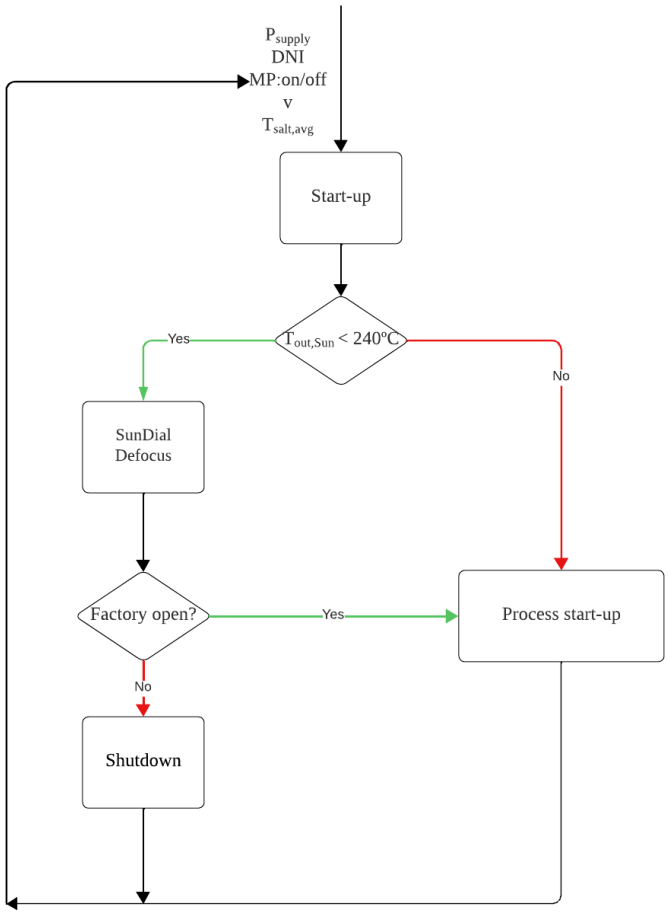

Figure 2.14: General flow diagram parallel configuration.

In the start-up diagram depicted in Figure 2.15, the first difference is noticed in the TES start-up. In this configuration, the TES can be in three different states: charge, discharge, or off. If the SunDial is off and the TES average salt temperature is lower than the process setpoint the TES will be off. Then, if the flow directed to the SunDial is lower than the demand flow of the outlet temperature of the SunDial is lower than the salts, the TES will be on discharge mode. Otherwise, it would be in charge mode. Differences can be also found in the SunDial start-up. Here, the flow sent to SunDial is checked and if it is zero the SunDial is shutdown, this means the SunDial minimum DNI is achieved.

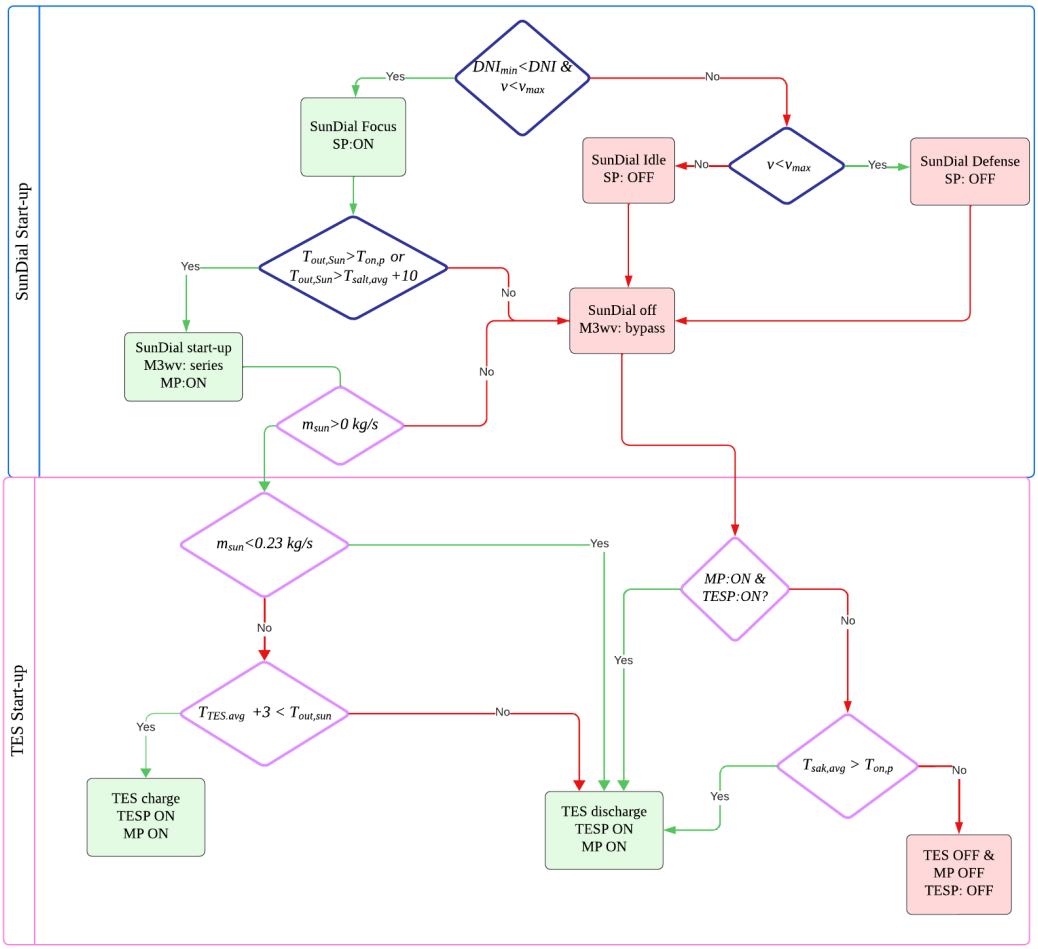

Figure 2.15: Start-up flow diagram for the parallel configuration.

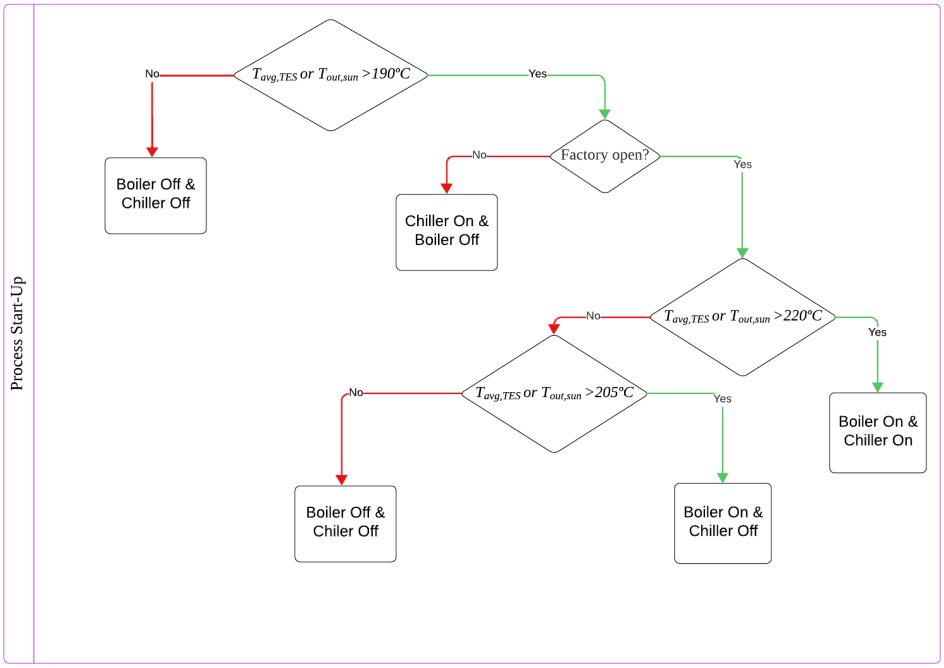

(a)

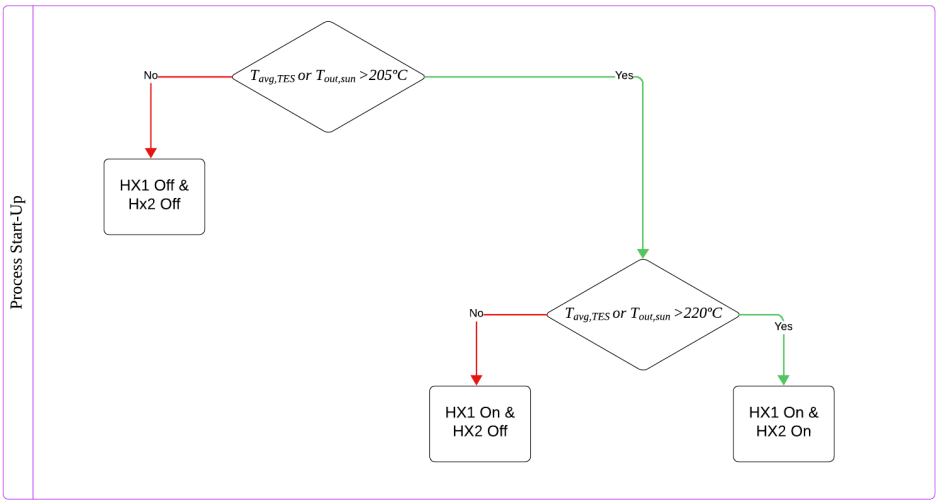

(b)

Figure 2.16: Process flow diagram for the dairy factory (a) and of the tube steel factory (b).

Finally the demand operation strategy is depicted in Figure 2.16 . In this case, the connection with the HXs is dependent on the TES average salt temperature and the SunDial outlet temperature instead of the TES outlet temperature. Like in the series layout, it can be seen that the operation of the dairy factory is more complex than the steel factory due to the priority to operate the boiler over the chiller in scenarios where the energy production of the SunDial is not enough for both. For example, if the factory is open and the temperature is

lower than 205 °C, the chiller and the boiler will be turned off. Therefore, the system will be preheating until the temperature of the boiler is achieved, and no energy will be produced at lower temperatures while the factory is open and the irradiation is low.

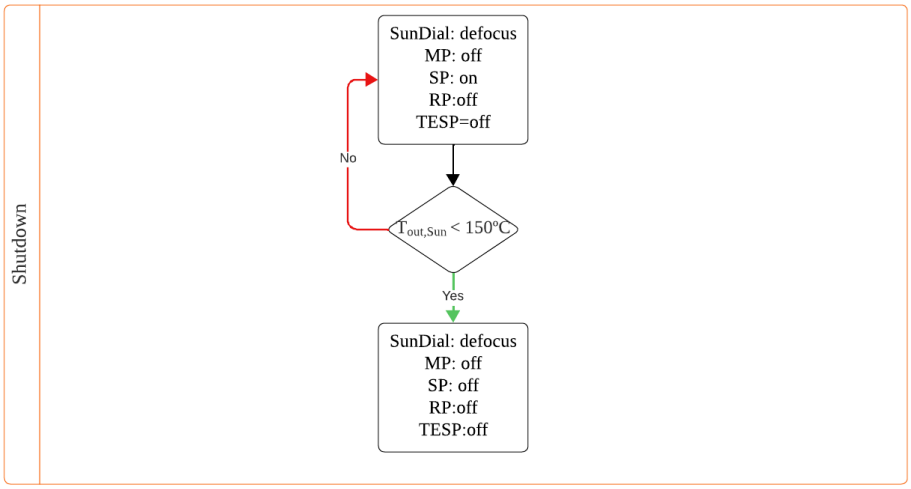

Figure 2.17: Shutdown flow diagram parallel configuration.

2.3 Findings

This chapter has outlined the configuration of the ASTEP concept. To derive this configuration, an initial exploration of the literature was conducted in Section 1.1.4, revealing the absence of a standardized arrangement for process heat plants. Instead, the optimal configuration is found for each particular application and depends on various factors, including the nature of the process, available space, integration point, TES, and accessible DNI.

Two possible system configurations were designed to allow flexible heat integration into the industry. This means the heat can be supplied at different temperature levels, increasing the system's efficiency. Furthermore, a comprehensive control strategy was developed to meet the requirements of both factories. A standard PID control scheme was selected due to the relatively low complexity of the system and the absence of experimental data available for the SunDial and the TES, which prevented the implementation of more advanced control methods. However, the resultant automated system eliminates the necessity for operator intervention and promotes more efficient system utilization. This enhanced efficiency contributes to lower maintenance requirements.

The selection of the final configuration solution will be grounded in the primary objectives of cost-effectiveness, user-friendly operation, minimal maintenance, and energy supply to the demand. Therefore, in the next chapters, theoretical models will analyze the system's performance and cost. However, only taking into account the inherent characteristics of the system, the following advantages and disadvantages for the series and the parallel configuration

can be identified:

The series configuration's principal advantage is that no action of the control system is required to change between the TES modes of charge and discharge because the outlet stream of the SunDial always passes through the TES. This means that the operational modes that the control system manages are reduced by 3: SunDial on and process on (operational modes 3,4 and 6), SunDial on and process off (operational modes 1 and 2), and SunDial off and process on (operational mode 5). The different modes are selected by the three-way on/off bypass valves. The disadvantage of this configuration is that SunDial has to overcome the thermal inertia of the TES in all operating modes.

The parallel configuration's main advantage is that the SunDial is directly connected to the process, so the TES can be bypassed, this implies more flexibility to the system. The principal disadvantage of this configuration is that the charge or discharge modes are controlled by the three-way valves. Another limitation is that the system requires an additional pump to ensure constant flow through the TES. Furthermore, the control of the temperature of the demand is more complex because it depends on the operating mode.

The outcome of this evaluation indicated that a TES connection in series presents the simplest system configuration, attributed to its reduced component count and operational modes relative to the parallel configuration. This translates to lower costs, streamlined operations, and reduced maintenance demands. The next chapter will look into the creation of a dynamic model, intended to simulate both configurations for each factory to analyze in detail the modes of operation of the system and verify that the control strategy designed achieves the target of temperature and heat delivered to the industry.

Chapter 3

ASTEP Modelling

This chapter's main objective is to develop a model to investigate the performance of ASTEP system. There is a noticeable absence of simulation tools tailored for solar concentrated systems utilized in industrial processes [64]. These tools hold significant importance in feasibility studies and early design phases, facilitating the development of successful solutions aligned with industrial process requirements. Most of the available tools are for yield annual calculations for Power Concentrated Plants and are based on steady-state energy balances [28]. For example, the well-known tool developed for the National Renewable Energy Laboratory (NREL), called System Advisor Model (SAM)[58], is mostly applied to estimate the levelized cost of electricity or heat estimations.

In the case of ASTEP concept, a dynamic model was required to develop the system control strategy and to have preliminary results of the heat performance to verify the system fulfills its purpose. The main target of ASTEP was to supply low-cost heat over 190 °C. Automated control systems can oversee the solar plant's operations without human intervention, reducing the likelihood of human errors and enhancing overall system efficiency. Furthermore, dynamic modeling can simulate transient situations such as start-ups, shut-downs, and clouds that are a daily occurrence in solar heat plants and can affect the system's performance.

In section 3.1, the dynamic model for ASTEP system is presented. The model was developed using Modelica language and serves as a tool to analyze various dynamic scenarios that require careful consideration and to compare the two configurations in series or in parallel proposed in the Chapter 2.

In Section 3.2 , the dynamic model is used to carried out several investigations over the ASTEP system. First, the parallel and series configurations of the TES system can be compared in terms of solar fraction, energy supply to the process, and the quality of energy supply, taking into account the effectiveness of the control system. Then, the different operational modes that may arise within the system were thoroughly examined. Subsequently, the impact of cloudy days is assessed, which is one of the challenges to overcome with this technology.

After selecting the more convenient configuration, an analysis of the thermal inertia exhibited by the system's pipelines was done. The solar systems include large pipe networks used to interconnect the subsystems with the process. These large pipe networks imply thermal losses

and thermodynamic behaviors that are interesting to include especially in small-scale solar systems due to the significant impact on heat production. Not considering the thermal inertia could have significant impacts on the calculations of start-up and cold down of the systems. In solar heat plants, the start-ups occur daily so an inefficient start-up routine could reduce significantly the amount of yield energy [41]. Therefore, it is important to analyze in detail the dynamic effects of thermal inertia in start-ups in daily simulations.

Then, a particular concern about the defocus controller accuracy was analyzed due to the novel tracking system of the SunDial collector. The defocus controller is required to limit the maximum achieved temperature to avoid damage to the system. SunDial is the first Fresnel collector to apply an azimuthal tracking system, hence an evaluation of the sensitivity required by the tracking system was carried out.

In Section 3.3, the adjustments made to the dynamic model for carrying out annual simulations are outlined. A simplified model will be employed to evaluate the yearly performance of the ASTEP system efficiently, assessing whether it can generate the expected annual energy output. The findings on annual heat production will form a crucial part of conducting a techno-economic analysis in Chapter 5.

3.1 Detail dynamic model for ASTEP

The dynamic model of the ASTEP system was constructed using the Modelica language within the Dymola software [25]. As it was seen in Section 1.1.4 the most implemented software to carry out dynamic simulation of solar heat plants was TRNSYS. The reason of this may be due to its large standard library with pre-design components that can be used easily to model solar thermal systems. However, as ASTEP systems involve novel components that are not included in TRNSYS library, the Modelica language was chosen for its flexibility in creating new elements necessary for both the SunDial and the TES components. Modelica is an object-oriented and equation-based language, these characteristics simplify the construction of new models. Furthermore, Modelica is an open language that incorporates a standard library [40], encompassing most of the essential components needed for modeling hydraulic circuits, including pumps, valves, pipes, controllers, and more. The primary reason for selecting Dymola software over OMEdit (an open-source Modelica software) was its robust solver capable of handling non-linear and extensive systems of equations [24].

In Modelica, each component is represented as a class, housing all the equations and data specific to that component. This design allows for easy reuse of components in different systems. Systems are constructed by interconnecting these components, often referred to as 'blocks,' using connectors or 'lines.' These connectors facilitate the exchange of three types of variables between models, following the principles of energy conservation [83]:

- Across variables (or Potentials): These variables, such as pressure and temperature, are equalized at connection points.
- Through variables (or Flow): The sum of these variables, such as mass flow rates, totals zero at connection points.

- Stream variables: These variables are employed for the bi-directional flow of matter, involving convective transport of specific quantities like enthalpy or chemical composition [35]

Another reason for selecting Modelica was its alignment with previous studies on dynamic solar thermal systems, many of which employed the Dymola software. The outcomes of these studies have contributed to the creation of open-source libraries such as ThermoPower [19], ThermoSysPro [29], and ThermoCycle [63]. Although these libraries were originally designed to model solar thermal systems for power generation, they include elements relevant to modeling ASTEP that can serve as sources of inspiration.

In the next sections, a detailed explanation of how all of the components of the ASTEP were modeled is presented. For most of the components of the system, pre-existing models were implemented from the Modelica standard library or other open-source libraries. But for SunDial and TES, which are novel prototypes, in-house models were developed in Dymola.

3.1.1 Heat transfer fluid

Modelica's open library includes an interface to model heat transfer fluid (HTF). This package is called Medium, and it contains a template that can be used to add fluids that are not included in the library. The Medium package includes the fluid-state equations to compute the thermodynamic state (depending on different input variables such as pressure, temperature, density, or composition) and functions to compute other properties, for example, viscosity, specific thermal capacity, and thermal conductivity. This package was used to include the Therminol 59 and 55 [27] as a partial medium of Modelica. The properties were added by temperature-dependent polynomial equations obtained from the provider's experimental data. The polynomials are described in Appendix A.

3.1.2 SunDial Model

The SunDial is a small-scale rotary Fresnel collector with an area of 44 and 47.5 m^2, for the SunDial-HL and SunDial-LL respectively, occupying a land space of 12 meters in diameter. They boast a nominal power capacity between 20 and 25 kW and can achieve temperatures of up to 240 °C. The SunDial model is comprised of two primary components: the receiver and the mirrors. The modeling of the mirrors was performed externally through ray tracing and was not included in the scope of this study, as previously documented [5]. Consequently, the incident power on the receiver and meteorological data were utilized as inputs for the dynamic simulation.

It's worth noting that the SunDial-HL and SunDial-LL models share an identical receiver configuration. Both prototypes incorporate two evacuated single tubes connected in series, spanning a length of 8 meters and an external diameter of 70 mm. The differentiation between the two SunDial prototypes lies in the efficiency of concentrating the solar energy that is taken into account in the ray-tracing simulation that generates the input data used to drive

the model, as illustrated in Figure 3.1. This input data is incorporated into the model using a CombiTable1Ds from the standard Modelica library, referred to as the 'Weather table.' The external information encompasses ambient temperature, wind velocity, and incident power on the receiver, with a temporal resolution of 1 hour for a complete Typical Meteorological Year (TMY). The table interpolates values corresponding to the simulation time, which is selected by the non-linear integration algorithms (DASSL, Radau) that applied variable integrator steps. Then, the data extracted from the table for each time step within the simulation is connected to the SunDial model via a connector aptly named the 'Weather Bus'.

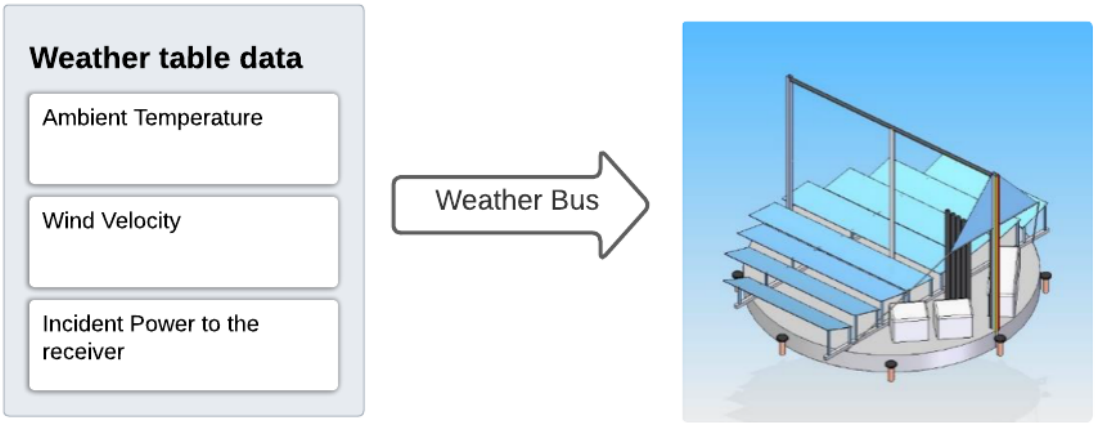

Figure 3.1: External input data to the model.

The receiver model is based on a methodology developed by Barbero et al. [10] that employs simplified analytical expressions dependent on physical parameters. To validate this model, experimental reports from Sandia National Laboratory were used and the coefficients were approximated from the experimental data. The model is suitable for calculating local efficiency and is divided into 66 segments with a maximum length of 0.25 m. However, it should be noted that one limitation of the thermal model is that the velocity of the fluid must exceed 0.58 m/s. Therefore, a simplification can be carried out by considering that the internal global coefficient (between the fluid and the external conditions) and the external (between the receiver surface and the external conditions of the receiver) are equal. In our Dymola model, this is not inconvenient because this condition is ensured by utilizing SunDial pump recirculation to maintain a constant flow velocity over 1 m/s. Another simplification in the model assumes convective heat transfer coefficients within the vacuum annulus are zero-valued.

Hence, the simulation of the absorber tube was conducted using a discretized Modelica dynamic pipe, which was divided into 33 nodes. This model represents a straight pipe with distributed mass, energy, and momentum balance for fluid flow in one dimension. To solve the partial differential equations, a finite-volume method and staggered grid scheme are applied to ensure accurate momentum balance. The length of each node in the absorber tube model is 0.25 m, except for the two ends which are 0.125 m long. Figure 3.2 provides a simplified representation of six nodes from the Dymola model used in this study. Each node within the absorber is connected through thermal ports that facilitate heat transfer

and temperature exchange between adjacent blocks. Additionally, a thermal conductance block links neighboring nodes together allowing efficient thermal communication throughout the system. To introduce incident power into the absorber nodes, we employed a Modelica block named "Prescribe Heat", which utilizes data from our Weather table as an input source. The heat transfer fluid boundary conditions are incorporated into the SunDial model via a fluid port. This connector facilitates the transfer of mass flow rate, pressure, and enthalpy between different models. The conduction and capacitance for the steel tube, as well as external convection in the outer layer of the glass tube, are modeled using Modelica blocks to represent respective heat transfer mechanisms.

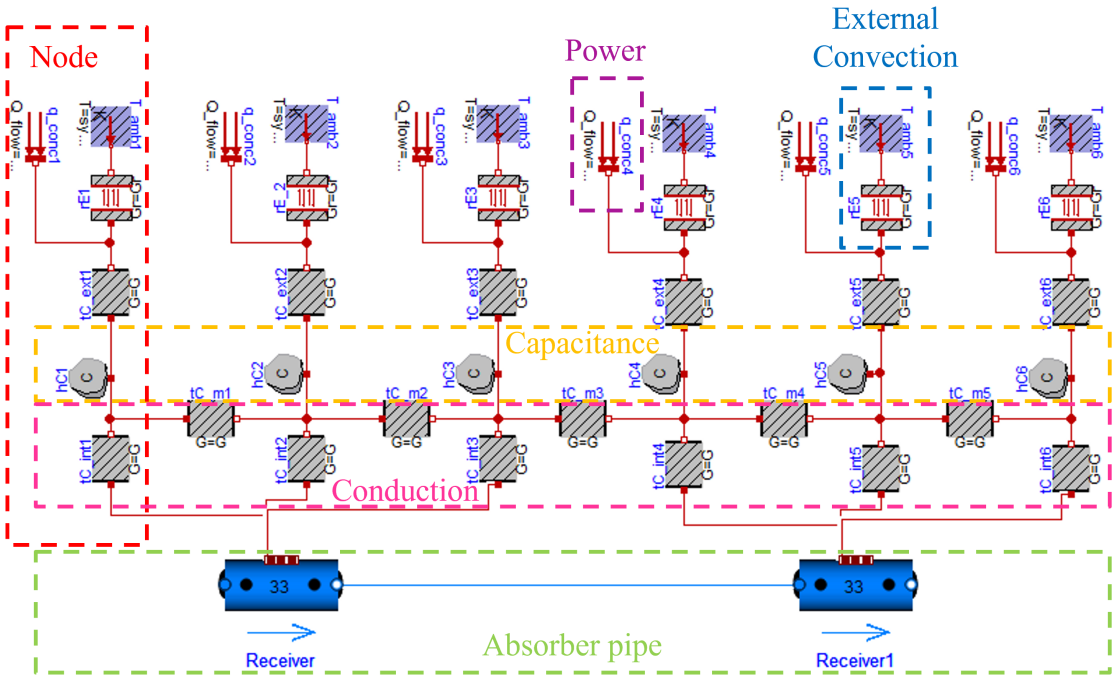

Figure 3.2: SunDial Dymola representation for 3 nodes for each receiver (the real model had 33 nodes).

The Modelica Dynamic pipe incorporates a heat transfer model to determine the heat transfer coefficient (h_i) between the bulk fluid and the segment boundary linked to the heat ports, specifically in this case, the absorber nodes. A suitable approach is applied by implementing equations from Barbero et al. [10], denoted as Equations 3.1 and 3.2, which represent an alternative Nusselt correlation formula within this model's framework.

$$\mathrm{Nu_n} = 0.0371 \cdot \mathrm{Re_n}^{0.8} \cdot \mathrm{Pr_n}^{0.33} \tag{3.1}$$

$$\mathrm{Nu_n} = \frac{h_{\mathrm{i,n}} \cdot D_\mathrm{i}}{k_\mathrm{n}} \tag{3.2}$$

Where the suffix n is the node number, Re is the Reynolds number, Pr is the Prandtl number, k is the thermal conductivity of the fluid and D_i is the internal diameter of the absorber.

The heat transfer caused by conduction through the metal absorber is simulated using a Modelica thermal conductivity block, which employs Equation 3.3. Each node of the absorber was divided into three distinct sections: the inner wall (G_{i}), outer wall (G_{o}), and interface between nodes (G_{m}).

$$\dot{q}_{\mathrm{k,n}} = G \cdot \Delta T_{\mathrm{n}} \tag{3.3}$$

Here ΔT is the temperature difference between the two faces: for the inner wall it is the fluid and the wall, for the outer wall it is the wall and the ambient temperature, and for the interface between nodes, it is the temperature of the adjacent nodes. The thermal conductance for the inner wall (G_{i}) was calculated with the Equations 3.4, 3.5 and 3.6:

$$G_{\mathrm{i}} = \frac{2 \cdot \pi \cdot k_{\mathrm{s}}}{\log\left(\frac{D_{\mathrm{m}}}{D_{\mathrm{i}}}\right)} \Delta x \tag{3.4}$$

$$G_{\mathrm{o}} = \frac{2 \cdot \pi \cdot k_{\mathrm{s}}}{\log\left(\frac{D_{\mathrm{o}}}{D_{\mathrm{m}}}\right)} \Delta x \tag{3.5}$$

$$G_{\mathrm{m}} = \frac{2 \cdot \pi \cdot k_{\mathrm{s}}}{\log\left(\frac{D_{\mathrm{o}}}{D_{\mathrm{i}}}\right)} \Delta x \tag{3.6}$$

$$\tag{3.7}$$

Where k_{s} is the thermal conductivity of the steel D_{m} is the mean diameter between the external and internal diameters and Δx is the length of the node. The values of the parameters of the absorber are illustrated in Table 3.1.

The heat stored in the wall due to the capacitance of the absorber (C) was modeled with a Modelica heat capacitance connected between the tube's inner and outer wall of each node using Equations 3.8 and 3.9, where T_{w} is the temperature in the absorber wall, c_{ps} is the specific heat of the steel, and ρ_s is the density of the steel.

$$\dot{q}_{cn} = C_n \cdot \frac{dT_{\mathrm{wn}}}{dt} \tag{3.8}$$

$$C = c_{\mathrm{p_s}} \cdot \pi \cdot \frac{(D_i^2 - D_e^2)}{4} \cdot \rho_s \cdot \Delta x \tag{3.9}$$

The radiative and external convective losses to the ambient are modeled using a Modelica body radiation approach, modified based on the model developed by Barbero et al. [10]. Equation 3.10 to Equation3.13 are used to calculate each node's radiative losses (q_{r}). The external heat transfer coefficient (Gr) is determined using a correlation that takes into account factors such as absorber temperature (T_{r}), wind velocity (v_{w}), and ambient temperature (T_{a}). Air properties are represented using the standard medium for air in Modelica.

$$q_{rn} = Gr_n \cdot \sigma \cdot \left(T_{wn}^4 - T_{\text{amb}}^4\right) \cdot \pi \cdot D_o \cdot \Delta x \tag{3.10}$$

$$Gr_n = 1.26 \cdot 10^{-4} \cdot (T_{wn} - 273.15) + 0.035, v < 0.5 \tag{3.11}$$

$$Gr_n = 0.000188 \cdot {Re_g}^{0.01428} \cdot (T_{wn} - 273.15) + \frac{1}{27.68 \cdot {\text{Re}_g}^{0.0302}}, v > 0.5 \tag{3.12}$$

$$Re_g = \frac{D_g \rho_a v}{\mu_a} \tag{3.13}$$

Where σ is the Stephan-Boltzmann constant equal to 5.67x10^{-8} W/m^2, D_{g} is the external diameter of the glass tube, Δx is the length of the node, ρ_a and μ_a are the density and dynamic viscosity of the air. The losses caused by shading of the receiver supports were considered constants and applied to node 16 of each receiver with a value of 124.6 W.

Table 3.1: Physical properties and dimensions of the absorber.

Parameter	Value	Unit
G_{i}	2394	W/K
G_{o}	2465	W/K
G_{m}	1214	W/K
C	440.8	J/K
D_{o}	0.07	m
D_{i}	0.066	m
D_{g}	0.115	m
f	0.978	-
η	0.9395	-

The heat transfer to the absorber is evaluated using the model developed by Barbero et al. in which the impinging power (q_{conc}) is multiplied by two factors. The impinging power values are provided externally through a table with corresponding values for each node, these values are calculated with the Monte Carlo ray tracing model and take into account the effective surface area of the receiver which considers end losses of the receiver tube [5]. The factor, η, depends on two coefficients: α_{r} (= 0.955) for heat absorbed in metal surfaces and α_{g} (= 0 .02) for heat absorbed in glass tubes. Lastly, parameter d represents the defocus fraction controlled by a proportional integrative controller (PI) and is limited between the values 0 and 1. The method to calculate d is explained in detail in the section 3.1.4.

$$q_{\text{abs}_n} = q_{\text{conc}_n} \cdot \eta \cdot d \tag{3.14}$$

$$\eta = \alpha_r \cdot (1 - \alpha_g) \tag{3.15}$$

3.1.3 Thermal Energy Storage Model

The Thermal Energy Storage (TES) system utilized a shell and tube heat exchanger design, consisting of 60 tubes connected in series with 'u' bends to create a spiral configuration. The fluid entered at the center of the spiral and exited at the external end of the tubes. These tubes were positioned within a tank containing a phase-change material (PCM). The heat transfer within the PCM was characterized by a model comprising seven distinct regions, each described by a set of differential equations. These equations were formulated based on the results obtained from a prior study involving computational fluid dynamics [2].

The TES model is subdivided into 60 nodes, corresponding to the number of tubes within the heat exchanger. For each node, an energy balance is computed, considering the heat transfer interactions between the heat transfer fluid and the salt, as outlined in Equations 3.16 and 3.17.

$$\dot{q}_n = U_n \cdot A_i \cdot (T_{f,n} - T_{p,n}) \tag{3.16}$$

$$U_n = \frac{1}{\frac{1}{h_{i,n}} + \frac{1}{h_{o,n}}} \tag{3.17}$$

Here, the suffix n is the node number, f is the HTF and p is the PCM; $\dot{q}$ is the heat flow between the HTF and the salt, **U** is the global heat transfer coefficient, A_i is the internal area of the tube, T_f is the HTF temperature and T_p is the PCM temperature.

The internal heat transference coefficient was calculated for each node with the equation of the Nusselt number presented in Equations 3.1 and 3.2. The energy balance between two adjacent nodes of the HTF can be expressed by Equation 3.18:

$$L \cdot \pi \cdot \frac{D_i^2}{4} \cdot \rho_{f,n} \cdot c_{pf,n} \cdot \frac{dT_{f\,n}}{dt} = \dot{m}_f \cdot c_{pf,n} \cdot (T_{f,\,n} - T_{f,n+1}) - \dot{q}_n \tag{3.18}$$

Here, L is the tube length and D_i is the internal diameter of the tube. The latent heat provided by the PCM is represented in Equation 3.19:

$$\dot{m}_p \cdot H_{fg} \cdot \frac{dx_n}{dt} = \left(1 - f_{q_n}\right) \cdot \dot{q}_n \tag{3.19}$$

Here, H_fg is the specific heat for the phase change, x is the liquid fraction, and f_q is the fraction of sensible heat. Lastly, the sensible heat transfer between the PCM nodes can be expressed by Equation 3.20:

$$\begin{aligned} &((1 - x_n) \cdot m_p \cdot c_{pps} + m_s \cdot c_{ps}) \cdot \frac{dT_{ps,n}}{dt} + m_p \cdot c_{pps} \cdot \frac{dx_n}{dt} \cdot (222 - T_{ps,n}) \\ &+ (x_n \cdot m_p \cdot c_{ppl} + m_s \cdot c_{ps}) \cdot \frac{dT_{pl,n}}{dt} + m_p \cdot c_{ppl} \cdot \frac{dx_n}{dt} \cdot (T_{pl,n} - 222) = f_{q,n} \cdot \dot{q}_n \end{aligned} \tag{3.20}$$

Where, m_{p} is the mass of PCM, c_{pps} and c_{ppl} is the specific heat capacity of the PCM in the solid and liquid state, m_{s} is the mass of steel of the tubes, and T_{ps} and T_{pl} are the temperatures of the PCM in the solid and liquid states. Equation 3.21 shows the relation between the PCM temperatures:

$$T_{p,n} = (1-x)\,.T_{ps,n} + x.T_{pl,n} \tag{3.21}$$

The external heat transfer coefficient and the fraction of sensible heat within the PCM are both influenced by various factors, including the temperature of the PCM, the fraction of liquid, and whether the TES system is in a charge or discharge mode. Consequently, to accurately characterize the behavior of the TES system, it was divided into seven distinct regions illustrated in Figure 3.3, each contingent upon these variables. This Figure shows the evolution of the salt temperature, the sensible heat fraction, the heat transfer coefficient, and the liquid fraction of one node through all the regions for a complete process of charge, from 190 °C to 240 °C, and discharge, from 240 °C to 190°C.

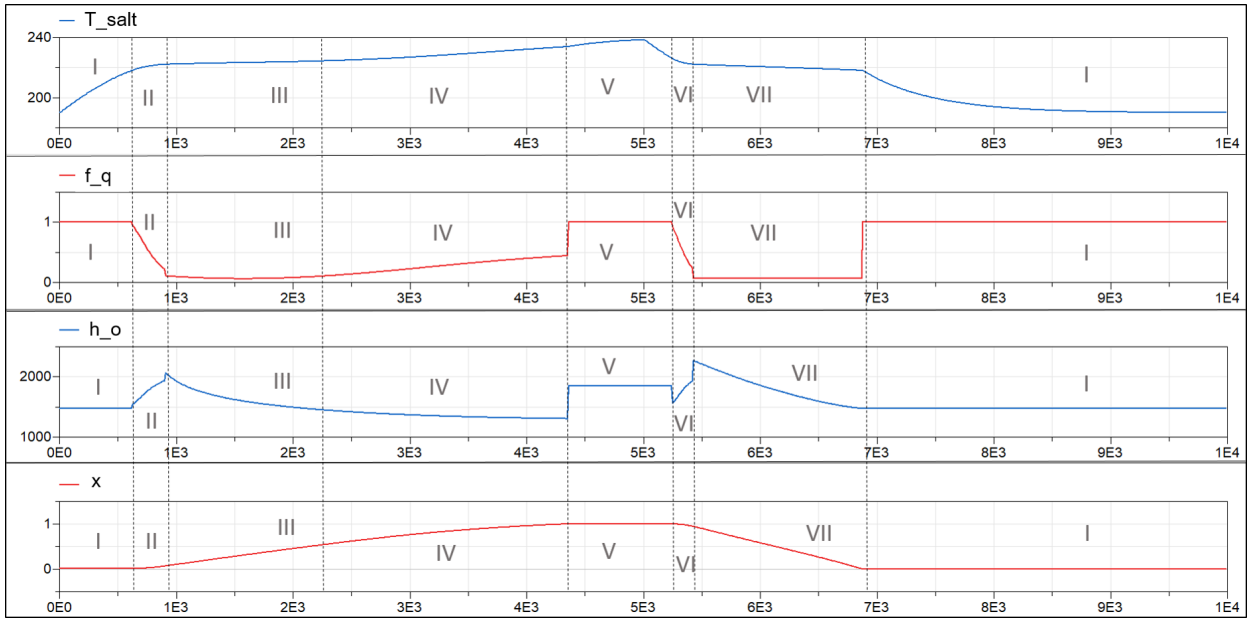

Figure 3.3: Evolution of the salt temperature, the fraction of sensible heat, the external heat transfer coefficient, and the liquid fraction of TES through the seven regions

The initial region assumes that the entire PCM is in a solid state, resulting in a constant value for the external heat transfer coefficient ($h_{\mathrm{o}} = 1475$ W/m^{2}K) and a fraction of sensible heat ($f_{\mathrm{q}} = 1$).

The second region commences when the mean temperature of the PCM reaches 218 °C, at this point the melting of the PCM initiates. Within this region, we apply Equations 3.22 and 3.23 to describe the behavior.

$$h_{o,n} = 1475 + 11.518 \cdot (222 - T_{p,n})^2 - 145.48 \cdot (222 - T_{p,n})^2 + 454.91 \tag{3.22}$$

$$f_{q_n} = \min(1, -0.0248 \cdot (222 - T_{p,n})^2 + 0.2802 \cdot (222 - T_{p,n}) + 0.0223) \tag{3.23}$$

The third region is marked by the melting process, which is described using Equations 3.24 and 3.25. In this region, the solid phase remains at the saturation temperature of 222 °C, while the liquid phase may experience superheating. This phase transition begins when the temperature of the PCM exceeds 222 °C, and the liquid fraction falls below 0.56.

$$h_{o,n} = 1302.64 \cdot (x_n)^{-0.17} \tag{3.24}$$

$$f_{q_n} = -0.7911 \cdot (x_n)^2 - 0.48268 \cdot x_n + 0.1337 \tag{3.25}$$

The fourth region is similar to the previous one; however, in this case, the predominant heat transfer mechanism shifts to convection. This region commences when the liquid fraction surpasses 0.56, and behavior for this phase is represented by Equations 3.26 and 3.27.

$$h_{o,n} = 1302.64 \cdot (x_n)^{-0.17} + 547.36 \cdot (x_n)^{6.424} \tag{3.26}$$

$$f_{q_n} = 4.1785e^{-6} \cdot {h_{o,n}}^2 - 1.16e^{-2} \cdot h_{o,n} + 8.1665 \tag{3.27}$$

The fifth region corresponds to the point at which the PCM has completely melted, with x=1, signifying that the fraction of sensible heat (f_{q}) equals 1. In this state, the heat transfer coefficient remains constant at h_{o} = 1850 W/m^2.K.

The sixth region marks the onset of the solidification process, with $x = 1$, but at a temperature lower than 226 °C. In this phase, the liquid fraction experiences superheating, while the solid phase remains at its saturation temperature. This region commences when the temperature exceeds 222 °C, and the equations governing this phase are represented by Equations 3.28 and 3.29.

$$h_{o,n} = 1475 + 11.518 \cdot (T_{p,n} - 222)^2 - 145.48. \, (T_{p,n} - 222)^2 + 454.91 \tag{3.28}$$

$$f_{q_n} = \min(1, -0.0248 \cdot (T_{p,n} - 222)^2 + 0.2802 \cdot (T_{p,n} - 222) + 0.0223) \tag{3.29}$$

In the final region, which is governed by Equations 3.30, 3.31, and 3.32, most of the PCM remains in the solid phase, but a portion is still in the liquid state. This phase begins when the temperature falls below 222 °C. In this region, the liquid fraction is at the saturation temperature, while the solid phase is subcooled.

$$h_{o,n} = 865 \cdot (x_n)^{1.5} + 1475 \tag{3.30}$$

$$f_{q_n} = -9.35 \cdot x_n + 1, x_n > 0.1 \tag{3.31}$$

$$f_{q_n} = 0.065, x_n < 0.1 \tag{3.32}$$

These equations were implemented in Dymola to create a new model. Within this model, the various regions are selected using conditional statements (if conditions), and the nodes are processed using a for-loop. To integrate this model with the simulation, a Modelica Partial Two Port is employed, similar to the approach used in the SunDial model. The properties utilized to characterize the PCM are detailed in Table 3.2.

Table 3.2: Properties of the PCM used in the TES.

Parameter	Value
Salt mass per tube [kg]	17.57
Liquid specific latent heat [J/kg.K]	1452
Solid specific latent heat [J/kg.K]	1400
Fusion heat [kJ/kg]	108
Salt density [kg/m^3]	1950

3.1.4 Controllers

The control system comprises actuators and sensors, Figure 3.4 shows a block diagram of a simple feedback controller based on Proportional, Integral, and Derivative (PID) control schemes. The sensors are used to measure the variable of interest (y) compared with the setpoint (y_{sp}) and send the difference, called error (e), to the controller. The controller sends a signal (u) to the actuator which can be a valve, a frequency driver, etc. For our control proposal, the derivative part is not required, so PI controllers are implemented. Equation 3.33 corresponds to a generic PI controller where K_c is the controller gain and T_c is the time constant.

$$u = K_c \cdot e(t) + \frac{K_c}{T_c} \cdot \int e(t) \cdot dt \tag{3.33}$$

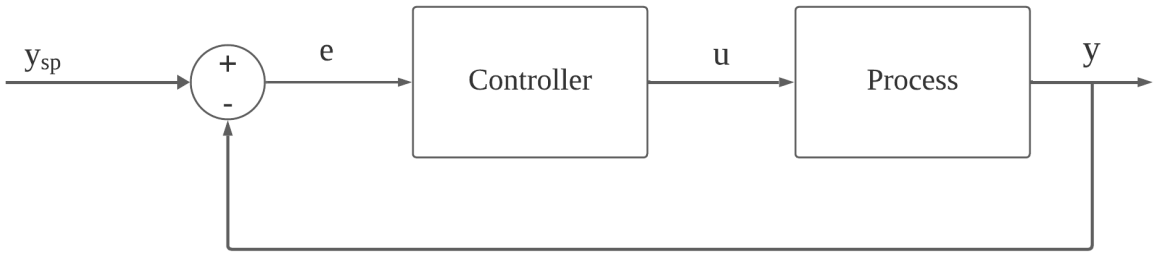

Figure 3.4: Block diagram of a simple feedback system

For temperature and flow control, Proportional-Integral controllers with bandwidth limitations were implemented to confine the manipulated variable within its operational range. Moreover, these controllers are equipped with an on/off switch that enables deactivation when control is not necessary.

For instance, in Figure 3.5 a diagram of the demand inlet temperature control is depicted. When the demand is not active, two switches (referred to as Sw1 and Sw2) deactivate this controller, causing both the pump and the controller to shut off. Disabling the Proportional-Integral (PI) controller ensures improved control by preventing the accumulation of errors in the PI signal. Additionally, the PI controller incorporates a bandwidth (BW) feature that restricts the pump flow to 0.23 kg/s, corresponding to the value of the demand mass flow.

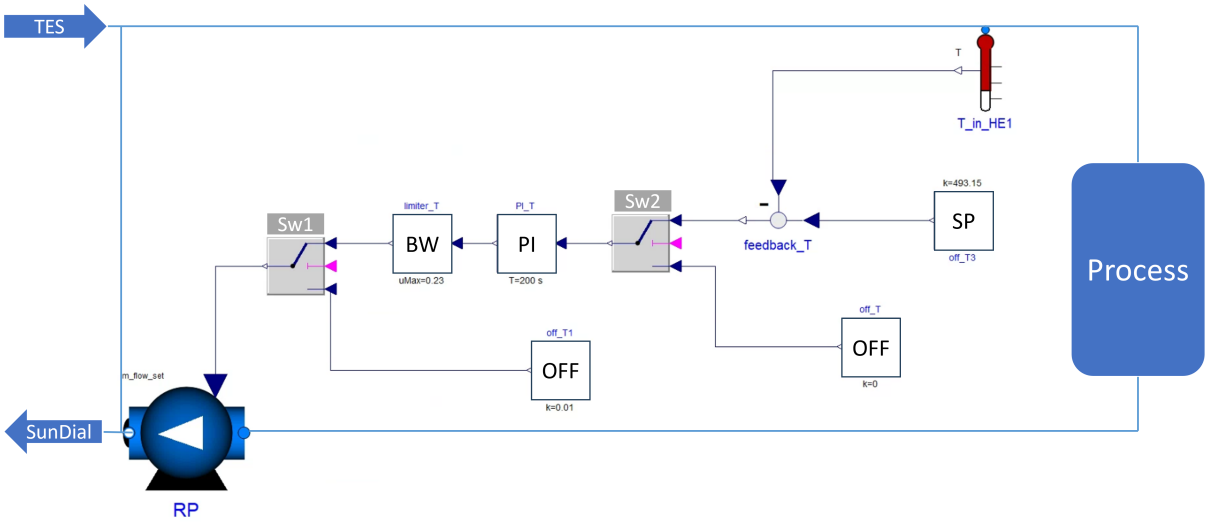

Figure 3.5: Demand inlet temperature controller diagram.

A similar approach is applied to the demand inlet mass flow controller, as is depicted in Figure 3.6. Switches Sw1 and Sw2 serve to deactivate the PI controller and close the valve when there is no demand. Subsequently, a bandwidth (BW) parameter is employed to confine the PI signal within the valve aperture range, which spans from 0 to 1.

Finally, the SunDial is equipped with a defocus PI controller, designed to prevent the maximum temperature of the system from being reached by adjusting the incident heat by defocusing the collector mirrors. Illustrated in Figure 3.7, this controller monitors the outlet temperature of the SunDial and compares it to a desired temperature set-point of 240 ^{o}C. The difference between these temperatures is computed and utilized as an input error for the PI controller. The output of this PI controller is equal to the defocus variable, called d, which multiplies the incidence power of the SunDial in Equation 3.14 from the SunDial model. The utilization of defocus control is restricted to instances of excess power compared to the demand requirements, which occur when the storage is full.

The controllers' constants were estimated with the Ziegler-Nichols method [9]. This method involves applying a step signal to the manipulated variable and observing its effect on the control variable. Figure 3.8 illustrates a step variation in the manipulated variable, such as the mass flow rate, and the corresponding response of the process control variable, e.i., the temperature.

The process response of this system is represented by a first-order system, which can be characterized by Equation 3.34. The parameters appearing in the first-order response are

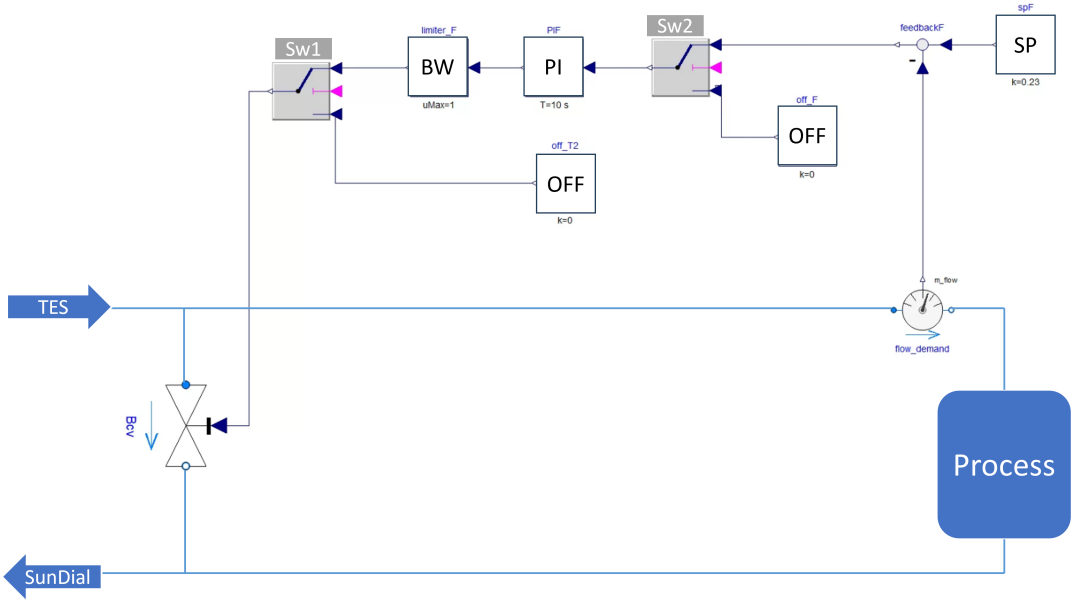

Figure 3.6: Demand inlet mass flow controller diagram.

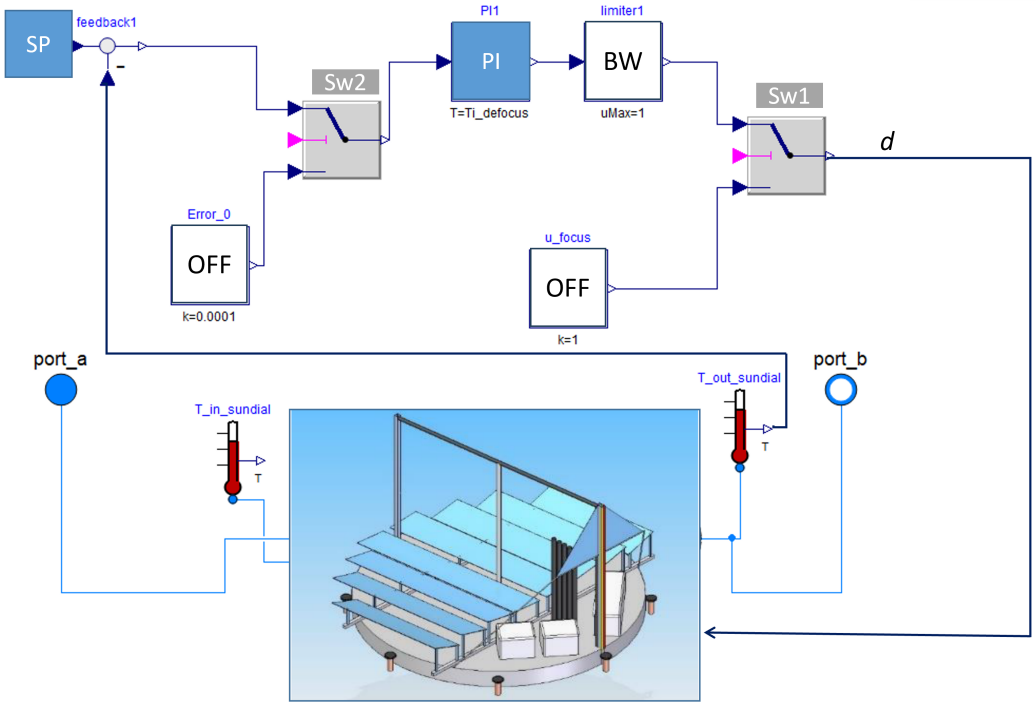

Figure 3.7: Demand inlet mass flow controller diagram.

termed the static gain (K_p), time constant (T_p), and delay (t_r), all of which can be determined from the curves depicted in Figure 3.8.

The time constant signifies the duration the process takes to reach 63% of the final value, which is the value obtained when the stationary state is attained. Meanwhile, the delay refers to the interval between the start of the step signal and the onset of the process response. In instances where the delay is zero, t_r can be approximated as the duration for the process to achieve 5% of the final value.

Lastly, the process gain is calculated utilizing Equation 3.35. It denotes the ratio between the variation of the process response from the initial value to when the steady state is once again reached and the variation of the step.

$$G(s) = \frac{K_p}{1 + T_p \cdot s} e^{-t_r \cdot s} \tag{3.34}$$

$$K_p = \frac{\Delta y_\mathrm{process}}{\Delta y_\mathrm{step}} \tag{3.35}$$

The controller constants can be calculated knowing the values of the process constants with the Ziegler-Nichols equations shown in Table 3.3. Then, with the calculated controller constants, the controller is applied in the dynamic simulation and is adjusted manually by increasing o reducing the constants' values, this process is called tunning. The tunning of the PID controllers is especially important to nonlinear systems such as solar plants [37]. A low gain can produce a slow response of the controller, but an aggressive controller can produce oscillations in the response.

Table 3.3: Controller constants calculated by Ziegler-Nichols

Controller	K_c	T_i	t_r
P	$\frac{\mathrm{T_p}}{\mathrm{K_p \cdot t_r}}$	-	-
PI	$\frac{0.9 \cdot \mathrm{T_p}}{\mathrm{K_p \cdot t_r}}$	$3t_\mathrm{r}$	
PID	$\frac{1.2 \cdot \mathrm{T_p}}{\mathrm{K_p \cdot t_r}}$	$2t_\mathrm{r}$	$0.5t_\mathrm{r}$

Table 3.4 provides the constants associated with the PI controllers, where K_c represents the proportional constant, T_c denotes the time constant, and u_min and u_max define the lower and upper limits accepted by the actuator. All these components have been modeled using the Modelica Standard Library.

3.1.5 Standard components of Modelica and other libraries

The remaining components of ASTEP are standard components commonly found in thermo-hydraulic systems. Therefore, we can leverage previously designed models available in the Modelica standard library or other specialized libraries for these components.

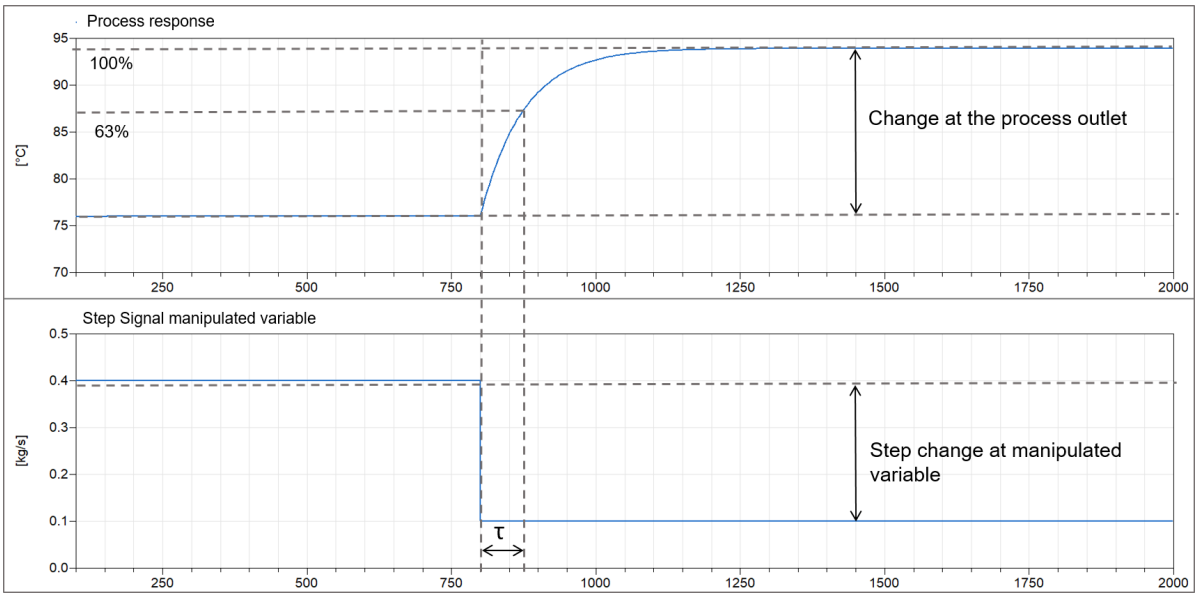

Figure 3.8: Step signal and process response.

Table 3.4: PI controllers constants.

Layout	Control variable	Actuator	K_c	T_c (s)	u_{min}	u_{max}
Series	Demand inlet temperature	RP	-0.1	200	0 [kg/s]	0.23[kg/s]
	Demand inlet flow rate	BPV	-78	3	0	1
	Defocus	SunDial platform	0.1	400	0	1
Parallel	SunDial outlet temperature	MP	-0.15	200	0 [kg/s]	0.54[kg/s]
	Demand inlet temp. charge	BPV	0.01	75	0	1
	Dem. inlet temp. discharge & SunDial	MP	-0.42	75	0 [kg/s]	0.23[kg/s]
	Demand inlet temp. discharge	BPV	-0.01	200	0	1
	Defocus	SunDial platform	0.1	400	0	1

Heat exchangers

The heat exchangers were modeled using the heat exchanger component from the Modelica Standard Library, which consists of two dynamic pipes connected by a wall, as illustrated in Figure 3.9. In Modelica, models are interconnected through ports that facilitate the transfer of variables between them. For instance, the ports between the pipe and the wall are responsible for linking temperature and heat flow variables. The flow direction within the heat exchanger followed a counterflow pattern. The heat transfer model assumes a constant heat transfer coefficient. The physical parameters employed for modeling the heat exchanger and the relevant data for the process streams are summarized in Table 3.6.

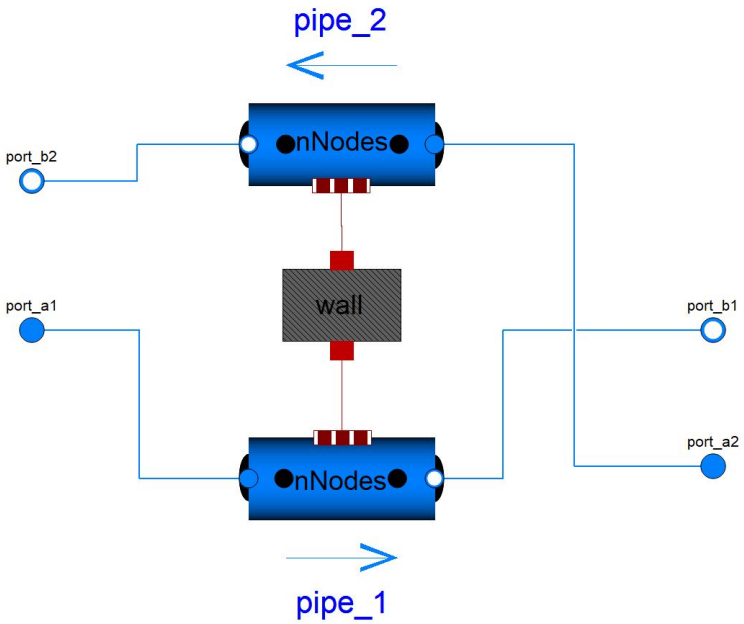

Figure 3.9: Screenshot of Modelica Standard Library Heat Exchanger.

Pumps, valves, sensors and expansion tank

Pumps, valves, and sensors are taken from the Modelica standard library. Table 3.7 shows the nominal parameters of these elements. The expansion tank is modeled with a closed volume from the Modelica Standard library and an expansion element from the Buildings open source library [56].

Pipelines

All the pipelines within the system have been represented as seven separate pipelines, labeled P1 to P7, as illustrated in Figure 3.10 [12]. These pipelines have been modeled using the Dynamic Pipe component from the Modelica Standard Library. The characteristics and parameters of these pipes are summarized in Table 3.9. With the exception of pipeline P1, all the pipelines have a nominal diameter of 20 mm and an insulation thickness of 102 mm. These specific parameters were chosen after analyzing the system's pressure and thermal losses to achieve a balanced compromise between them. Pipeline P1, on the other hand, has a larger nominal diameter of 40 mm and a thicker insulation layer measuring 127 mm. This

Table 3.6: Parameters used to model the heat exchangers.

Parameter	Value	Unit
Cross-sectional area HX1 & HX2	0.0005	m^2
Length HX1	2	m
Length HX2	7	m
Flow channel perimeter HX1 & HX2	0.08	m
Heat transfer area HX1	0.16	m^2
Heat transfer area HX2	0.56	m^2
Heat transfer coefficient HX1 & HX2	15699	$W/m^2.K$
Wall thickness HX1 & HX2	0.005	m
Wall thermal conductivity HX1 &HX2	43	W/m.K
Wall specific heat capacity HX1 &HX2	473	J/kg.K
Wall density HX1 &HX2	7.8	g/cm^3
Flow HX1	0.54	kg/s
Temperature HX1	195	°C
Flow HX2	0.54	Kg/s
Temperature HX2	182	°C

difference in parameters for P1 is attributed to its higher flow rate, which is associated with the SunDial receiver's requirements of a minimum velocity of 1 m/s.

The inertia of the seven pipelines depicted in the ASTEP process diagram (Figure 3.10) has been modeled using components from the Modelica library, as illustrated in Figure 3.11. This model takes into account various factors, including the conductance of steel and insulation (mineral wool), capacitance of steel and insulation, internal and external convection, and radiation to the environment. The temperatures across the radial pipe model can be seen in Figure 3.11 and Figure 3.12. The thermal properties and the external heat transfer coefficient (h_o) are considered constants and are listed in Table 3.9.

Figure 3.12 provides a cross-sectional view of the pipe, highlighting the principal dimensions detailed in Table 3.9. The Modelica local pipe calculates the internal heat transfer coefficient (h_i) using Nusselt correlations for laminar and turbulent single-phase flow with forced convection in pipes. The heat flux due to convection ($\dot{q}_i$) is computed using Equation 3.36 within the Modelica element. External convection is modeled using Modelica Convection, which employs Equation 3.37.

$$\dot{q}_{i,j} = h_{i,j} \cdot A_{i,j} \cdot (T_{f,j} - T_{w,j}) \tag{3.36}$$

$$\dot{q}_{o,j} = h_{o,j} \cdot A_{o,j} \cdot (T_{mw,j} - T_{amb,j}) \tag{3.37}$$

Here, the suffix j represents the number of the pipe, A_i represents the internal area of the pipe, T_f is the temperature of the fluid, and T_w is the temperature of the internal wall of the steel tube. A_o is the external area considering the insulation, T_{mw} is the temperature on

Table 3.7: Nominal Parameters for the Pumps and Valves. The nominal aperture for the valves is in parenthesis.

Layout	Element	Nominal mass flow rate [kg/s]	Nominal delta pressure [bar]
Series	Pump - MP	0.5	1.3
	Pump - RP	0.23	0.2
	Pump- CRP	0.59	0.2
	Pump-SP	4	0.1
	Valve- BPV (0.5)	0.5	0.15
	Valve-Cbpv (0.5)	0.19	0.1
Parallel	Pump - MP	0.5	1.3
	Pump - PP	0.23	0.4
	Pump- CRP	0.59	0.2
	Pump-SP	4	0.1
	Pump - TESP	0.5	0.4
	Valve- BPV (0.3)	0.13	0.2
	Valve- BPV1(0.5)	0.13	0.3
	Valve-Cbpv (0.5)	0.19	0.1

the exterior wall of the insulation, and T_{amb} is the ambient temperature. The environment temperature is set at 20 °C.

Where T_f is the temperature of the fluid, T_w is the temperature of the pipe, T_{mw} is the temperature of the insulation and T_{amb} is the ambient temperature

In Figure 3.12 r_i is the internal radius, r_o is the external radius of the pipe, r_{mw} is the external radius of the insulation, T_f is the temperature of the fluid, T_w is the temperature of the pipe, T_{mw} is the temperature of the insulation and T_{amb} is the ambient temperature.

The thermal inertia of the pipes was modeled with Modelica Heat Capacitor and calculated with the parameters in Table 3.9 and Equation 3.38 for the heat capacity of the steel tube and the insulation. The heat capacitor uses Equation 3.39 for the heat stored in the pipe ($\dot{q_c}$):

$$C_j = \left(\pi \cdot (r_{o,j}^2 - r_{i,j}^2) \cdot \rho_s \cdot Cp_s + \pi \cdot (r_{mw,j}^2 - r_{o,j}^2) \cdot \rho_{mw} \cdot Cp_{mw}\right) \cdot L_j \tag{3.38}$$

$$\dot{q_{c}}_j = C_j \frac{dT_{wj}}{dt} \tag{3.39}$$

Where C_j is the capacitance, r_i , r_o , and r_{mw} are the internal, external, and insulation radius, ρ_s and C_{ps} are the density and the specific heat capacity of the steel, ρ_{mw} and C_{pmw} are the density and the specific heat capacity of the mineral wool, L_i is the length of the pipe, T_w is the temperature of the pipe wall.

The Modelica Thermal Conductor is used to model the heat conduct through the pipe and

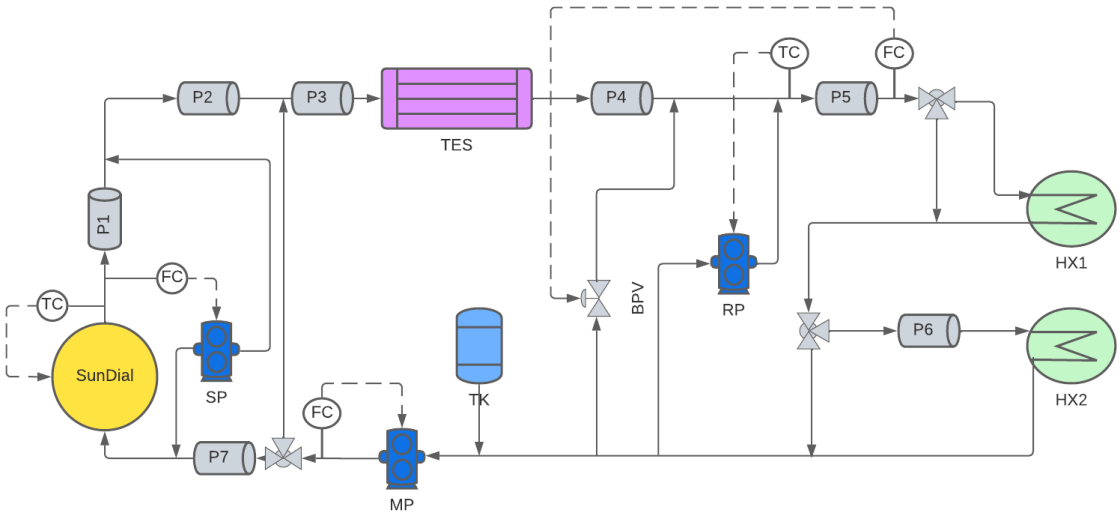

Figure 3.10: Process flow diagram for the ASTEP system P1 to P7 are the number of the pipelines 1 to 7.

the insulation. This model uses Equation 3.40 to calculate the heat flow ($\dot{q}_k$) through the steel or the insulation. G_s and G_{mw} (Equations 3.41 and 3.42) are the thermal conductance of steel and the insulation, which represents the inverse of the thermal resistance.

$$\dot{q}_{k,j} = G_j \cdot \Delta T_j \tag{3.40}$$

$$G_{s,j} = \left(\frac{2 \cdot \pi \cdot k_s}{\log\left(\frac{r_{o,j}}{r_{i.j}}\right)} \right) \cdot L_j \tag{3.41}$$

$$G_{mw,j} = \left(\frac{2 \cdot \pi \cdot k_{mw}}{\log\left(\frac{r_{mw,j}}{r_{o.j}}\right)} \right) \cdot L_j \tag{3.42}$$

Where k_{mw} and k_s are the thermal conductance of mineral wool and steel, and ΔT is the temperature difference between the two faces. For the steel pipe, it is the temperature difference of the fluid ($\mathrm{T_f}$) and the temperature of the steel tube (T_{w}); and for the insulation, it is the temperature difference between the steel tube ($\mathrm{T_w}$) and the external temperature of the insulation (T_{mw}). Finally, Modelica Body Radiation was used to consider the thermal losses due to radiation. This model calculates the heat flow to the ambient due to radiation ($\dot{q}_r$) with Equation 3.43, where Gr_i is the net radiation conductance (Equation 3.44). Where ε is the emissivity for the aluminum cover and σ is the Stephan-Boltzmann constant.

$$\dot{q}_{\mathrm{r_j}} = Gr_{\mathrm{j}} \cdot \sigma \cdot (T^4_{\mathrm{mwj}} - T^4_{\mathrm{amb}}) \tag{3.43}$$

$$Gr_{\mathrm{j}} = \pi \cdot 2 \cdot r_{\mathrm{mw_j}} \cdot \varepsilon \cdot L_{\mathrm{j}} \tag{3.44}$$

Table 3.9: Parameters used to model the pipelines [12]

Parameter	Value	Unit
L_1	16	m
L_2	16	m
L_3	5	m
L_4	6	m
L_5	6	m
L_6	6	m
L_7	21	m
$r_{\mathrm{i,DN20}}$	0.01032	m
$r_{\mathrm{o,DN20}}$	0.01335	m
$r_{\mathrm{mw,DN20}}$	0.06415	m
$r_{\mathrm{i,DN40}}$	0.02047	m
$r_{\mathrm{o,DN40}}$	0.02415	m
	0.08765	m
k_{s}	45.5	$\mathrm{W/m \cdot K}$
k_{mw}	0.042	$\mathrm{W/m \cdot K}$
C_{s}	536	$\mathrm{J/kg \cdot K}$
C_{mw}	920	$\mathrm{J/kg \cdot K}$
ρ_{s}	7700	$\mathrm{kg/m^3}$
ρ_{mw}	128	$\mathrm{kg/m^3}$
h_{o}	2.58	$\mathrm{W/m^2.K}$
ϵ_{a}	0.04	-

3.1.6 ASTEP System

As previously mentioned, the sub-models of the components can be interconnected using links to build a complete system. Additionally, the inclusion of a medium package is necessary, which encompasses the state equation and physical properties of the Heat Transfer Fluid (HTF). Furthermore, a system component is required to define the boundary conditions such as ambient conditions, flow direction, and initialization values.

Figure 3.13 and Figure 3.14, illustrates a screenshot of the Dymola diagram for both the dairy and tube steel factory configurations. In these diagrams, all the previously described models are interconnected in a series layout to represent the entire system.

The startup and shutdown procedures for the various sub-components (SunDial, Heat Exchangers, and Thermal Energy Storage) are executed by controlling the on/off valves positioned at their respective inlets, as well as the system's pumps. When a component is operational, its valve is open, allowing the Heat Transfer Fluid (HTF) to enter, while non-operational components have the HTF bypassed.

The pumps labeled SP and MP will operate at their nominal flow rates when they are activated. However, when they are turned off, a very small flow rate set at 0.001 kg/s will be

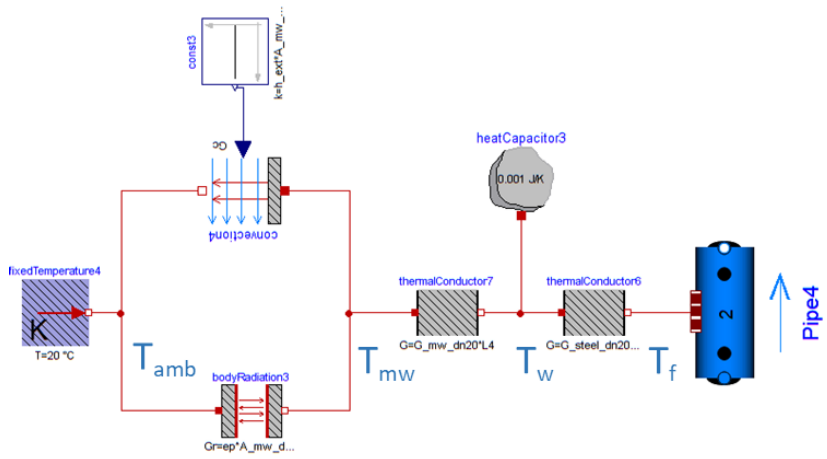

Figure 3.11: Diagram of pipelines inertia model in Dymola with profile temperatures identified .

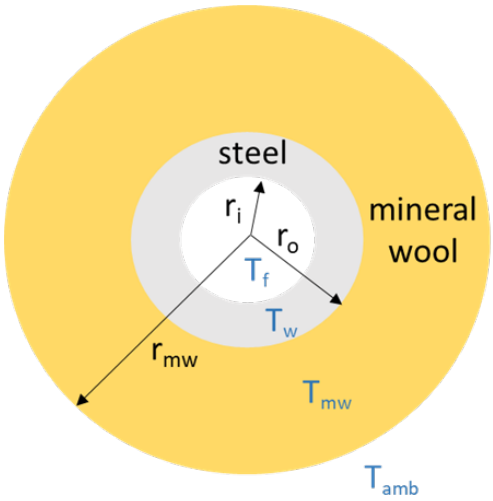

Figure 3.12: Pipelines cross-section.

set to maintain some circulation within the system because the pump model of the Modelica standard library requires a flow greater than zero. The recirculation pump (RP) flow is overseen by a dynamic controller to achieve the process inlet temperature setpoint.

The startup and shutdown conditions have been implemented in the algorithm section of the Modelica model using conditional statements (when conditions).

3.2 Dynamic analysis of ASTEP system

The main objective of developing a dynamic simulation is to analyze transient impact in the ASTEP system. This is important because transients occurs frequently in solar heat plants, like daily start-ups and clouds events. This intermittency of the solar source is one of the the

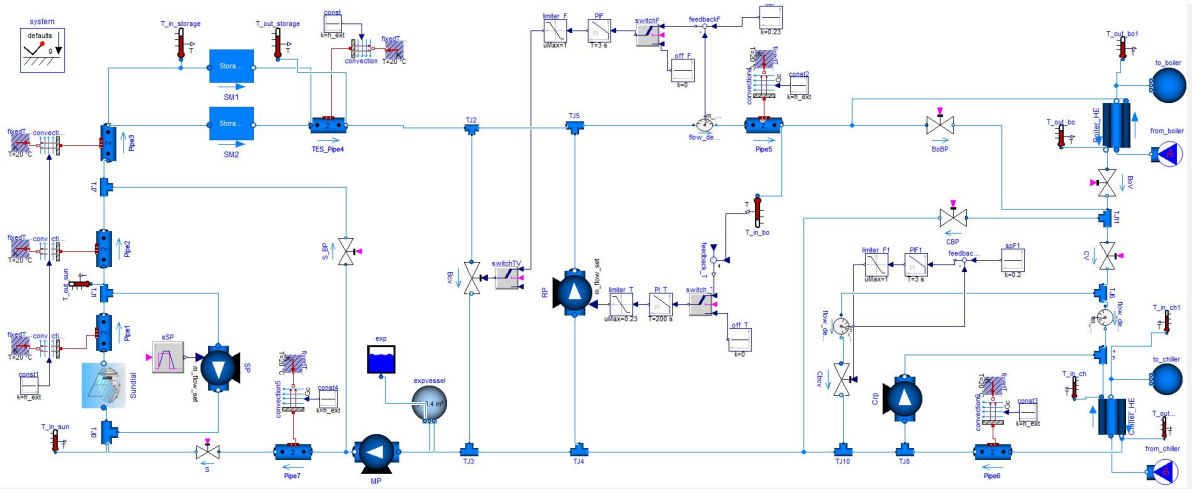

Figure 3.13: Screenshot of the Dymola diagram of the ASTEP system for the dairy factory.

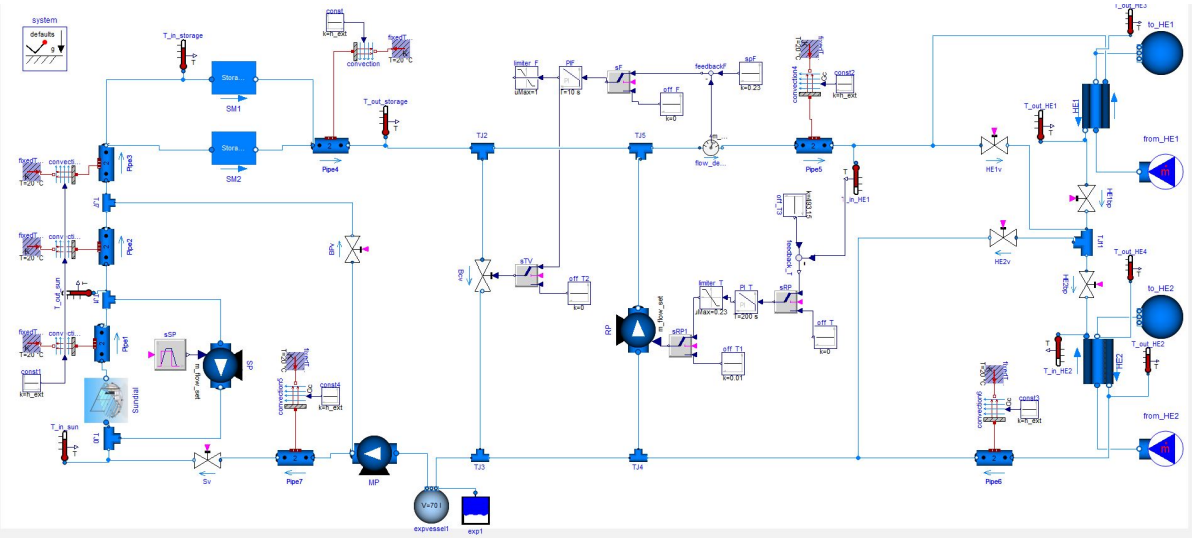

Figure 3.14: Screenshot of the Dymola diagram of the ASTEP system for the tube steel factory.

main barriers of implementing this technologies in the industry. ASTEP system wants to be a reliable solution to the process industry. This can be achieve thanks to the TES and the design of simply and robust control system. Therefore, the second objective of the dynamic simulation is to test the control strategy and the quality of the controllers.

Some of the challenges of ASTEP system is that the SunDial and the TES are newly prototypes so no experimental data is available on their performance. Furthermore, the small scale of the SunDial, 25 kW, and the large number of pipes to the interconnection with the industries could imply significant heat losses to the ambient. This implies, that the thermal inertia of the pipelines could have an impact on the ASTEP start-up and energy produced. Finally, the SunDial is the first rotatory Fresnell collector, so a new defocus startegy is designed by the rotation of the collector, and this controller is analyzed in detail to find the precision required for the SunDial prototype.

As previously mentioned, Dymola is a block diagram modeling software, which provides a convenient framework for creating various configurations of the ASTEP concept and assessing their performance. In this section, both the parallel and series configurations of the TES system are simulated and compared. The comparison will focus on key performance indicators such as energy supplied to the process, solar fraction, and the quality of the control system. Additionally, the analysis will involve studying the temperature time-profiles of the controlled variables, allowing for a comprehensive evaluation of these different TES configurations. This approach provides valuable insights into the system's efficiency and helps decide which configuration best suits the specific requirements and objectives of the application.

3.2.1 In parallel versus in series configuration for the TES

Two configurations were designed for ASTEP in Section 2.2 : Option 1 which connects the TES in parallel with the solar collector and the process, allowing the solar collector outlet stream to be directed to either the TES or the process. Option 2 connects the TES in series with the solar collector and the process, ensuring that the solar collector outlet stream always passes through the TES before reaching the process. In this section, we present a comprehensive comparison based on results obtained from dynamic simulations conducted over two consecutive days across three distinct seasons (summer, fall, and winter) for both the series and parallel configurations. It is important to note that, for the sake of simplicity, we have limited this comparison to the dairy factory, which represents the more intricate system owing to the inclusion of process heating and cooling components.

The dynamic simulation results are analyzed to determine the optimal configuration (whether it is connecting the TES in series or parallel) for the ASTEP system. Three different aspects will be evaluated to choose the optimum configuration: the energy supplied to the process, the simplicity of the system, and the quality of the control system. The system's control quality is assessed by analyzing simulation results to determine if the temperature and flow targets at the inlet of the process heat exchanger are met under different weather conditions. The amount of energy supplied to the process is calculated as the sum of transferred energy in both heat exchangers for each simulation. Additionally, the solar fraction is computed and compared. Finally, a thorough evaluation of system simplicity takes into account reduced component usage and fewer operational modes required while maintaining equivalent energy performance levels.

To reduce the computational time required for simulating two consecutive days, certain simplifications were implemented in the Dymola detailed model, which was previously outlined in Section 3.1. These simplifications included the elimination of the system's pipelines. Importantly, these simplifications were made with the understanding that their impact, or lack thereof, would be consistent across both configurations being compared. The pipe's inertia will be analyzed in detail for the selected configuration in Section 3.2.5.

Secondly, the model used to simulate the process HXs was simplified and replaced with a heat sink modeled by a dynamic pipe and a prescribed heat source from the Modelica standard library. The heat source is programmed to extract the power required by the process when

the conditions for the start-up are met. For example, the boiler will extract 8 kW when the temperature factory is opened, and the conditions are reached. The simulation with the heat exchanger will be carried out for the selected configuration. This simplification translates to the exclusion of HX inertia and the modeling of process fluids. Please note that the impact of these simplifications on both configurations will be consistent, ensuring a fair and meaningful comparison. Figures 3.15 and 3.16 present the Dymola models reflecting these simplifications.

To rapidly compare the effectiveness of the control system, the results of the two configurations are plotted in the same graph. Figure 3.17 shows the SunDial power and the power supplied to the boiler and the chiller, in a continuous line for the series configuration and in a dashed line for the parallel configuration. The power of the different components is calculated by Equation 3.45 where the subscript i can be changed for the name of the variable: SunDial, chiller, boiler. Then, Figure 3.18 shows the boiler and the chiller inlet and outlet temperatures for the two configurations.

$$P_{\mathrm{i}} = \dot{m}_{\mathrm{i}} \cdot c_{\mathrm{p}} \cdot (T_{\mathrm{out,i}} - T_{\mathrm{in,i}}) \tag{3.45}$$

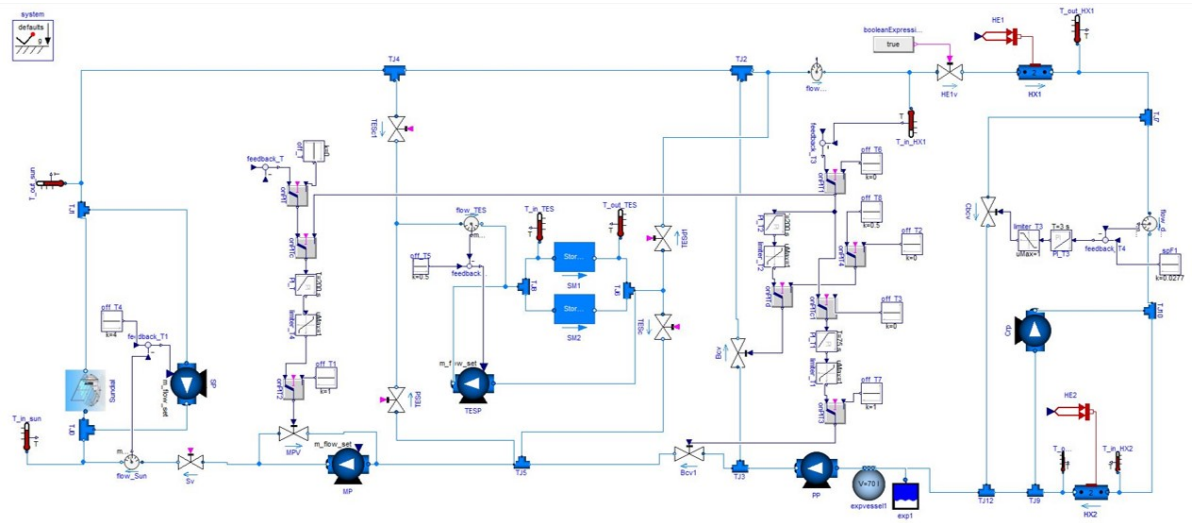

Figure 3.15: Screenshot of the Dymola diagram with the TES connected in parallel .

The results of power for both configurations are similar except for the start-up time for the chiller, which occurred one hour earlier in the parallel simulation. The reason for the delay in the series start-up is caused by the thermal inertia of the TES. In the case of the parallel configuration, the SunDial is directly connected to the process. But in the series, the SunDial needs to preheat the TES before it can supply heat to the process. In the temperature graph, it can be seen that although the inlet process temperature is controlled at the setpoints in both scenarios, a better result is achieved in the series layout. In the case of the parallel layout, we noticed a deviation of 5 °C of the temperature setpoint at the start-up and the shutdown. To numerically compare the precision of the controllers in each configuration, the mean absolute error (MAE) between the temperature setpoint and the demand inlet temperature was calculated and is shown in Table 3.10, and as it was predicted looking at the graph, the error is lower in the series configuration.

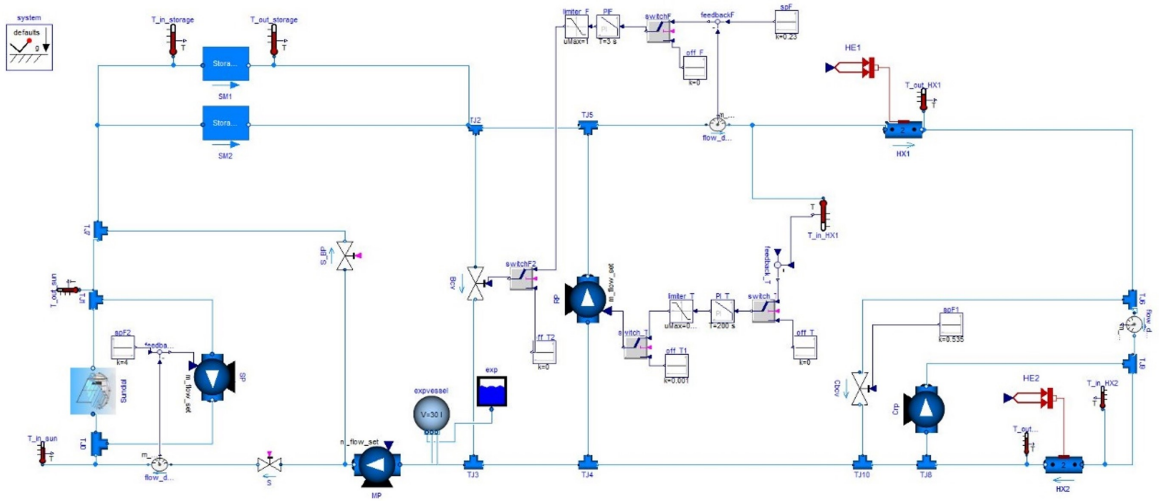

Figure 3.16: Screenshot of the Dymola diagram with the TES connected in series .

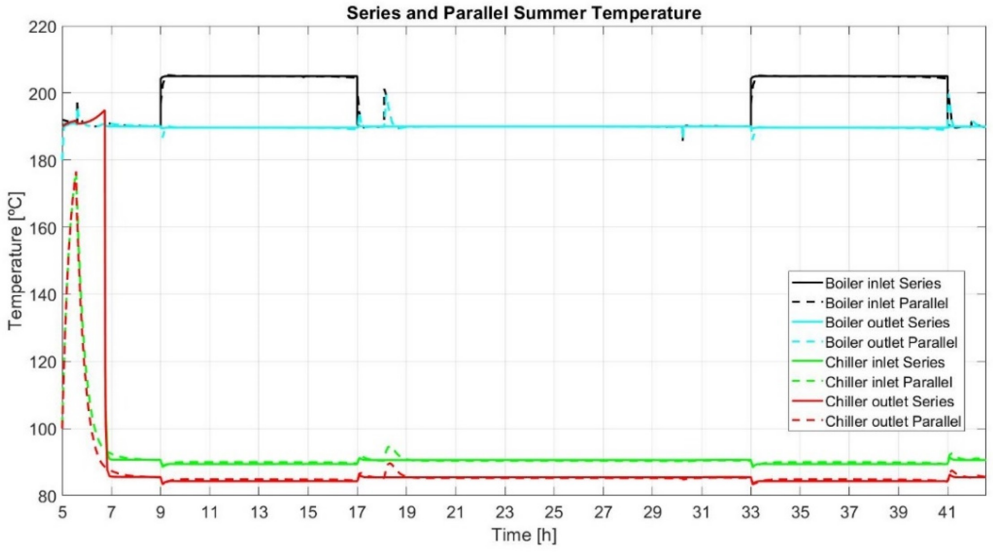

Figure 3.18: Temperature results for summer in series vs. parallel connection of the TES.

Table 3.10 also shows the energy at the end of the simulation, calculated by Equations 3.46 and 3.47 , and the final temperature for the average temperature of the TES salts. The energy produced by the SunDial is the same in both configurations. However, the energy sent to the process is 1.5 % higher in the parallel configuration. One of the causes may be related to the energy added to the systems by the enthalpy increased by the pumps. The parallel configuration consumes 31 % higher energy than the series configuration due to the larger number of pumps.

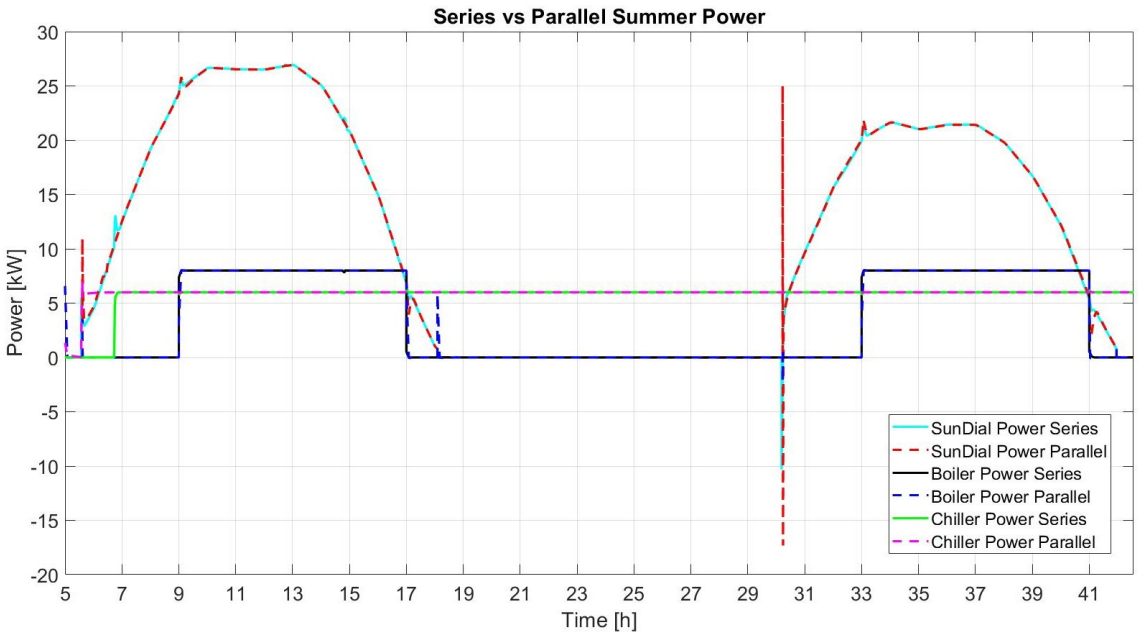

Figure 3.17: Power results for summer in series vs. parallel connection of the TES .

$$\frac{dE_{\text{sun}}}{dt} = P_{\text{sun}} \tag{3.46}$$

$$\frac{dE_{\text{hx}}}{dt} = P_{\text{hx1}} + P_{\text{hx2}} \tag{3.47}$$

Table 3.10: KPI for series and parallel configuration in summer

Parameter	TES in series	TES in parallel
SunDial Energy [kWh]	420.7	420.8
Process Energy [kWh]	342.9	348.2
Pumps Energy [kWh]	3.5	5.1
TES Energy [kWh]	80.0	74.6
MAE T_{sp}	0.129	0.515

Following the procedure employed for the summer scenario, the fall scenario was also simulated, and the results are depicted in Figures 3.19 and 3.20. It can be observed that the boiler operates between 10 and 16 hours in both configurations; however, the chiller starts earlier in the parallel layout. In the series configuration, the chiller starts operating before the factory opens on the second day, whereas it does not in the parallel layout. This discrepancy arises from the fact that in the parallel layout the condition for start-up depends on the SunDial outlet, while in the series configuration, it is related to the TES outlet, which exhibits lower temperatures due to the thermal inertia of the storage.

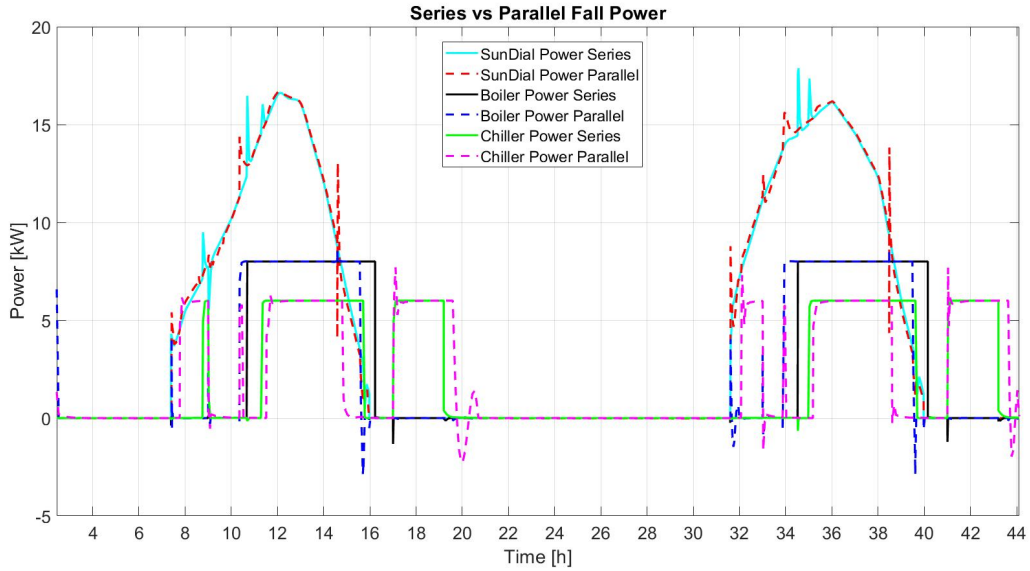

Figure 3.19: Power results for fall in series vs. parallel connection of the TES

Regarding the temperature profiles, it can be noticed that in the series configuration, the inlet temperatures of the boiler and the chiller are instantly conducted to the setpoint. However, in the parallel configuration, it is observed a transient in the chiller start-up. This may be explained by the control strategies implemented in each configuration: in the series layout, the TES outlet temperature is reduced with the cold stream of the recirculation pump (RP), while in the parallel layout, the SunDial outlet temperature is reduced with the cold stream of the bypass valve (BPV). Therefore, the dynamic behavior of the valve is different from the behavior of the pump, which has a fast response.

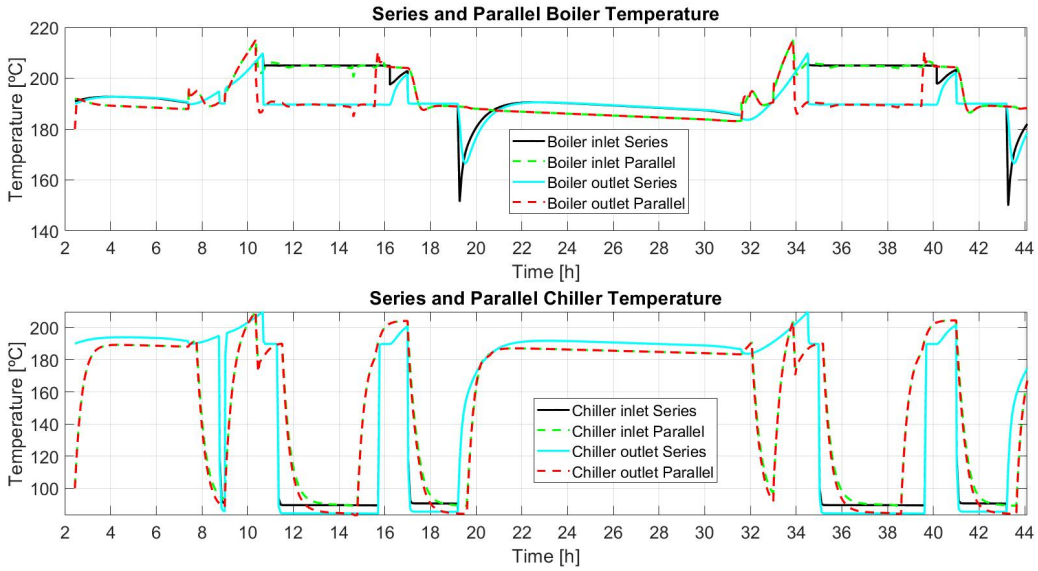

Figure 3.20: Temperature results for fall in series vs. parallel connection of the TES

Table 3.11 shows the kpis for the fall scenario. No signifucant difference in the energy production is observed in this case,less than 1% more energy is supplied by the parallel configuration. Neither in the temperature MAE with the setpoint, which is higher than in the summer simulations.

Table 3.11: KPI for series and parallel configuration in fall

Parameter	TES in series	TES in parallel
SunDial Energy [kWh]	185.2	185.4
Process Energy [kWh]	171.8	172.4
Pumps Energy [kWh]	2.3	3.5
TES Energy [kWh]	14.9	15.2
MAE T_{sp}	2.25	2.3821

Lastly, the results for the winter scenario are shown in Figures 3.21 and 3.22. On the first day, the series and the parallel configuration presented different results. In the parallel layout the boiler is operative for a longer time and the chiller a shorter in comparison with the series layout. In contrast, on the second day, both configurations present a similar behavior, only the chiller is operational after the factory is closed due to the setpoint condition to prioritize the boiler.

Regarding the temperatures graph, in the parallel graph, when the chiller starts for the first time, it can be seen that the time to control the chiller inlet temperature is slower than the operation time, and the chiller is shut down before the setpoint is achieved. In the series layout, the chiller start-up occurs later in the parallel layout due to the thermal inertia of the TES.

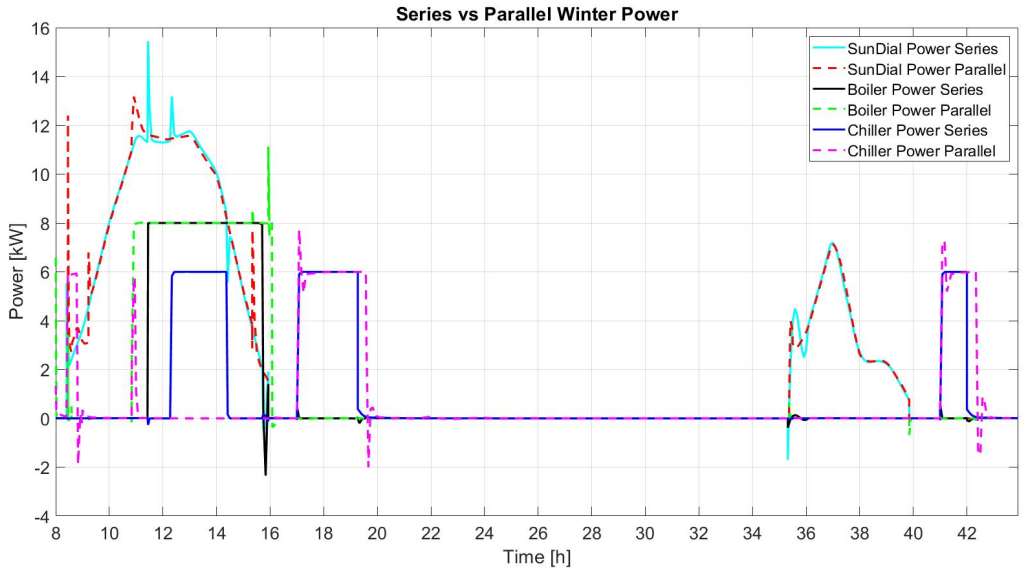

Figure 3.21: Power results for winter in series vs. parallel connection of the TES .

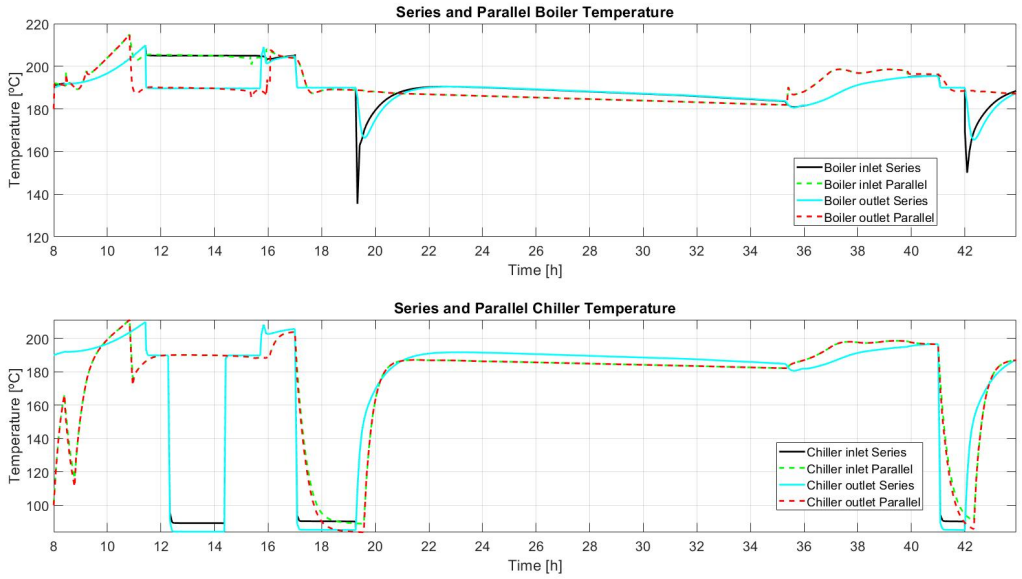

Figure 3.22: Temperature results for winter in series vs. parallel connection of the TES.

The energy difference between configurations is larger in this scenario, as is depicted in Table 3.12. Also, the MAE with the temperature setpoint is higher than the previous scenarios, being lower for the series. The energy supplied to the process is 3 % higher in the parallel configuration. However, the energy added by the pumps is 38 % higher in parallel layout. The difference in the SunDial total energy can be explained because of the variation of the SunDial thermal efficiency during the transient in the simulation. In Figure 3.23 the inlet and outlet temperature of the SunDial and the thermal efficiency are illustrated. The thermal efficiency was calculated as the ratio between the SunDial power and the concentrated power in the receiver. When the SunDial temperatures oscillate due to a transient caused by a start-up or shut down the efficiency of the SunDial also presents an oscillation. The thermal efficiency when the system operates in a steady state takes values between 0.7 and 0.88.

Table 3.12: KPI for series and parallel configuration in winter

Parameter	TES in series	TES in parallel
SunDial Energy [kWh]	77.9	78.7
Process Energy [kWh]	66.5	68.4
Pumps Energy [kWh]	2.1	3.4
TES Energy [kWh]	12.6	12.3
MAE T_{sp}	3.24	4.1579

Additionally, the solar fraction was calculated for each simulation dividing the current energy supplied to the process by the nominal demand energy. The nominal demand energy corresponds to 416 kWh and is calculated by Equation 3.48, where the boiler's nominal power is 8 kW and the total hours of operation are 16 hours; the chiller nominal power is 6 kW, and

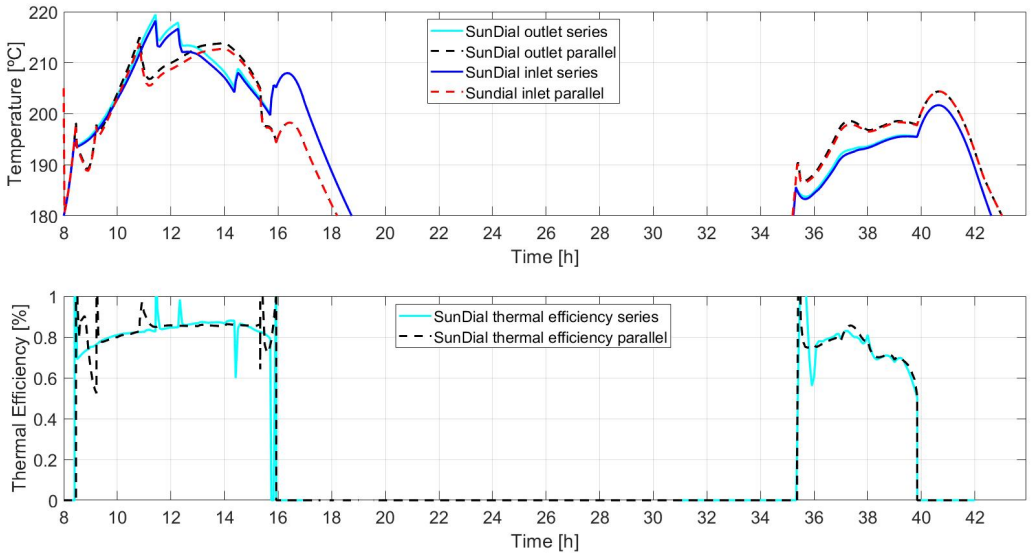

Figure 3.23: Thermal efficiency for winter in series vs. parallel connection of the TES.

the hours of operation are 42 hours. The results are presented in Table 3.13 and indicate that the performance of the two configurations is very similar.

$$E_{nom} = 8\text{kW} \cdot 16\text{h} + 6\text{kW} \cdot 42\text{h} = 416\text{kWh}. \tag{3.48}$$

Table 3.13: Solar fraction for the series and parallel configuration on different seasons.

Solar Fraction	TES in series	TES in parallel
Summer	0.824	0.837
Fall	0.413	0.414
Winter	0.160	0.165

Analysis of the effects of clouds.

One of the disadvantages of solar energy compared to conventional sources is its local intermittency due to factors such as cloud cover, which are difficult to prevent. To address this concern, we conducted tests to evaluate SunDial's response to different cloud patterns and ensure that the ASTEP control system consistently delivers heat to the industrial process.

To compare the two configurations under sudden changes in irradiance, a cloud scenario is simulated. The results of power and temperature for both configurations are depicted in Figures 3.24 and 3.25. When clouds appear, SunDial power becomes zero, but heat production can still be backed up by the TES (the TES power has been included in Figure 3.24). From the power graph, it can be observed that in parallel layout, the chiller operation starts one

hour earlier. However, a small deviation is noticed in boiler power during cloudy periods despite having sufficient charge in TES to meet demand.

Regarding the results of the temperature control, in the series configuration, the inlet temperature of the boiler remains constant thanks to the stabilized effect of the series connection of the TES. But in the parallel configuration, the demand inlet temperature presents a deviation from the setpoint between 1 and 5 °C when the clouds appear. This deviation is a consequence of the direct connection of the SunDial with the demand. The MAE with the setpoint for this scenario is 0.38 for the series and 1.72 for the parallel.

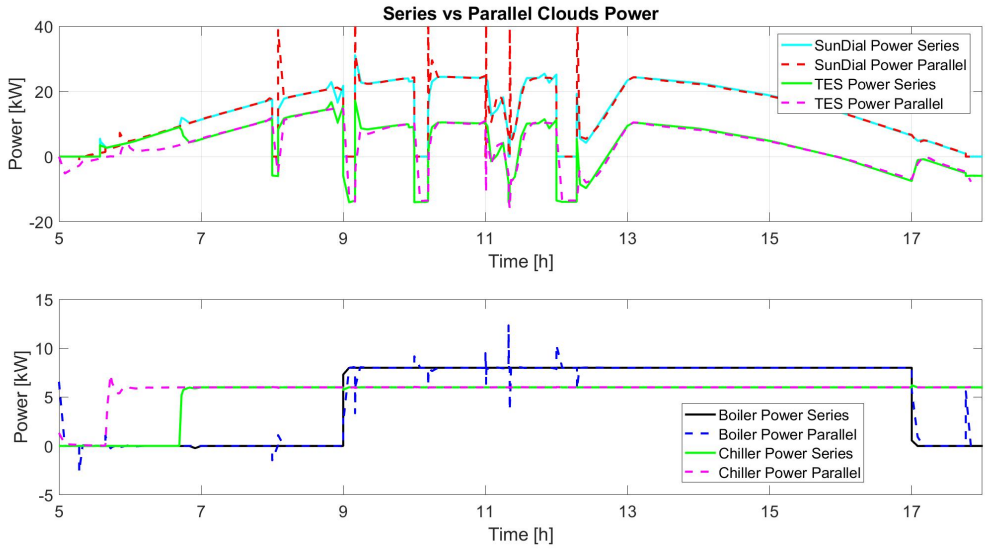

Figure 3.24: Power results for a day with clouds in series versus parallel connection of the TES.

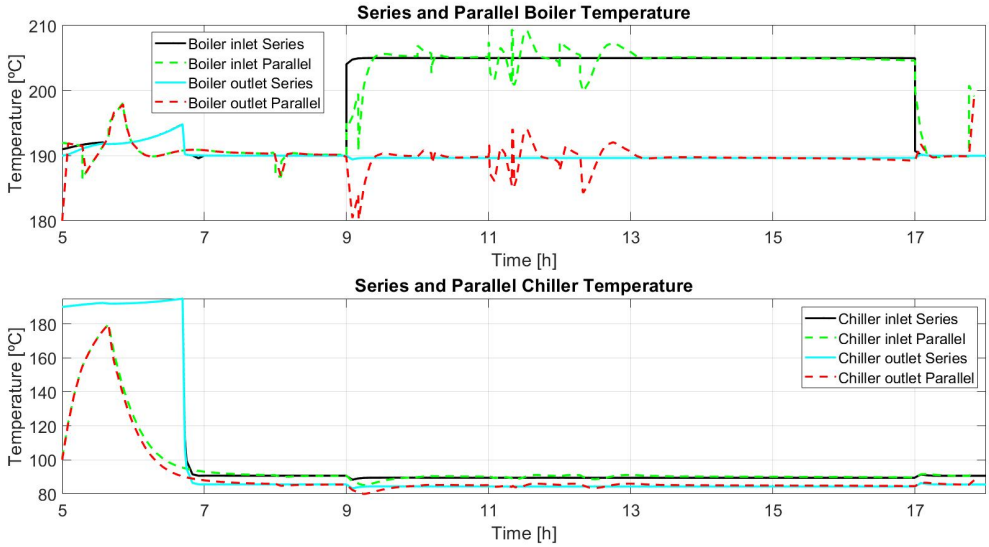

Figure 3.25: Temperature results for a day with clouds in series vs. parallel connection of the TES.

The stable response during the clouds that the series configuration presented due to the thermal inertia of the TES can be understood by analyzing the evolution of the TES node temperatures depicted in Figure 3.26. The effects of the clouds are clearly shown by the abrupt decrease in the oil inlet temperature during the clouds. However, the oil outlet temperature did not present any deviation during the clouds. Paying attention to the temperature in the salt nodes, one can notice that the impact of the clouds is both delayed and reduced as it propagates from node to node within the TES.

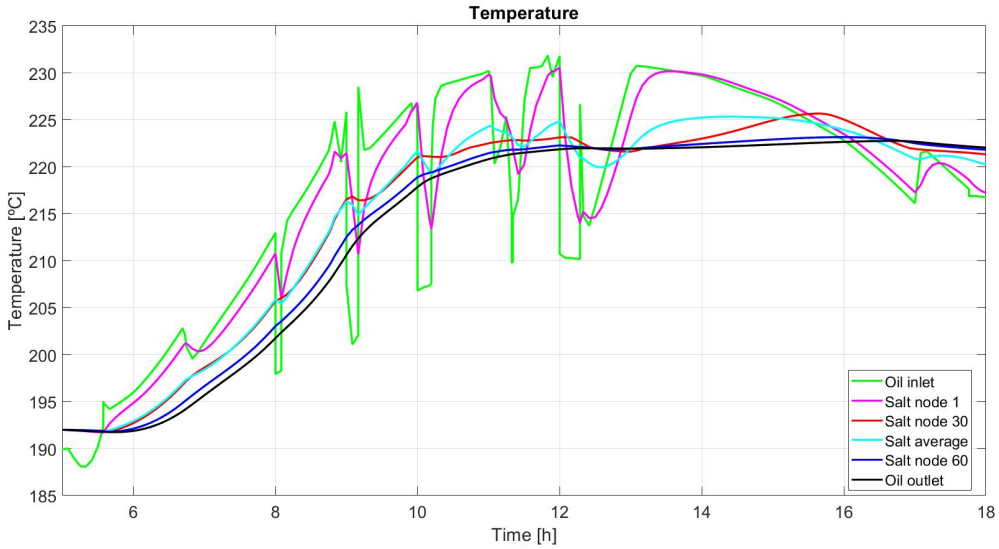

Figure 3.26: Temperature evolution for the TES salts in the series configuration for a cloudy day.

3.2.2 Selection of the configuration

In Section 3.2.1, the development of dynamic models for both configurations was undertaken and subsequently, a comparative assessment in terms of energy production, solar fraction, and control quality was conducted. With the results obtained from this assessment, the next conclusions can be deduced:

- The parallel layout exhibits a marginal energy production advantage, generating between 0.35 % and 3.2 % more energy than the series configuration. Nevertheless, it's important to highlight that the parallel configuration incurs higher pumping energy consumption, accounting for approximately 31 % to 38 % of the total energy consumed by the pumps. This increase in energy consumption can be attributed to the greater number of pumps incorporated into the parallel configuration.
- Regarding control quality, the simulation results indicate that the series-connected TES configuration demonstrates a smoother control response across various irradiance scenarios, including simulations on cloudy days. This robust control performance against irradiance fluctuations is attributed to the thermal inertia of the TES system, which helps stabilize the system under varying solar conditions. However, when it comes to the

heat supply to the process, the start-up occurred one hour earlier in the parallel TES configuration. This shift in start-up timing is due to the direct connection between the SunDial and the demand, bypassing the need for TES preheating. In a border context, both systems show poor results in terms of control in the scenarios with low irradiance.

- Upon analyzing the two configurations, and considering their respective levels of simplicity, the series connection of the TES system with the SunDial collector and the process heat exchangers was selected as the more straightforward solution. The parallel TES configuration required the management of a greater number of variables: namely, the outlet temperature of the SunDial, the operational mode of the TES (charging or discharging), and the inlet temperature of the secondary heat exchanger (the chiller). This elevated the complexity of the control system and demanded the inclusion of supplementary components. These additions included an auxiliary pump for TES recirculation, two three-way valves that enable the selection of the TES connection in either charge or discharge mode, a Proportional-Integral (PI) controller tasked with overseeing the chiller inlet temperature, as well as another PI controller assigned to manage the primary recirculation valve.

Therefore, the series configuration was selected to be applied to the ASTEP system due to its simplicity, as the parallel TES connection would entail a complex system with a higher number of elements, consequently leading to higher costs. Remarkably, the results demonstrate that both systems yield very similar outcomes in terms of solar fraction.

It is essential to recognize that the choice between series and parallel configurations should be contingent on the specific needs and objectives of the application. In diverse applications or alternative systems, the advantages offered by a parallel configuration, such as accelerated startup times, could indeed be a decisive factor favoring the adoption of that particular configuration.

In summary, the series connection of the TES emerges as the selected solution for the ASTEP system, aligning with ASTEP's objectives of achieving a cost-effective and straightforward approach to generate heat for the process industry. This configuration demonstrates robust control performance across various irradiance scenarios and aligns well with the system's goals.

3.2.3 Modes of operation for series configuration

As previously illustrated in Section 2.2, the ASTEP system can be operated in six different operational modes. The transition between the operational modes is automatically driven by the control system. To analyze the performance of the system against different levels of irradiance, a pack of simulations of the pre-selected days for high and low irradiance (in Section 2.1.2) was accomplished.

Furthermore, the operation strategy for SunDial differs from the typically implemented in SHIP, where the mass flow variation controls the collector's outlet temperature and the solar collector has a constant temperature difference [37]. In the ASTEP system, the inlet

temperature of the SunDial is variable and will increase as the TES is charged until the maximum temperature is achieved. In consequence, the outlet temperature of the SunDial will also increase, but the temperature difference of the collector will be variable and dependent on the incident power and the state of charge of TES.

The power of the different components, except for the impinging power that is an input to the simulation, is calculated by Equation 3.45 , these are the power produced by the SunDial, the power feed to the boiler and the chiller, and the power exchange by the TES. The power exchanged by the TES will be positive in charging and negative during the discharging. Then, the TES charge percentage is calculated with Equation 3.49, which considers the heat stored in the PCM salts and the thermal losses to the environment. The TES state of charge starts at zero with a PCM salt temperature of 190 °C, so if the salt temperature is below 190 °C the state of charge will be negative. This can happen at night due to thermal losses to the environment. The SunDial inlet temperature and inlet flow are measured before the SunDial recirculation.

$$TES_{\text{charge}} = \frac{E_{\text{TES}}}{E_{\text{TES,full}}} \cdot 100 \tag{3.49}$$

Other variables of interest are the temperature profiles of the outlet temperature of the TES and the outlet temperature of the SunDial because the transition between modes depends on these variables. Finally, the inlet and outlet temperatures of the process HX which are the control variables are included in the plot, to examine the quality of the controllers. Additionally, the different modes of operation are distinguished on the graph by color squares.

Modes of operation for the dairy factory

Fig, 3.27a and 3.27b show the power and the temperature results respectively of the summer simulation (8^{th} of July) for the dairy factory in Corinth, Greece, for the series configuration. The initial temperature is 110 °C for the SunDial absorber and the thermal oil inside and 190 °C for the TES. The simulation starts at 5 a.m. at sunrise when the SunDial begins in the preheat mode, this lasts approximately 1 hour and finishes when the temperature is 5 degrees higher than the salts. Then, the SunDial is connected and the Main Pump (MP) is turned on to charge the TES.

At 7:30 a.m., the TES outlet temperature reaches the chiller start-up setpoint. Consequently, the system connects with the chiller heat exchanger, and both the flow rate and temperature are controlled at the HX inlet. Initially, the HX inlet temperature matches the TES outlet temperature until the temperature controller becomes active. Furthermore, the outlet temperature of the HX remains consistent with the process fluid temperature until the HX is engaged. The primary goal of the control system is to maintain a steady temperature and flow rate at the HX inlets to ensure a constant power supply to meet the demand. The outlet temperature of the TES exhibits greater stability compared to the SunDial's outlet temperature due to the high capacitance of the storage. Finally, the controllers fine-tune the values to align with the desired setpoint.

The inlet temperature of the boiler is regulated at 205 °C when the boiler is operational and

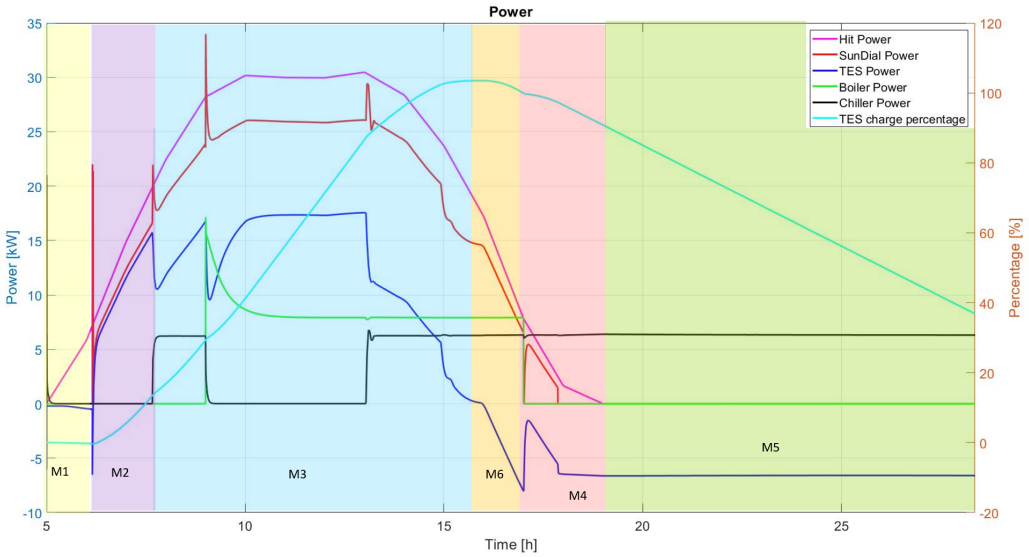

(a)

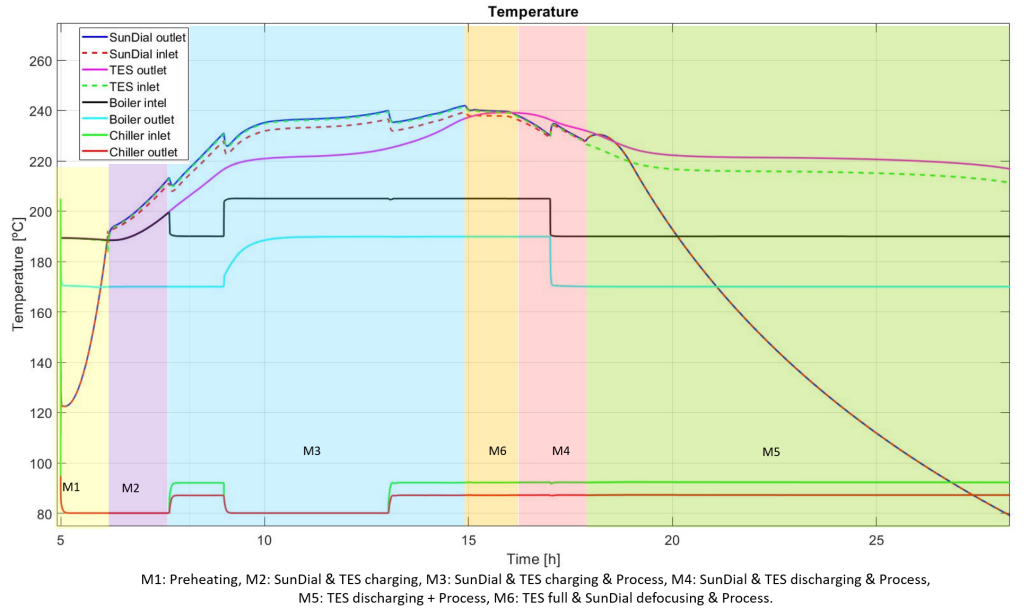

(b)

Figure 3.27: Dairy factory results for the series configuration in summer: (a) Power and (b) Temperature.

190 °C when the boiler is inactive but the chiller is operational. Figure 3.28 illustrates the temperature controller's action, with the upper plot demonstrating how the inlet temperature setpoint shifts between 205 °C and 190 °C. This control is managed by the frequency driver of the Recirculation Pump (RP) to modulate the flow and manipulate the inlet temperature of the HX. Figure 3.29 portrays the response of the flow controller, where the inlet flow rate of the process HX is maintained at a constant level by diverting excess flow through the Bypass Valve (BPV).

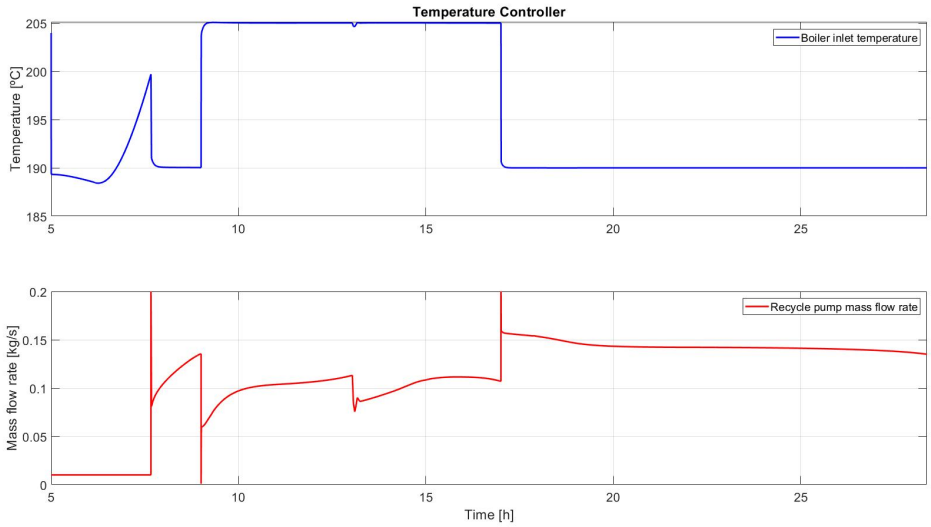

Figure 3.28: Temperature controller manipulated (bellow) and controlled (above) variables of the dairy factory for summer.

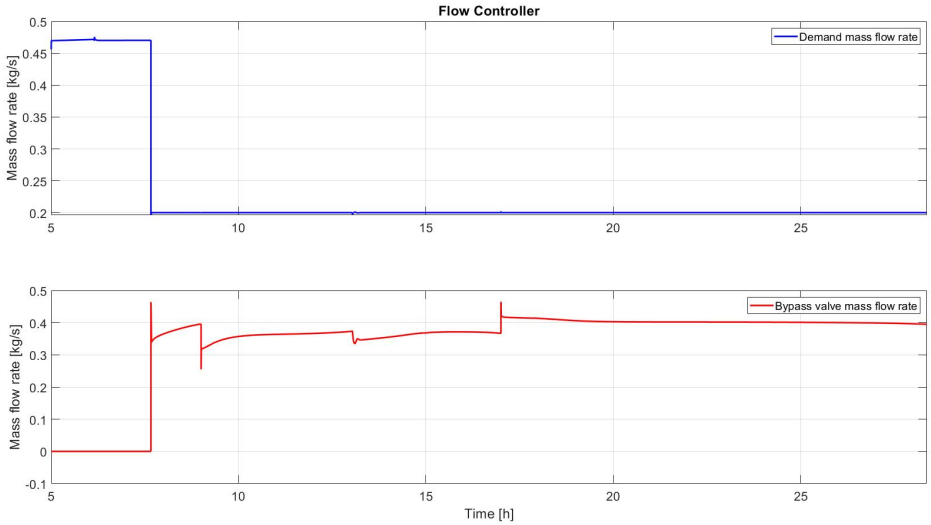

Figure 3.29: Flow controller manipulated (bellow) and controlled (above) variables of the dairy factory for summer.

At 9 a.m., the factory opens, and the conditions for supplying heat to the boiler are established. During the startup phase, the boiler's power initially exceeds the nominal value but quickly stabilizes to reach the nominal output. This initial power surge is necessary to raise the temperature of the heat exchanger, which starts at the process temperature that is a lower temperature than the nominal value. The control system prioritizes the operation of the boiler rather than the chiller. Consequently, the chiller is temporarily shut down to ensure that the boiler receives adequate energy. The chiller is restarted at 1 p.m. when the energy generated by the SunDial becomes sufficient to power both HXs simultaneously.

Around 3 p.m., the TES reaches its full capacity, prompting the SunDial defocus controller to commence controlling the SunDial's outlet temperature to the maximum allowable value of 240 °C. In Figure 3.27a it can be seen that at 3 p.m. the SunDial power is reduced more than expected in comparison with the Hit power. This discrepancy signifies the energy being diverted by the SunDial as a result of partially defocusing its mirrors. Figure 3.30 illustrates the SunDial's outlet temperature and the focus percentage. Notably, the minimum focus level is set at 85 %, resulting in a 15 % reduction in power output due to defocusing.

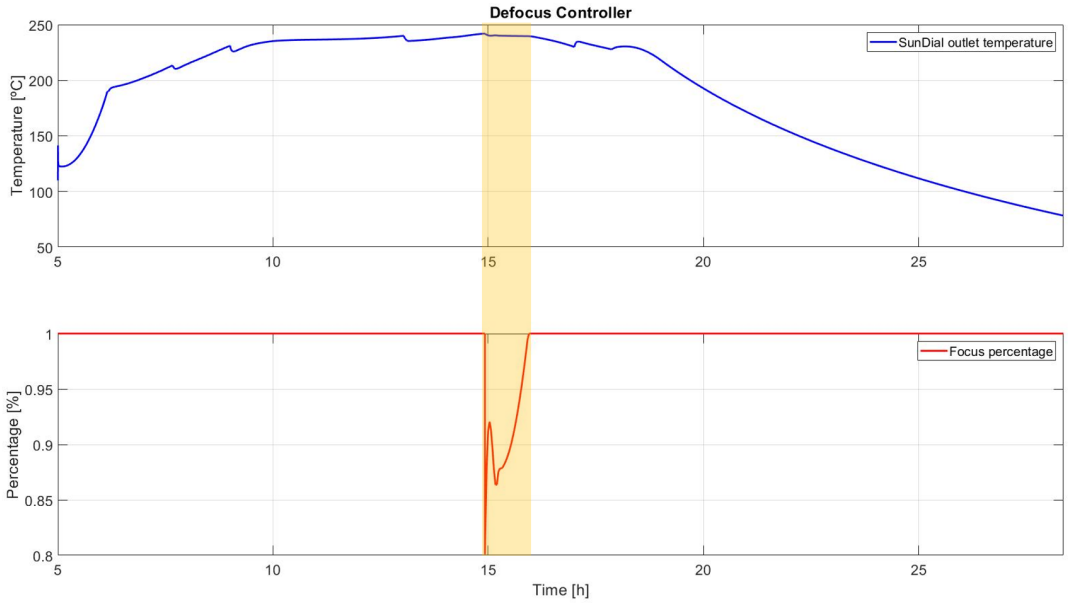

Figure 3.30: SunDial outlet temperature (above) and focus controller percentage (bellow) of the dairy factory for the summer day.

At 4 p.m., the SunDial's energy output becomes insufficient to meet the demand. However, since the TES is fully charged at this point, the system initiates the TES discharge process. This operational mode continues until 6 p.m. when there is no longer DNI available to operate the SunDial effectively. Subsequently, the system continues to supply energy to the chiller using the stored energy until the simulation's conclusion.

The dynamic behavior of the system is clearly evident in the temperature profiles, as depicted in Figure 3.27b, particularly during the startup of various components within the system.

For instance, when the SunDial initiates its startup sequence, the temperatures experience a sudden decrease as colder fluid from the rest of the system enters. However, due to the considerably higher flow rate within the SunDial compared to that driven by the Main Pump, the temperatures rise rapidly. Similarly, during the startup of the boiler, the temperature reduction effect is observed in the SunDial temperatures. Additionally, the inertia of the HX is apparent in the outlet temperature of the boiler, which takes approximately an hour to reach its nominal value.

Regarding the temperature profiles of the TES, Figure 3.31 provides insights into the inlet and outlet temperatures of the thermal oil, as well as the salt temperatures for nodes numbered 1, 30, and 60. The average temperature, calculated by adding the temperature values at each node and dividing by the total number of nodes, is also displayed. At the beginning of the simulation, the SunDial is connected to the TES, and the charging mode is activated. Initially, the salt is in the solid phase, and the first node of the salt is close to the value of the inlet temperature of the oil. The salt temperature of node 30 exhibits a similar trend to the average salt temperature, while the last node (60) aligns with the outlet temperature of the oil. When the salt temperature reaches the phase change temperature of 222 °C, there is a notable change in the behavior of the salt temperature curves. They tend to stabilize around the phase change temperature of the Phase Change Material (PCM) and increase more gradually. Upon reaching full capacity, all node temperatures reach the maximum value of 240 °C. Towards the end of the simulation, as the TES discharges, the salt temperatures trend towards the average salt temperature. It is worth highlighting that the effects of variations in the inlet temperature of the oil become less pronounced as the HTF traverses through the nodes of the TES, which can be noticed at the oil outlet temperature.

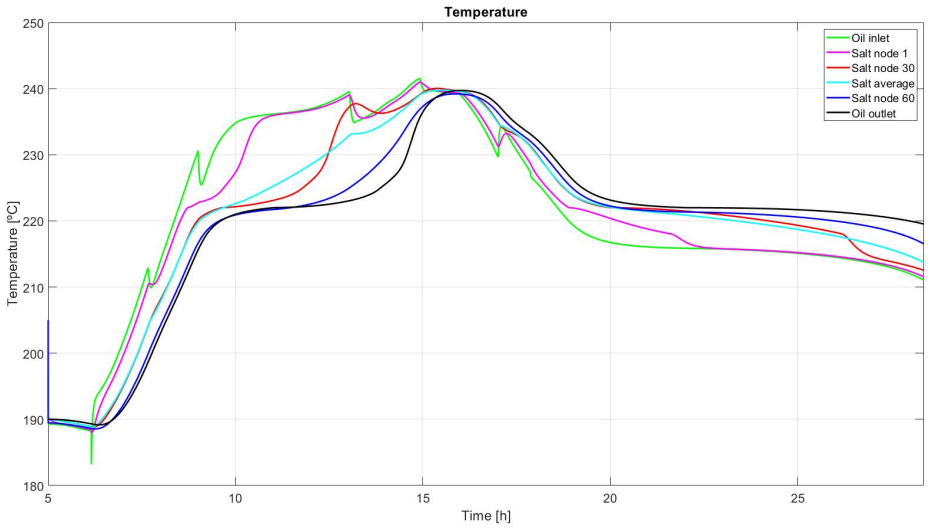

Figure 3.31: TES temperatures for different nodes of the model of the dairy factory for a summer day.

The results of the winter day (8^{th} of February), are shown in Figure 3.32a and 3.32b. In contrast to the summer simulation, here the SunDial commences operation after 9 a.m. when the factory opens. However, initially, the energy generated is insufficient to supply the boiler,

so it is utilized to charge the TES. After 12 p.m., the boiler's startup setpoint is achieved, and heat for the boiler is provided by both the SunDial and the TES. At 1 p.m., for a brief period of one hour, the SunDial simultaneously charges and meets the demand. Finally, the chiller is started-up when the factory is closed, which lasts for less than three hours. Regarding the dynamic behavior, similar effects to the ones observed in the summer simulation can be discerned during the startup of various components.

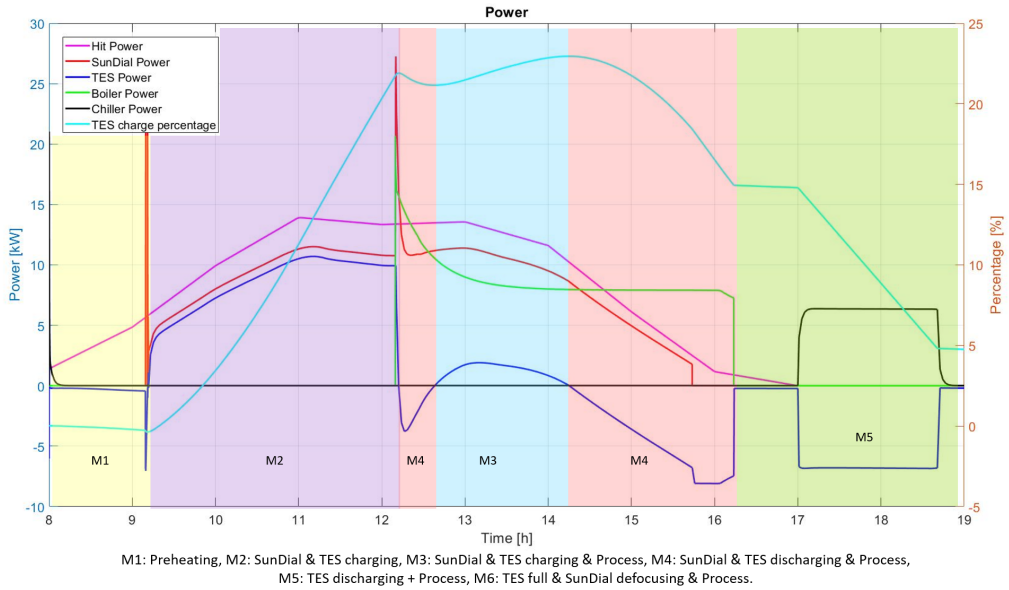

(a)

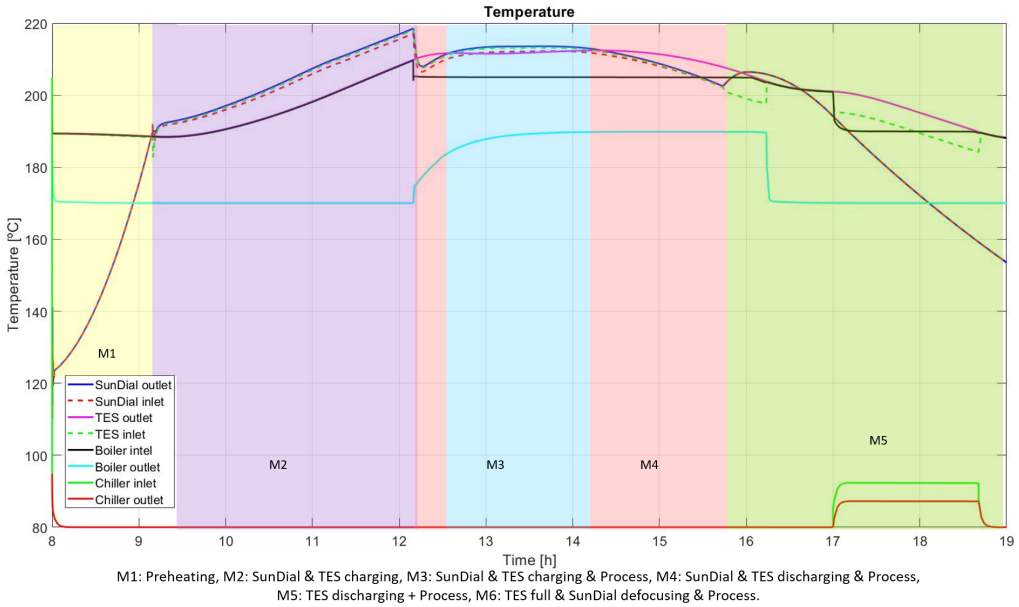

(b)

Figure 3.32: Dairy factory results for the series configuration in winter: (a) Power and (b) Temperature.

The energy production for each day also deserves some attention. Figure 3.33 shows the daily energy production by the SunDial and Process, which are calculated by Equation 3.46 and 3.46, and the target of energy of the ASTEP system defined in Section 2.1.1.

The energy supplied to the process during the summer day exceeds the target by 33%, whereas on the winter day, it falls short by 7 %. However, it's important to note that this winter shortfall may not be representative of all winter days, and a comprehensive assessment of the energy target should be conducted on an annual basis, taking into account variations in solar irradiance throughout the year. This will be analyzed in Chapter 5 where a simplified model was developed to carry out annual simulations. The amount of energy stored at the end of the day in summer is 42.9 kWh and in winter 5.4 kWh. So the amount of energy lost was higher in winter, approximately 10 %.

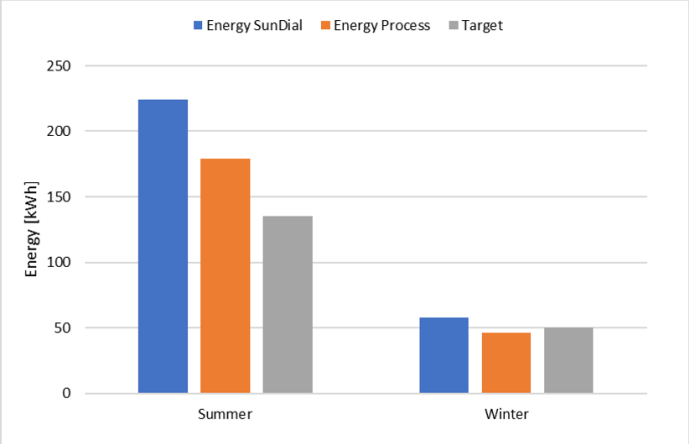

Figure 3.33: Energy results of winter and summer simulations of the dairy factory.

Modes of operation for the tube steel factory.

A similar analysis has been conducted for the tube steel factory in Iasi, Romania. Figures 3.34a and 3.34b presents the power and temperature results for a summer day (August 20th). The inlet temperature of the HX2 is not plotted because it is the same as the outlet temperature of HX1. Unlike the previous case, this factory operates continuously, 24/7. The initial temperatures for the TES and SunDial are set at 200 °C and 100 °C, respectively. The simulation begins with the SunDial in preheating mode.

At 6:30 a.m., the SunDial reaches its startup temperature and is subsequently connected to the system. Notably, the maximum power achieved by the SunDial-HL in this scenario is lower than the summer scenario for the dairy factory with the SunDial-LL (20 kW vs. 25 kW). Subsequently, at 9:00 a.m., the temperature controller initiates the overseen of the inlet temperature of HX1, setting it to 220 °C. From this moment onwards, HX1 operates at a constant power level. At 1:30 p.m., HX2 begins to operate, and finally, at 3:30 p.m., the TES switches to discharge mode due to insufficient SunDial energy to supply both HXs. The maximum temperature of the SunDial is not achieved in this scenario as in the dairy factory, because the TES does not achieve it is total capacity.

The results for the winter scenario (March 7th) are depicted in Figures 3.35a and 3.35b. As

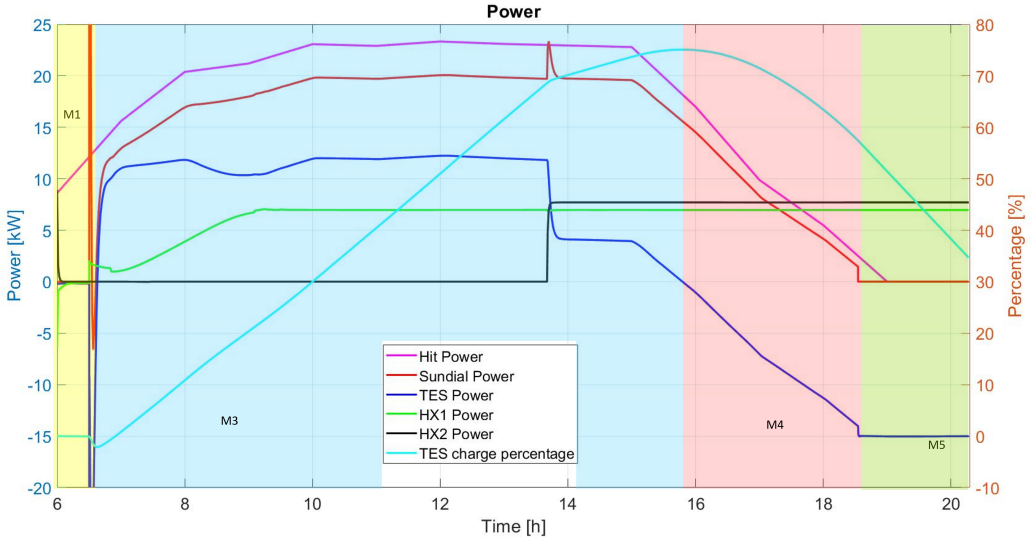

(a)

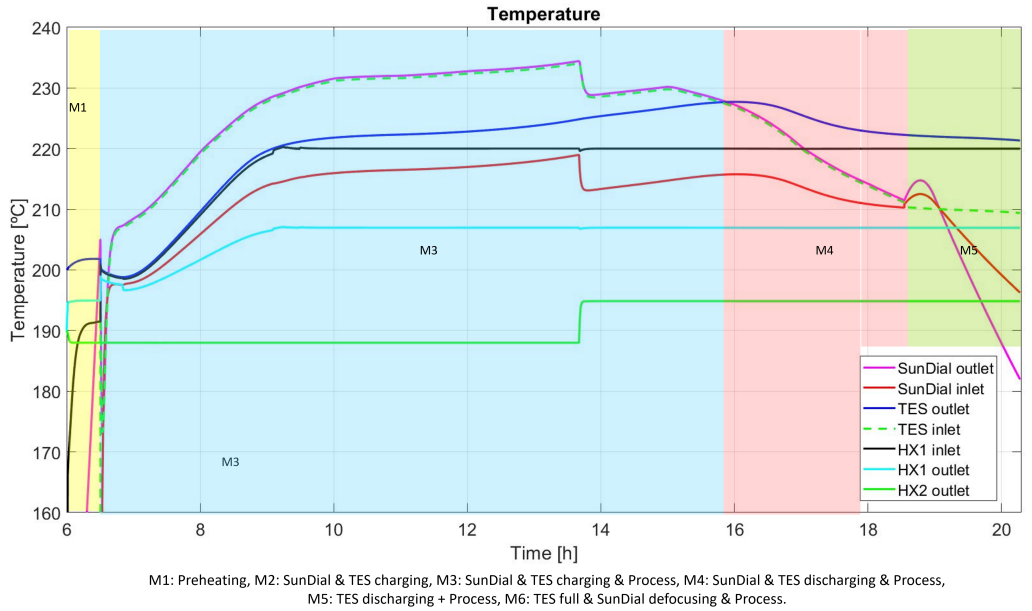

(b)

Figure 3.34: Tube steel factory results for the series configuration in summer: (a) Power and (b) Temperature.

can be observed in the power graph, the solar irradiance is exceptionally low during this day, preventing the HX2 from ever turning on. The first HX operates at variable power levels throughout the day. This situation arises because the temperature setpoint of 220 °C is never reached, rendering the temperature controller inactive. However, HX1 begins operation around 9 a.m. and remains operative until 6 p.m.

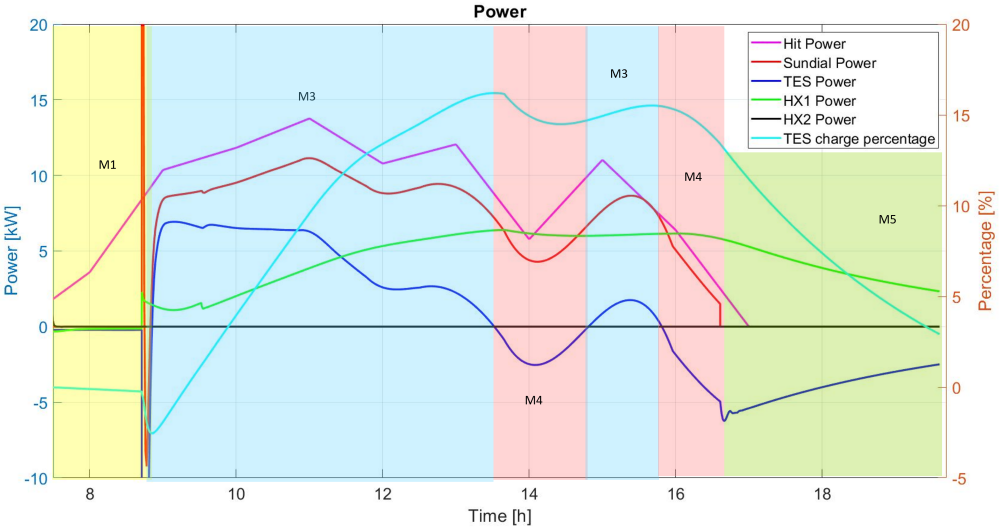

(a)

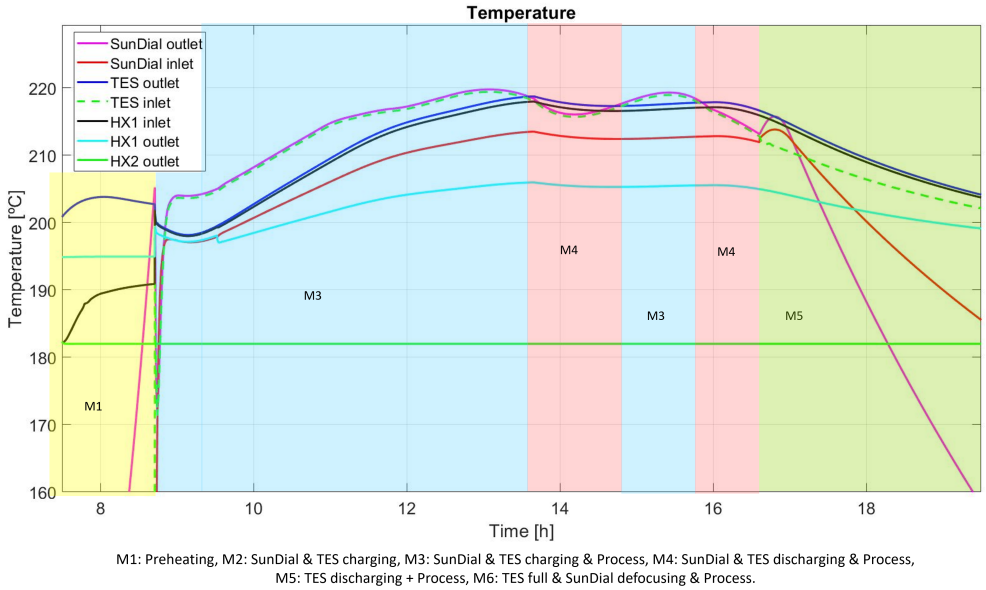

(b)

Figure 3.35: Tube steel factory results for the series configuration in winter: (a) Power and (b) Temperature.

The energy graph (Figure 3.36) illustrates that the energy targets are successfully met both in summer and winter. In the winter simulation, the proportion of the lost energy is 16.8 %

and is also higher than in the summer simulation, as in the dairy factory.

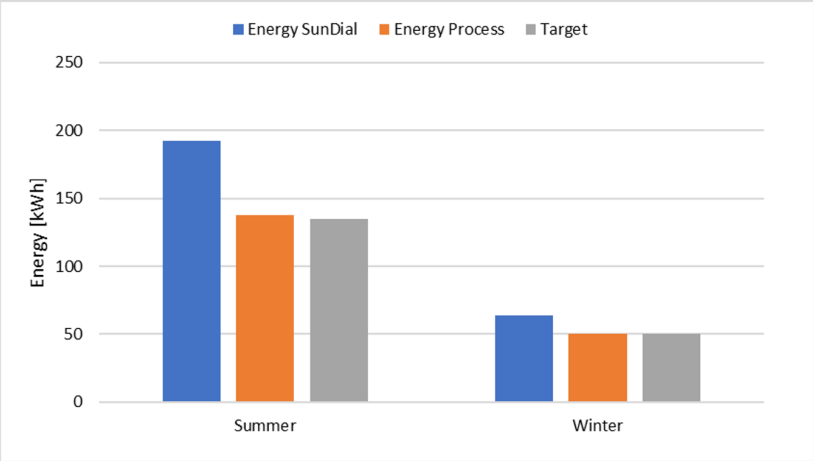

Figure 3.36: Energy results of winter and summer simulations of the tube steel factory.

3.2.4 Start-up setpoint for the dairy factory

In Section 2.2 the control strategy was defined as a flexible heating integration (FHI). This FHI involves using two heat exchangers connected in series so that the system can supply energy at different levels of power and temperature. This is particularly useful for solar systems due to the seasonal characteristics of solar irradiation. Hence, the solar system with FHI has more efficiency compared with a standard system, particularly in winter.

The FHI was applied by adjusting the particular needs of the dairy factory, which has two defined demand temperature levels: the heat that is produced by the boiler and the heat that is consumed by the chiller. Furthermore, the demand periods are different: the cooling produced by the chiller is required 24 hours a day, but the boiler is only operative between 9 and 17 hours. Hence, during the opening hours, the FHI will be prioritized for producing heat at high temperatures to replace the boiler.

The chiller is a low-temperature demand so, its setpoint is lower than the high-temperature demand of the boiler, 190 °C and 205 °C respectively. Thus, if both HXs can not operated at the same time, the chiller will start first the days with insufficient radiation for both HXs, reducing the hours of the boiler operation. This can be avoided by applying a setpoint to operate both HXs at the same time between the hours the factory is open higher than the one to operate individually.

To analyze the effect of the setpoint value for allowing the operation of the two heat exchangers simultaneously, four different conditions for the setpoint have been simulated: no setpoint condition for both HX, 210 °C, 220 °C and no chiller. The no setpoint condition will imply that each HX will start when its own target is reached. The no-chiller simulation is carried out to calculate the maximum scenario for the boiler. These four scenarios were simulated for two consecutive days in summer, fall, winter, and spring.

Figure 3.37 illustrates the power results for the spring days. The simulation with no setpoint condition is the one that supplies more energy to the process but the least to the boiler. The simulation with only the boiler is the one that provides the maximum power the boiler could have received. As the setpoint for both HX is increased the chiller operation is restricted and the boiler can operate for more hours.

In summer solar irradiation is very high so the boiler is operating all the hours the factory is open independent of the condition, in spite of the chiller operation is restricted by the setpoint condition. In contrast, in winter if there is no condition the boiler does not even operate. And no difference is obtained between the setpoints 210 °C and 220 °C.

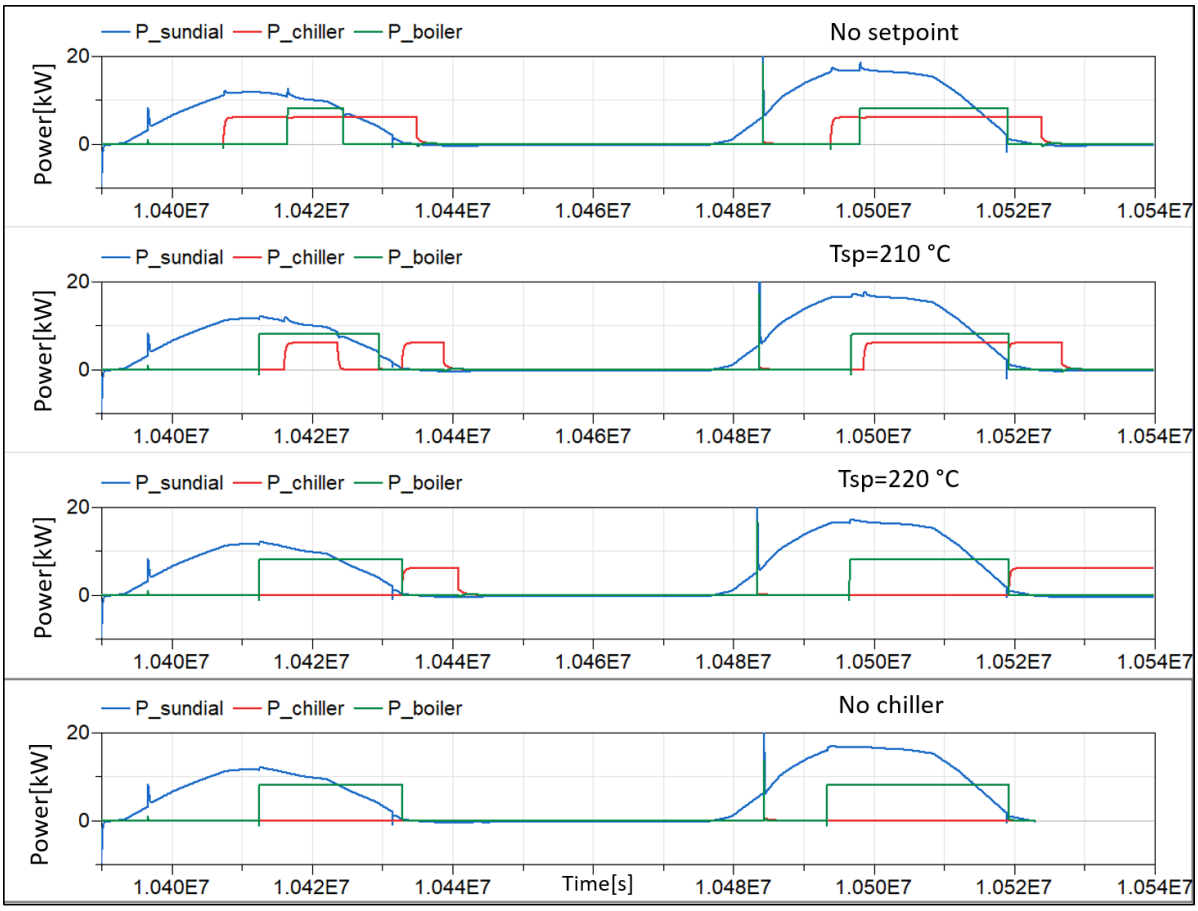

Figure 3.37: Power results for two spring days with different setpoint conditions for both HXs operations.

The results in terms of total energy and energy send to the boiler obtained in the four simulations for the different seasonal days were compared in Figure 3.38 . The no setpoint scenario implies a disadvantage for the high-temperature demand, the boiler, which in the winter days never turns on. The total energy supply to the process is 10 % more in most scenarios except winter.

For the simulation with no chiller, the maximum increase of the boiler energy is presented in the winter simulation with a 20 % increase. However, for summer and fall no difference is

present. This means that the maximum target for the energy is achieved with the 220 ° C. The total energy supply is highly reduced for all scenarios if the chiller is not implemented, with a maximum difference of 60 % less power in summer. This shows that the FHI can leverage more energy than using one unique integration point, in this case, the boiler.

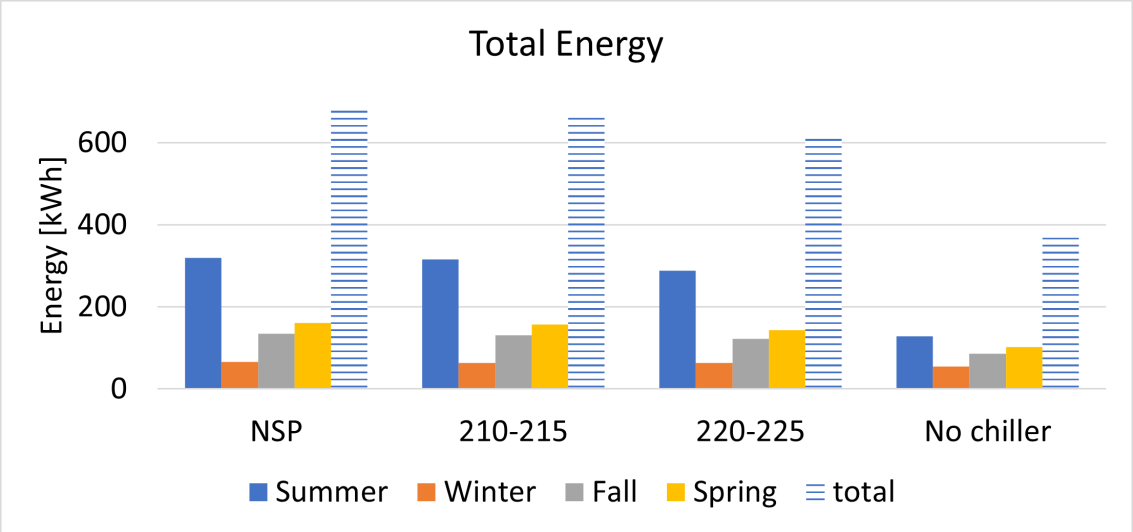

(a)

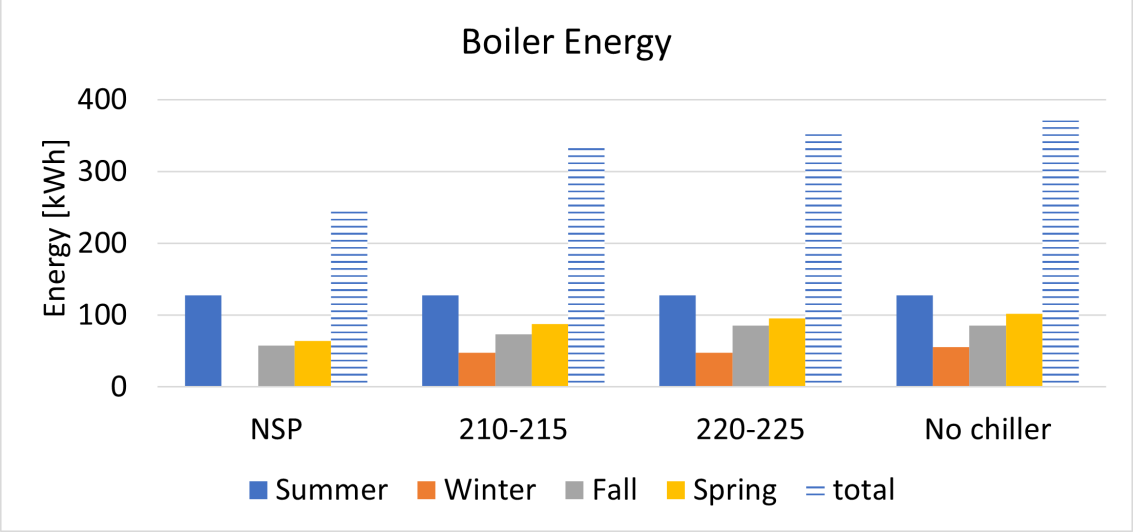

(b)

Figure 3.38: Energy results for the different scenarios: (a) total energy and (b) boiler energy.

Finally, the 210 °C setpoint shows a reduction in all scenarios except the winter, between 8.4 % and 14.4 % in the energy sent to the boiler. But the total energy feed to the demand increased by 10 %. The sum of all the results is depicted in the total series, the boiler decreased a 5.7 % with the 210 °C setpoint and the total feed energy increased a 8%.

For the ASTEP system, the setpoint of 220 °C was selected because the objective was to prioritize the boiler to the maximum and to leverage extra power with the chiller. The no-chiller option represents a total of 40 % less energy, making interest to resign to gain less

than 4 % more power sent to the boiler.

3.2.5 Impact of the piping thermal inertia

The influence of thermal inertia and heat losses in pipe networks is a significant concern when it comes to solar thermal energy. Pipe networks connecting the solar collector field, thermal energy storage, and process heat exchangers can be quite long depending on the size of the solar field and its distance from industrial processes. Furthermore, in a small system, the relation between the heat production and the piping thermal losses could be high, above 10%. In this study, two different systems were developed using Dymola software to investigate the impact of these pipelines in a tube steel factory scenario. The only difference between these systems is that one considered the inertia of the piping network, which incorporates modeling for both steel tube capacitance and insulation capacity, while the other system does not include this consideration. Furthermore, the effect of different irradiance levels and different setpoints for the demand temperature were analyzed. For this reason, two models one with pipes with capacitance and the other without were developed. Therefore, by comparing the different outcomes of the results, the effect of piping thermal inertia in small SHIP systems was found. The tube steel factory has been selected to carry out this analysis.

Previous studies have analyzed the effect of piping thermal inertia in solar systems, and have found delays in the simulation in comparison with the experimental results. For example, Rodat et al. [67] carried out a Dirac impulsion test, which consisted of generating a cold wave in the inlet of the solar field. They found a delay of 7.4 min in the experiment by comparing the results with a simulation, which considers a pipe of 1 mm thickness without insulation. They also compared the results of a daily simulation with those of the experimental facility and found a 15-minute delay in the solar field start-up. Sartor et al. [73] found a delay of 3.33 min in their model with a step change in solar radiation. Tascoini et al. [81] found that the delay in the process start-up produced by the inertia of the pipes was longer in winter than in summer. However, these studies were focused on larger systems than ASTEP.

Overall, the differences in start-up delays observed in various studies highlight the importance of considering system-specific factors, including scale, control strategies, insulation, and seasonal variations when designing and analyzing solar thermal systems. These factors can significantly influence the transient behavior of the system during start-up and shutdown processes.

Figure 3.39 displays the power output of the SunDial and the two heat exchangers (HX1 and HX2) for the two simulated systems, one with pipelines inertia and the other without, during the first scenario, during a summer day. The initial temperature for the SunDial and the pipelines is 80 °C and for the TES is 205 °C. By comparing the results of both simulations, one can notice a time shift in the start-up of the SunDial: the simulation without inertia starts at around 6:30 a.m., while the one with inertia begins about 13 minutes later.

To gain a better understanding, it is useful to examine the trend of the outlet temperature of the SunDial, depicted in Figure 3.40. In this simulation, the operation of the SunDial begins once the outlet temperature reaches 205 °C. As evident from this figure, during the

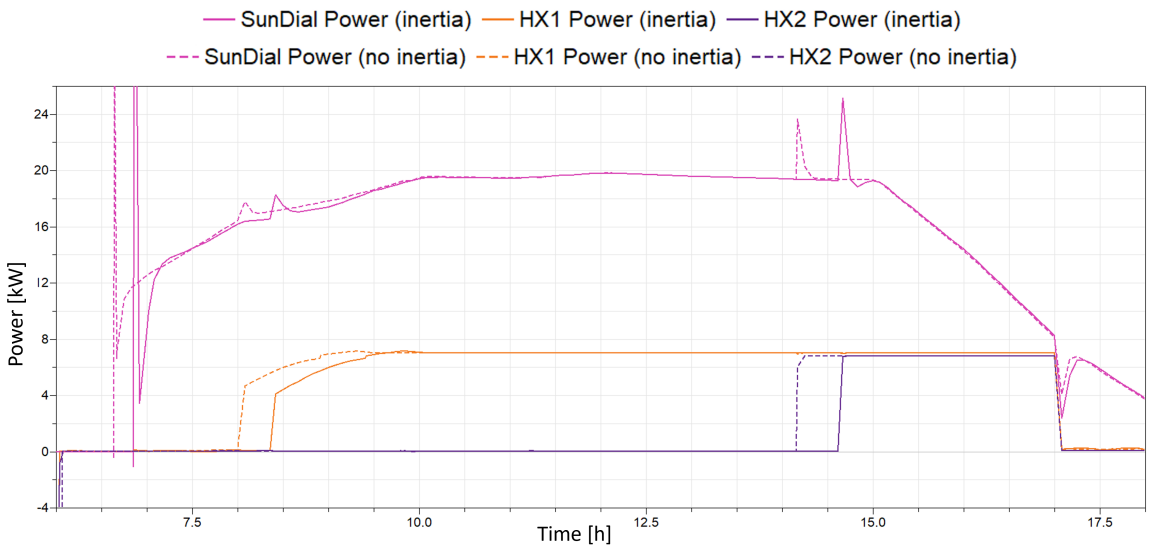

Figure 3.39: Power results of the SunDial and the heat exchangers (HX1 and HX2) for a summer day simulation with controller setpoint at 220 °C, represented in dashed line the simulation without pipelines inertia, and in continuous line the one with inertia

inertia simulation, temperatures initially exhibit lower values. Consequently, there is a delay in start-up operations which rely on attaining specific temperatures. Under this circumstance, SunDial must preheat not only the heat transfer fluid within the receiver but also pipeline P1. Thus, a portion of heat energy gets consumed by heating both steel and insulation present within pipeline P1 instead of being utilized solely for heating up fluid content.

Regarding the heat exchangers, there is a noticeable difference in the operation of the process HX. In the simulation without inertia, when the factory opens at 8 a.m., the thermal energy storage has already been charged sufficiently to supply HX1. This is determined by monitoring the outlet temperature of TES which exceeds the start-up setpoint of 210 °C. However, in the model with inertia, when the factory opens, TES outlet temperature is below 210 °C and as a result, there is a delay of 21 minutes for HX1 start-up. Similarly, for HX2 start-up there is a delay of 28 minutes until TES outlet temperature reaches 225 °C. The reason for this larger delay in both cases can be attributed to using part of solar heat to preheat a larger length of pipes in comparison with the SunDial start-up.

A comprehensive examination of irradiance impact was conducted through the execution of two simulations employing a temperature setpoint of 220 °C, representing a winter day scenario. The first difference we can notice with the summer results is that due to the low irradiance in winter, the power produced by the SunDial is neither sufficient to turn on the HX2, as is shown in Figure 3.41; not to reach the temperature setpoint of 220 °C for the controller start-up, depicted in Figure 3.42. This also implies that the HX1 works at variable power all the simulation time. Due to the low radiation, the HX1 began to operate more than an hour after the factory was opened.

The start-up delays of the different components are higher for the winter season than the

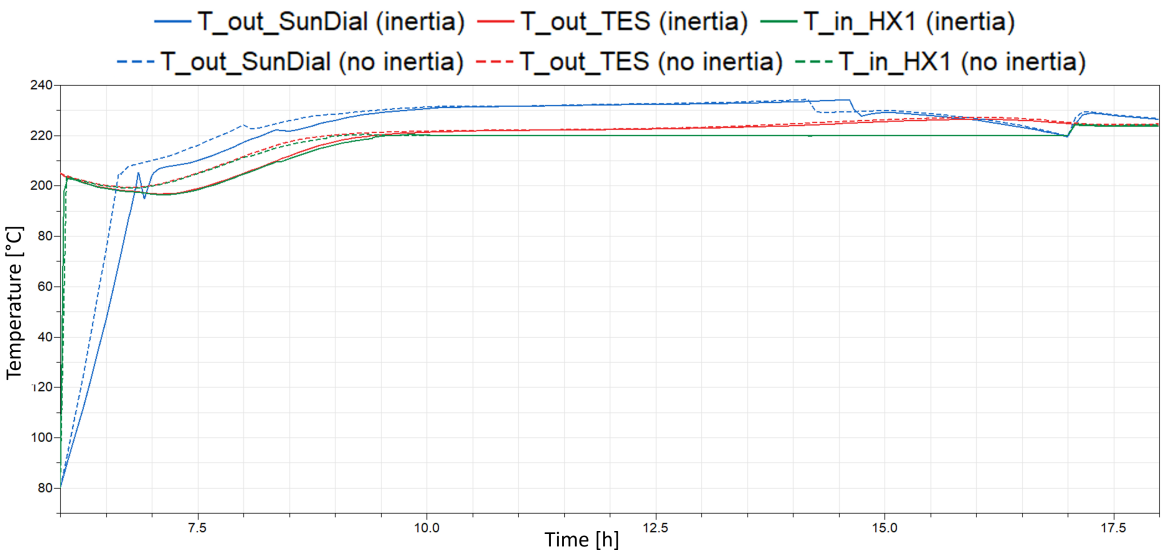

Figure 3.40: SunDial outlet temperature, TES outlet temperature, and HX1 inlet temperature for a summer day simulation with controller setpoint at 220 °C, represented in dashed line the simulation without pipelines inertia, and the one in continuous line with inertia.

summer: the SunDial start-up delay is 25 minutes, and HX1 of 38 minutes. These delays are longer compared to the summer scenarios where start-up times were 13 and 21 minutes. The primary reason for these longer delays is the lower solar irradiance in winter, which results in a longer time required to preheat the pipes. Furthermore, it is pertinent to highlight that the inertia inherent in the pipeline components contributes to an oscillatory behavior, characterized by intermittent shutdowns of the SunDial shortly after initiation. This oscillation manifests in the outlet temperature of the SunDial during its initial phases, a phenomenon absent in simulations devoid of inertia. When the SunDial is preheating, the flow circulates only through the SunDial and pipeline P1. But when the preheat is finished and the SunDial is connected to the rest of the system, which is at a lower temperature, the SunDial outlet temperature decreases abruptly, and the SunDial shuts off to start preheating again. This can be avoided by incrementing the start-up temperature setpoint as it was analyzed in Section 3.2.4.

In summary, the simulation results reveal that the inertia of the pipelines introduces a significant delay in the start-up of the SunDial and the heat exchangers for the demands. The residence time, which is the total volume divided by the volumetric flow rate, is calculated to be 1.27 minutes for the entire system. This residence time is relatively short and unlikely to cause significant delays in the controllers. The observed delays in the SunDial and the second heat exchanger start-up in the presence of pipeline inertia are much longer, on the order of 13 and 28 minutes in the summer scenario. Therefore, the primary factor contributing to these delays is the heat capacity of the piping system, which results in lower fluid temperatures while the pipeline is transitioning to thermal steady-state conditions. This effect is particularly pronounced during periods of low solar irradiance, such as in winter.

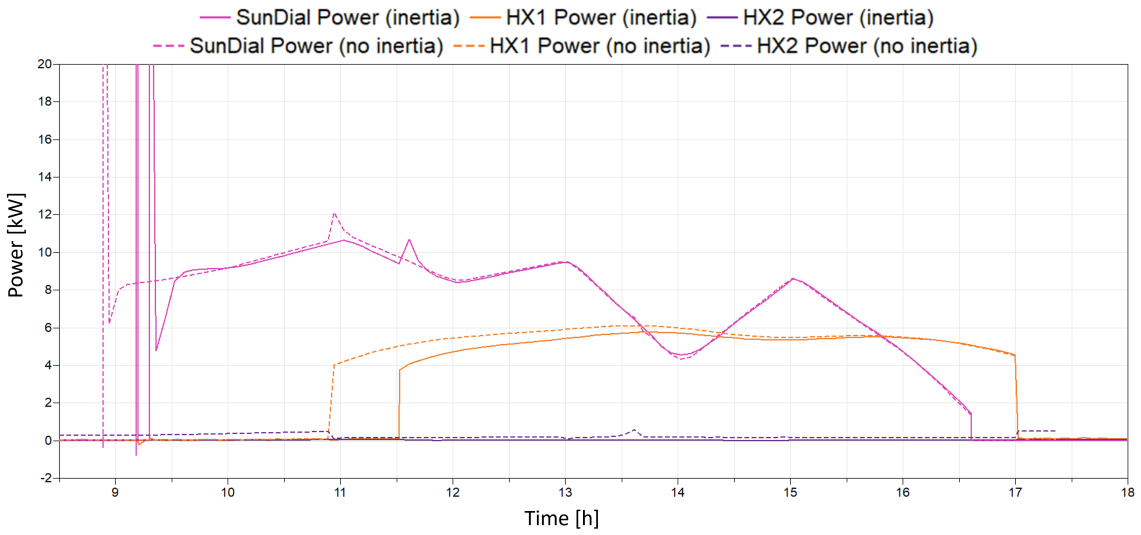

Figure 3.41: Power results of the SunDial and the heat exchangers (HX1 and HX2) for a winter day simulation with controller setpoint at 220 °C, represented in dashed line the simulation without pipelines inertia, and the one in a continuous line with inertia .

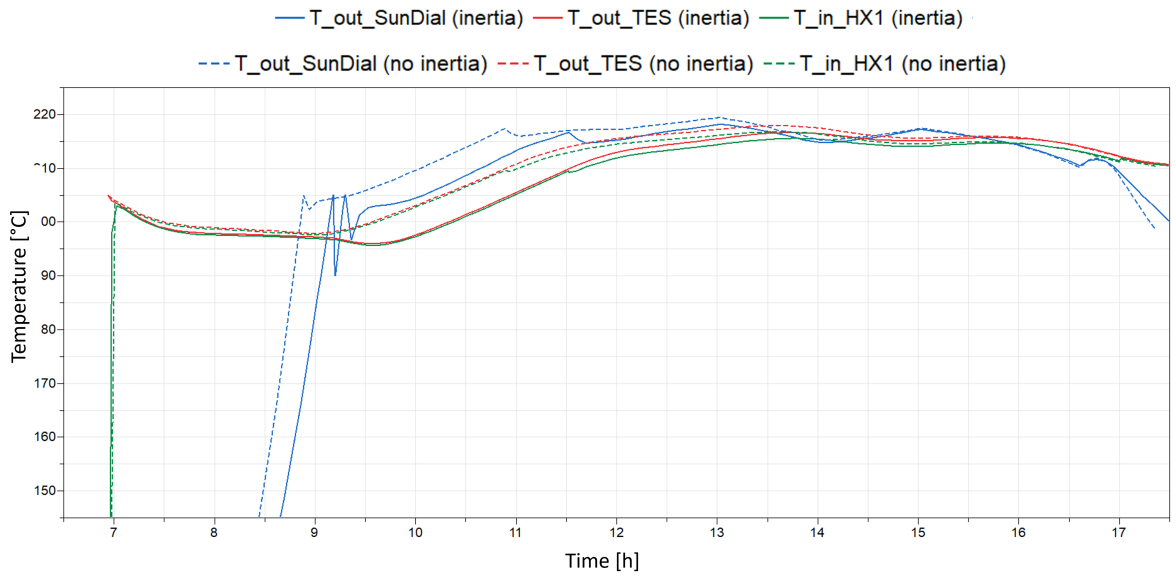

Figure 3.42: SunDial outlet temperature, TES outlet temperature, and HX1 inlet temperature for a winter day simulation with controller setpoint at 220 °C, represented in dashed line the simulation without pipelines inertia, and the one in a continuous line with inertia .

Compared with the results of other studies, ASTEP showed a longer delay in equipment startup. Therefore, the difference in the results between these studies and ours could be due to several factors:

- The scale of the solar system: ASTEP system was designed for small-scale industrial heat (around 20 kW and mirrors area of 44 m^2), while the other studies were for larger systems used in district heat and electric generation (of 400 and 1000 m^2).
- The insulation: The 104 mm of insulation was designed to minimize thermal losses to 10 % of the power produced: ASTEP prototype had high thermal losses due to the small scale of the system.
- The control strategy: principally when the controller's actions are dependent on a temperature.

Another interesting result to compare is the total energy supplied by the SunDial and the total energy sent to the process HXs, which are calculated with Equations 3.46 and 3.47. Concerning the total energy supplied to the process, differences were found between the simulations with and without inertia (Figure 3.43). The energy supplied to the demand at the end of the summer day for the non-inertia simulation was 81.3 kWh, while for the inertia simulation, it was 75.3 kWh, which represented 7.3 % less. Finally, in the winter simulation, SunDial produced a third of the amount of energy produced in summer (Figure 3.44). In this case, the difference in the energy supplied to the demand was 18 % lower in the inertia simulation.

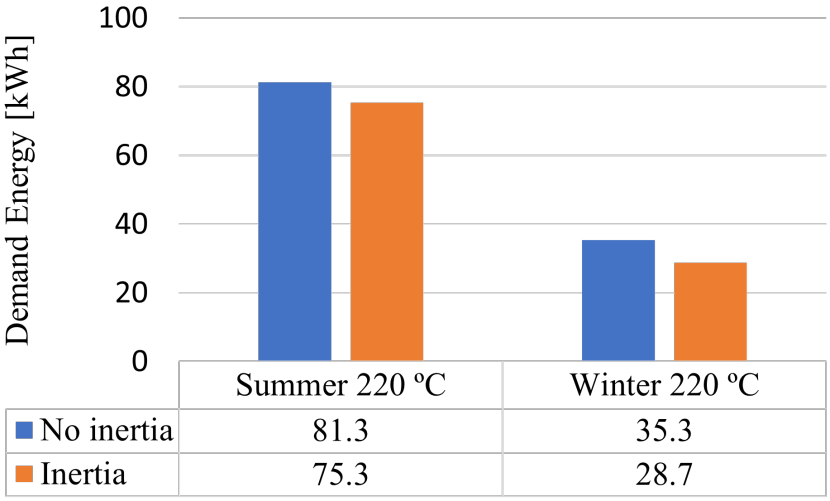

Figure 3.43: Total energy supplied to the process at the end of the simulation.

In conclusion, the impact on the total energy supplied to the demand was lower in the inertia simulation, with a 7 % difference observed in summer and an 18 % difference in winter. This underscores the significance of dynamic simulations in providing more representative results compared to quasi-static models, which tend to overestimate the total energy production. Moreover, the results obtained suggest that dynamic simulations hold greater importance in small systems like ASTEP than in larger systems analyzed in previous studies. This is due to

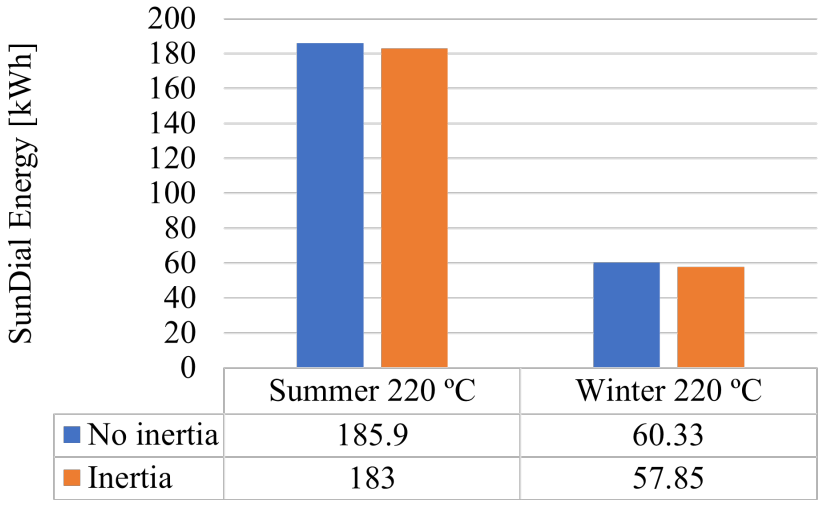

Figure 3.44: Total energy provided by the SunDial at the end of the simulation.

the more substantial disparities between the outcomes of dynamic and quasi-static models. Furthermore, we calculated thermal losses to the ambient due to the pipelines, amounting to 13 % of the total losses. This calculation was derived by subtracting the energy in the TES and the energy supplied to the demand from the energy generated by the SunDial, the energy provided by the pumps was not considered.

3.2.6 Sensitivity analysis of the defocus controller

The SunDial is characterized by its azimuthal tracking system performed by the rotation of the collector. This type of tracking differs from commercial solar collectors such as the PTC or LFC. Hence, it is of interest to analyze the dynamic behavior of this tracker. One of the uncertainties was to calculate the sensitivity required by the controller to achieve an acceptable result with no deviations from the maximum temperature admitted by the system. Therefore, a dynamic simulation of a defocus controller including an aleatory generated tracking error was developed for the ASTEP series configuration.

The effectiveness of the defocus in reducing the temperature by rotating the platform was tested by implementing the model shown in Figure 3.45 in the ASTEP simulation. This controller was added to the SunDial model, previously explained in Section 3.1.2.

Figure 3.46 illustrates a block diagram of the new defocus controller. The primary objective of this controller is to maintain the outlet temperature of the SunDial below the prescribed maximum limit of 240 °C. The outlet temperature of the SunDial is continuously monitored, and the resulting value is subtracted from the predetermined setpoint to calculate the error between the two. This error is then input to the PI controller, which generates a control signal sent to the defocus matrix. Before entering the defocus matrix, a tracking error is introduced into the signal. This defocus matrix contains data about the reduction in incident solar power resulting from changes in the azimuthal orientation of the platform.

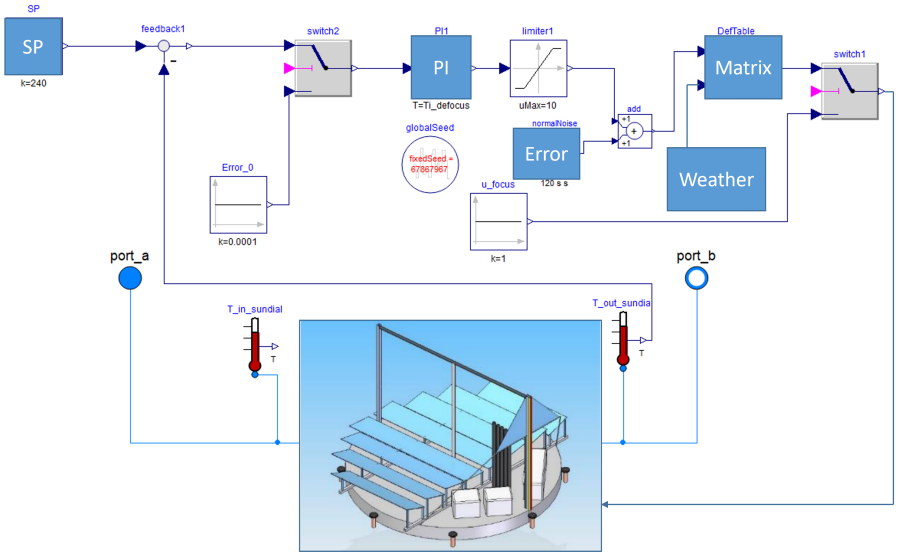

Figure 3.45: Dymola model for the defocus controller by rotating the platform

Figure 3.47 displays the details of this matrix, which has been computed in advance using ray-tracing techniques [5]. The matrix serves as an input to the defocus controller. The impinging power, as Figure 3.47 illustrates, relies upon both the defocus angle and the zenith solar angle. Consequently, a larger defocus angle is required when dealing with higher zenith angles. Ultimately, the controller transmits a signal to a variable-frequency drive, which activates a motor connected to a gear train. This motorized system, in turn, adjusts the orientation of the platform's wheels, leading to the desired defocusing of the mirrors.

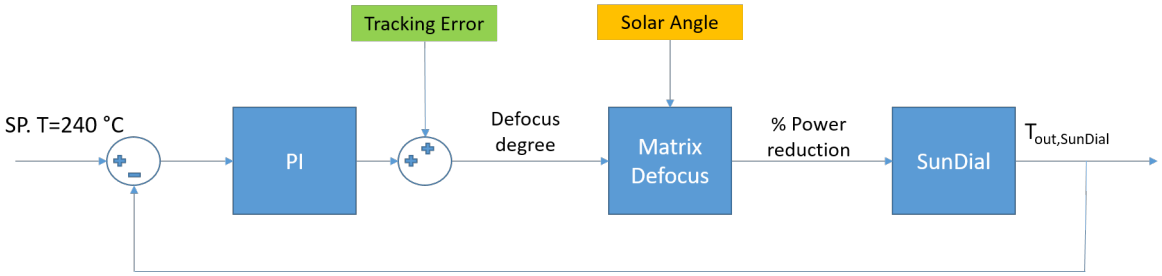

Figure 3.46: Box diagram of the defocus controller.

The controller has an on/off switch with a band wide to prevent the controller from saturation. The band wide will be dependent on the tracking error, with a higher error a larger wide band is required. The outlet of the PI controller is limited between the ranges of 0-10°. The platform movement error, which was modeled with a normal noise, is added to the outlet of the PI. To analyze the required precision of the controller, we implement three different errors as a normal standard deviation with the values: 0.1°, 0.2°, and 0.5°. Defocus matrix data and the typical meteorological year (TMY) are introduced as tables. In this case, we selected the TMY from Corinth, Greece, where the dairy factory is located.

Figure 3.48 presents temperature results from a simulation incorporating a 0.5° tracking error. Both the TES salts and the HTF initially commence at a temperature of 190 °C.

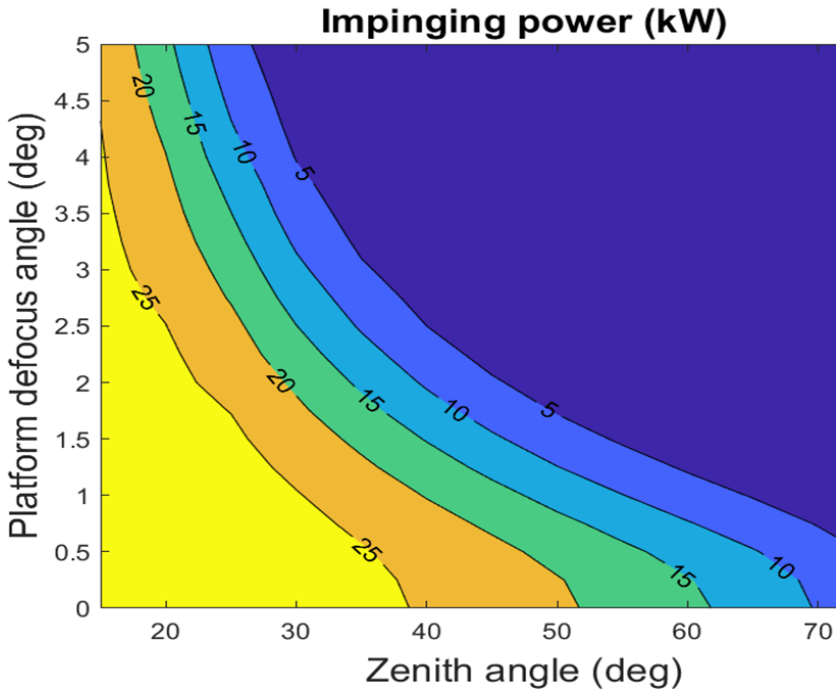

Figure 3.47: Defocus degree, zenith angle, and impinging power.

Subsequently, the SunDial outlet temperature (indicated in green) experiences a gradual increase, culminating in a temperature of 241.5 °C, at which point the defocus controller becomes active. The temperature were the controllers becomes active depended of the error, being 1.5, 1 and 0.5 degree respectively. Remarkably, the controller effectively maintains the temperature at a steady 240 °C by repositioning the platform away from its focal point, aligning it with the solar azimuth for that specific date and time.

Figure 3.49 illustrates the adjustments made to the platform's orientation, guided by the PI signal, which represents the defocus angle relative to the Sun's azimuthal position. The orange PI signal represents the aleatory error feed to the controller and the purple the actual output signal, when this signal is constant means that the controller is turned off. In Figure 3.48, it can bee seen that the average temperature of both the TES salts (indicated in red) and the HTF at the TES outlet converge to 240 °C approximately half an hour after the SunDial outlet temperature. The oscillations in the SunDial temperature are attenuated in the TES system, as a consequence of the TES thermal inertia. The inlet temperature supplied to meet demand (depicted in magenta) is regulated to remain at 190 °C.

The maximum defocus angle required is 1.5° and this implies a power reduction of 90%, as Figures 3.49 and 3.50 illustrate. It is evident that the defocus controller initiated its operation at 15:20, coinciding with a sudden decrease in impinging power (depicted in magenta). Importantly, the oscillations induced by the defocus controller within the SunDial power do not impact the power supply, which remains consistent due to the buffering capacity of the TES.

As illustrated in Figure 3.47, when the zenith angle is elevated, the required defocused angle

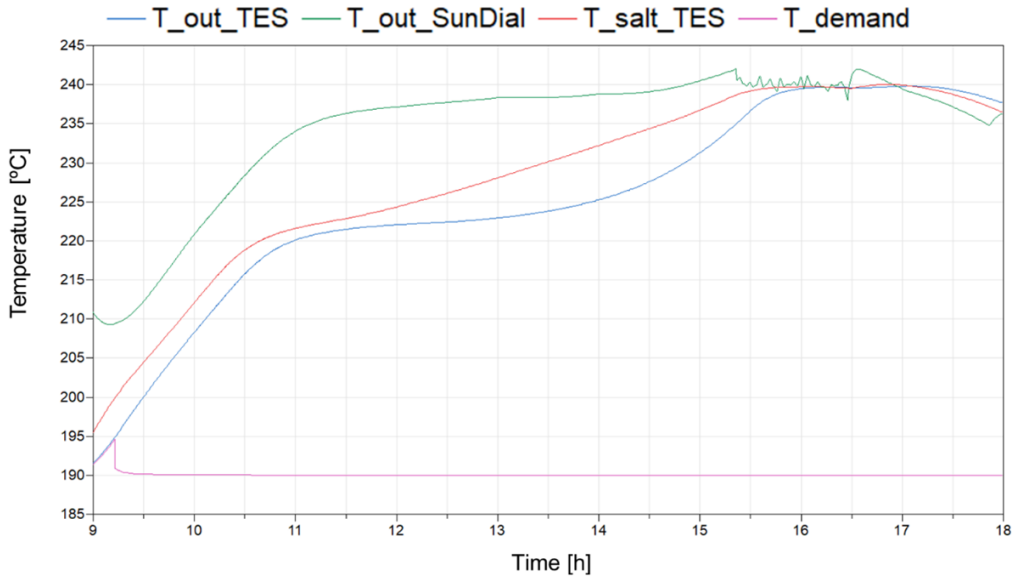

Figure 3.48: Temperature results for the simulation with an error of 0.5°.

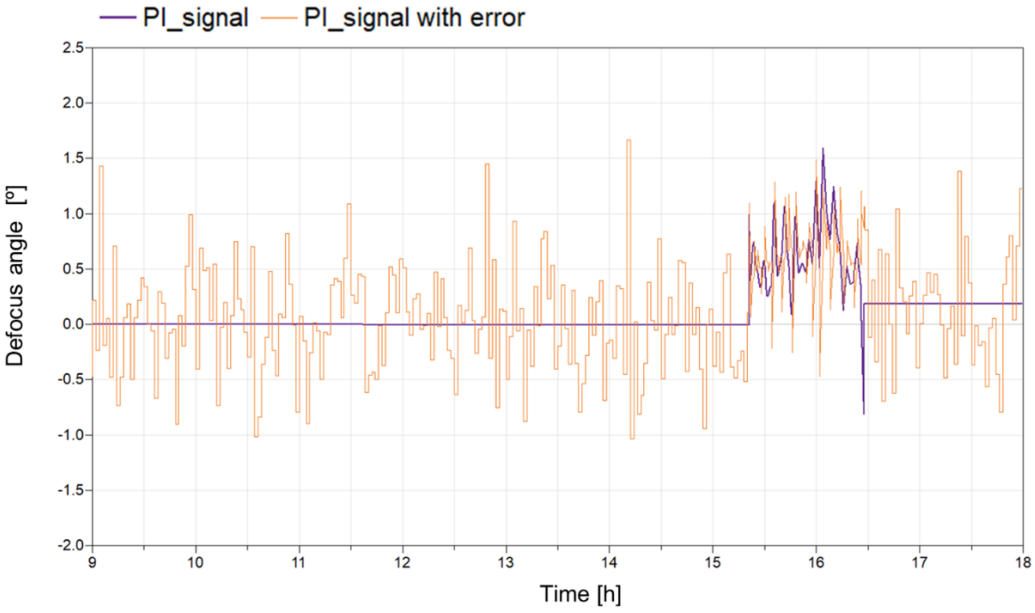

Figure 3.49: Controller signal in degrees of defocus for the simulation with an 0.5° error.

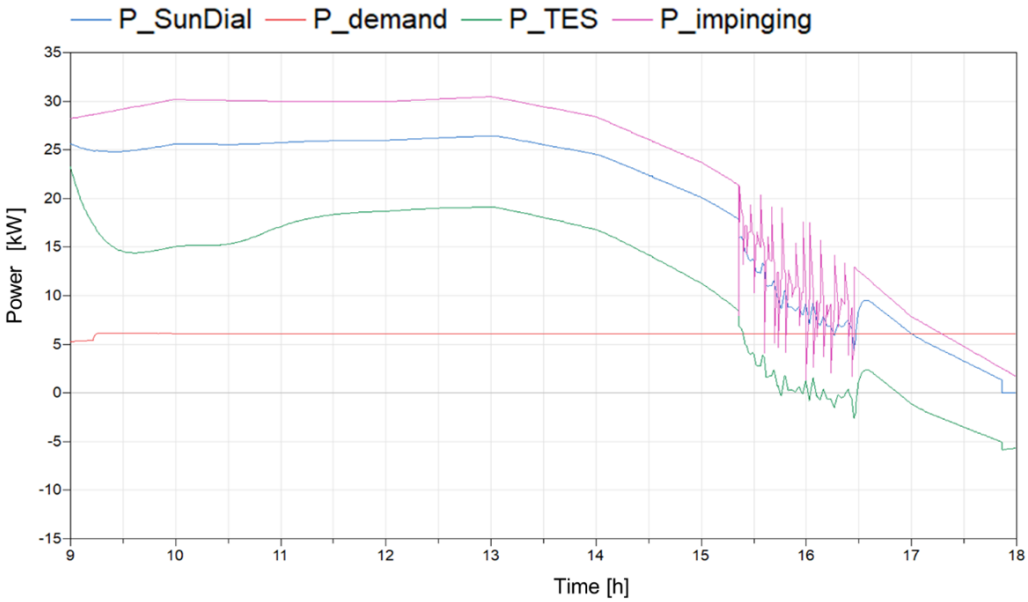

Figure 3.50: Power results for the simulation with an error of 0.5°.

is relatively small. An interesting finding arises when comparing the defocusing efficacy of the SunDial with that of a PTC: the SunDial demonstrates higher sensitivity. Figure 3.51 presents a typical curve for a PTC collector, indicating that a 4° defocus is necessary to achieve a 10 % efficiency of the defocus controller. This means that the power production of the PTC is reduced to 90 % of the one that can be generated if it is totally focused. In contrast, the SunDial demands only a 1.5° defocus to attain a similar level of efficiency.

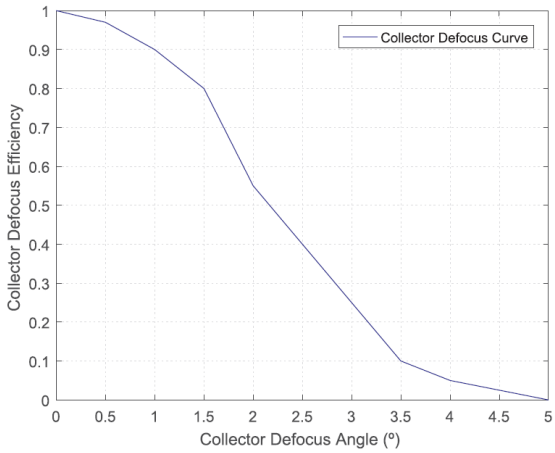

Figure 3.51: Collector defocus angle vs defocus efficiency for a PTC [71]

Figure 3.52 illustrates the variation in outlet temperature of the SunDial for different tracking errors. The controllers with tracking errors of 0.1° and 0.2° effectively maintained temperatures close to the set point of 240 °C throughout the simulation period. In contrast, oscillations were observed in the controller with a tracking error of 0.5°, resulting in a temperature below the lower limit at 16:20 (238 °C). Figure 3.53 presents data on defocus angle, demonstrating

constant back-and-forth movement when simulating a tracking error of 0.5°. Notably, this magnitude caused twice as much defocus angle compared to simulations with smaller errors.

In conclusion, the SunDial tracking system necessitates a more precise controller compared to the one utilized in larger commercial concentrators. This is due to the fact that the SunDial requires a small degree of movement to achieve a defocusing equivalent to that of a parabolic trough collector. Therefore, for optimal performance, it is essential for the tracking system to have an azimuthal position resolution of at least 0.2 degrees. However, since the rotation movement occurs through a wheel with a diameter of 0.2 meters located at a distance of 8.1 meters from its center, this translates into an effective motor resolution equivalent to 8 degrees.

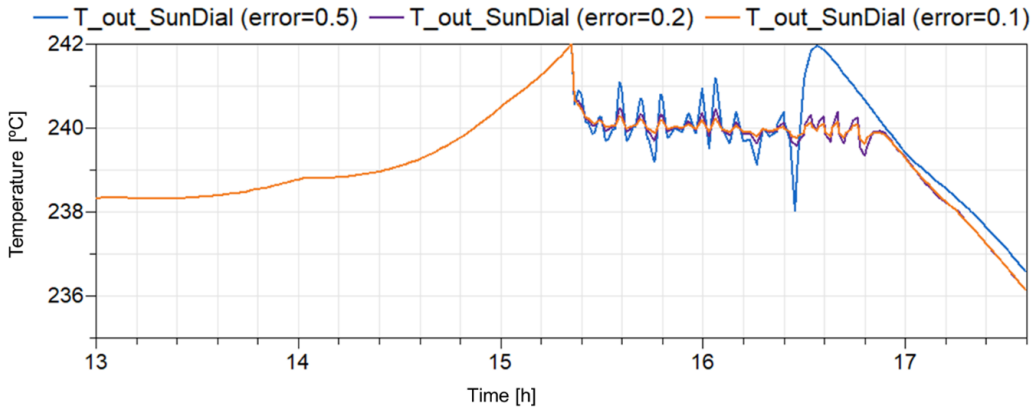

Figure 3.52: SunDial outlet temperature for different tracking errors.

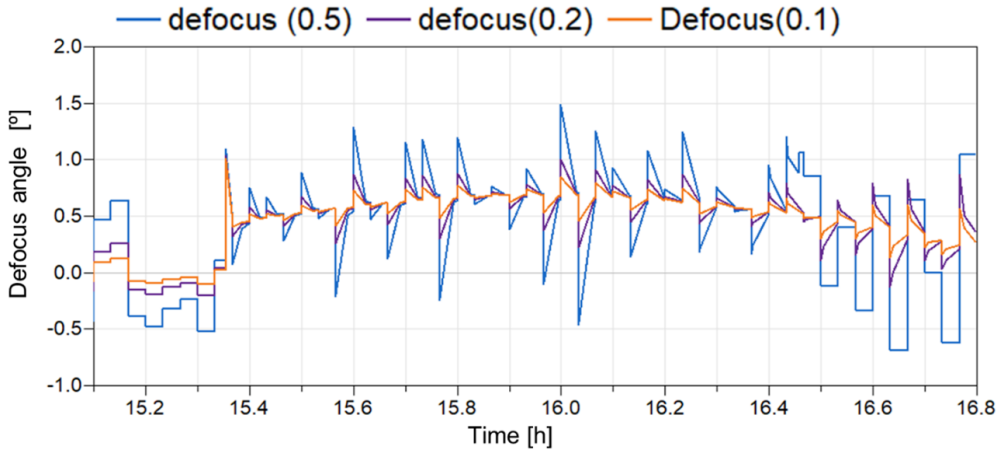

Figure 3.53: Defocus angle for different tracking errors.

Fortunately, there are tracking systems that can achieve an accuracy of 0.2°, such as the one proposed by Sidenk et al. [74]. This system is composed of a microcontroller that calculates the sun's trajectory through an algorithm, a GPS and a digital compass sensor that are used

to determine the tracker's position, and an encoder and PID controller to increase the position accuracy.

An additional observation is that the fluctuations in the outlet temperature of the SunDial system were mitigated by the use of a Thermal Energy Storage unit, which was connected in series. Consequently, this ensures a consistent heat supply to the process during all simulations, even when the defocus controller is active.

3.3 Simplified model for annual calculations

One of the goals in creating a simplified model is to calculate the yearly performance of the ASTEP system, ensuring that it meets the target of 25 MWh/year of energy. The complexity of the dynamic model for ASTEP systems results in high computational costs. Thus, various simplifications were implemented to enable annual simulations within a reasonable CPU time. Additionally, the yearly simulation outcomes will enable a parametric examination to enhance the ASTEP system for reducing LCOH. This analysis involves adjusting various system parameters like solar multiple, maximum temperature, or SunDial size to determine the optimal ASTEP system. The results of this techno-economic assessment will be elaborated in Section 5

The screenshot of the Dymola diagram for the ASTEP simplified model is depicted in Figure 3.54. The first simplification was to reduce the SunDial node number from 66 to 6. The 66 nodes were selected following the assumptions carried out by the Barbero et. al [10] model, which implies a maximum length per section of the receiver of 0.24 m. The second simplification was to consider the properties of the heat transfer fluid constant with the temperature. Each property was set to the average result for the simulation and they are shown in table 3.14. This may be the main limitation of the model, due to the actual variation of the properties with the temperature. However, if we only take the operative range of the system of 190-240 °C the properties vary in the next range: viscosity between 0.0005 and 0.00038 cp, density between 849 and 811.5 kg/m^3, the thermal conductivity 0.105 and 0.1003 J/K.m, and the specific heat between 2243 and 2362 J/K.kg.

Table 3.14: Heat transfer fluid constant properties

Property	Value
c_p [J/K.kg]	2325
ρ [kg/m^3]	860
μ [cp]	5.2E-4
k [J/K.m]	0.104

Then, all the system pipes were merged into two pipe models: one for the SunDial pipes, which are ND 50 and sum a total of 24 m in length, and the other for the BOP pipes, which are ND 20 and a total of 40 m in length. The pipes model considered the thermal inertia as it significantly impacts the results. The HXs were modeled with the same model used in Section 3.2.1, which includes a pipe with a heat source. The dairy factory demand was also

simplified and it is considered that the boiler operates all days between 9 and 17, instead only between Monday to Friday, and the chiller 24 hours.

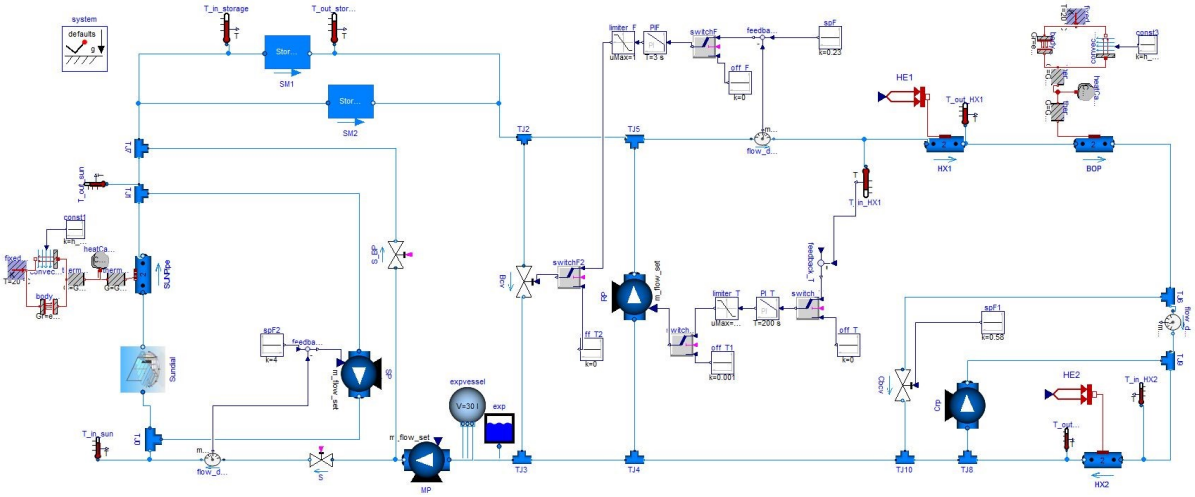

Figure 3.54: Dymola screenshot of the simplified system for annual simulations.

Lastly, the thermal energy storage system was simplified by merging two regions, resulting in a total of 6 regions. Region 4, dominated by convection in the liquid phase, was merged with region 3, dominated by solid fusion. These regions, as was explained in section 3.1, include a set of equations used to calculate the global heat transfer coefficients and the fraction of sensible heat. The simulation time was reduced by a programming improvement. It was found that by a reduction in the number of "if" loops the time of simulation drastically was reduced. This was made using two boolean variables, the first, called "charge", is used to select the state of the TES: charge or discharge, and the second, called "sat", defines the saturation condition. These boolean variables multiply the equations to calculate the fraction of sensible heat and the global heat exchange coefficient, thus, the corresponding equation is activated depending on the charge state and the saturation.

The impact of various simplifications on CPU time is assessed by simulating a single day using a combination of different sub-models. For instance, a system incorporating the detailed model for SunDial and simplified models for TES and HTF is constructed. To evaluate the influence of solar irradiation, simulations were conducted for three days representing different seasons (summer, fall, and winter). The graph in Figure 3.55 depicts the CPU time utilized in these simulations with mixed sub-models.

Figure 3.55a presents the CPU time in hours for the detailed dynamic model incorporating a combination of a simplified sub-model for one component. The most significant time savings occur with HTF simplification for 84 times ratio reduction, followed by SunDial, and finally TES model. In contrast, Figure 3.55b illustrated the CPU time in minutes for the simplified model with one detailed sub-model included. The time for the simulation with the whole simplified model achieves a reduction from 8 hours to less than 1 minute. In concordance with the detailed simulations, using simplified models alongside detailed HTF sub-model necessitates the highest CPU time while using detailed SunDial models requires the lowest CPU time.

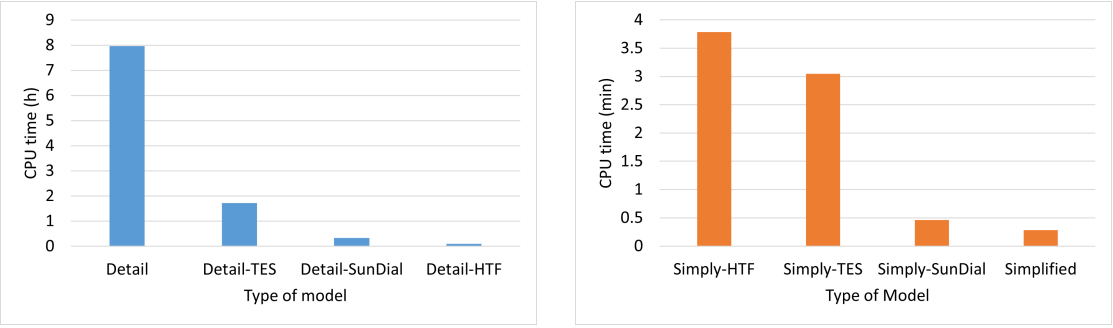

(a) **(b)**

Figure 3.55: (a) CPU time in hours for the full detailed model and mix with simply sub-models (b) CPU time in minutes for the full simply model and mix with detailed sub-models

To assess the discrepancy in energy calculations among the various models, the ratio of energy for different components in the detailed model compared to other models is computed. The findings, displayed in Figure 3.56, reveal that there is greater consistency among models on summer days. However, discrepancies are more pronounced for certain components such as TES and pumps. Notably, a larger disparity between models was observed during winter days, with even the demand showing a ratio distinct from 1.

The power outcomes of the simplified model (dashed line) and the detailed model (continuous line) for summer, fall, and winter are depicted in Figure 3.57 to provide a visual representation. The results show that during the summer simulation, the outcomes are comparable. However, during fall and winter simulations, there are similar discrepancies where the behavior of demand in the simplified model is delayed by 18 minutes.

Results of the annual model

A complete TMY was simulated for the Sundial-LL in Corinth and the SunDial- HL in Iasi. The annual performance was compared for both configurations in series and parallel. Furthermore, a simulation without flexible heat integration (FHI) was performed in the tube steel factory. This means that the integration with the process was done with one HX with a power of 14 kW and a setpoint of 220 °C, instead of the two HX of 7 kW each and the two temperatures setpoints (205 and 220 °C). The results depicted in Figure 3.58 show that despite the SunDial achieving a heat production over the ASTEP target of 25 MWh, the amount sent to the process is lower due to the high thermal losses in the piping and the TES, which represents 35-40 %.

The annual results for the two layout configurations, the in series versus the in parallel, aligned with the previously analyzed in Section 3.2.1. The parallel configuration supplies 4 % more energy in the dairy factory and 1.6% in the tube steel factory. This difference is caused by the transients which produce oscillations in the SunDial profile of temperatures, resulting in higher energy production in the parallel configuration. However, the parallel consumes double the pumping energy of the series, 0.5 MWh/year more in the dairy factory and 0.8 MWh/year in the tube steel factory, these values match with the surplus energy in the parallel. The piping thermal losses are also 0.4 and 0.7 MWh/year higher in the in-parallel configuration.

Fall

Energy	Detail-HTF	Detail-SunDial	Detail-TES	Simplified	Simply-HTF	Simply-TES	Simply-SunDial
SunDial	1.00	1.00	1.00	1.00	1.00	1.00	1.00
Demand	1.00	1.00	1.00	0.99	0.99	1.00	0.99
TES	1.00	1.00	1.01	1.01	1.01	1.00	1.02
Pumps	0.95	0.99	1.01	0.97	1.01	0.95	0.97

Summer

Energy	Detail-HTF	Detail-SunDial	Detail-TES	Simplified	Simply-HTF	Simp-TES	Simply-SunDial
SunDial	1.00	1.00	1.00	1.00	1.00	1.00	1.00
Demand	1.00	1.00	1.00	1.00	1.00	1.00	1.00
TES	1.01	1.00	1.00	1.01	0.58	1.00	1.01
Pumps	0.94	1.00	1.00	0.95	1.00	0.95	0.95

Winter

Energy	Detail-HTF	Detail-SunDial	Detail-TES	Simplified	Simply-HTF	Simply-TES	Simply-SunDial
SunDial	1.00	1.00	1.00	1.00	1.00	1.00	1.00
Demand	1.00	1.00	1.02	1.02	1.02	1.00	1.02
TES	1.02	0.98	0.60	0.64	0.60	1.02	0.63
Pumps	0.95	1.00	1.01	0.99	1.02	0.95	0.99

Figure 3.56: Energy ratio between the detailed model and the mix of models for 3 different days of the year

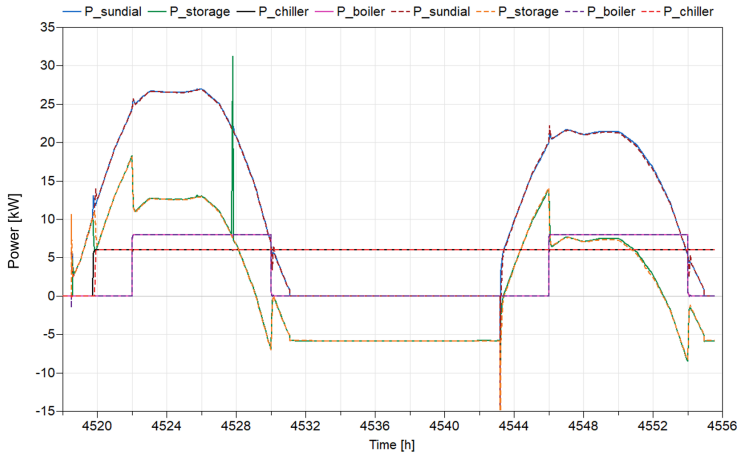

(a)

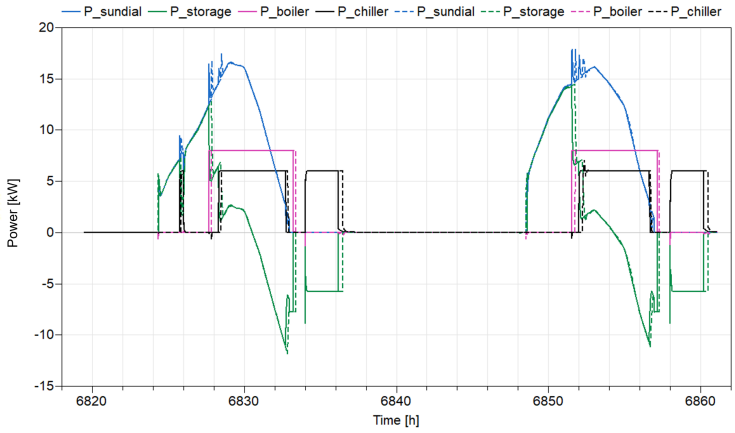

(b)

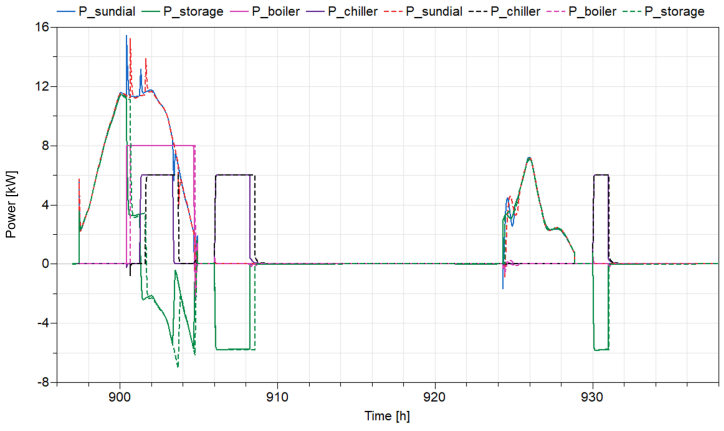

(c)

Figure 3.57: Results for the simplified model (dashed line) vs the detailed model (continuous line) in different seasons: (a) Summer, (b) Fall, and (c) Winter.

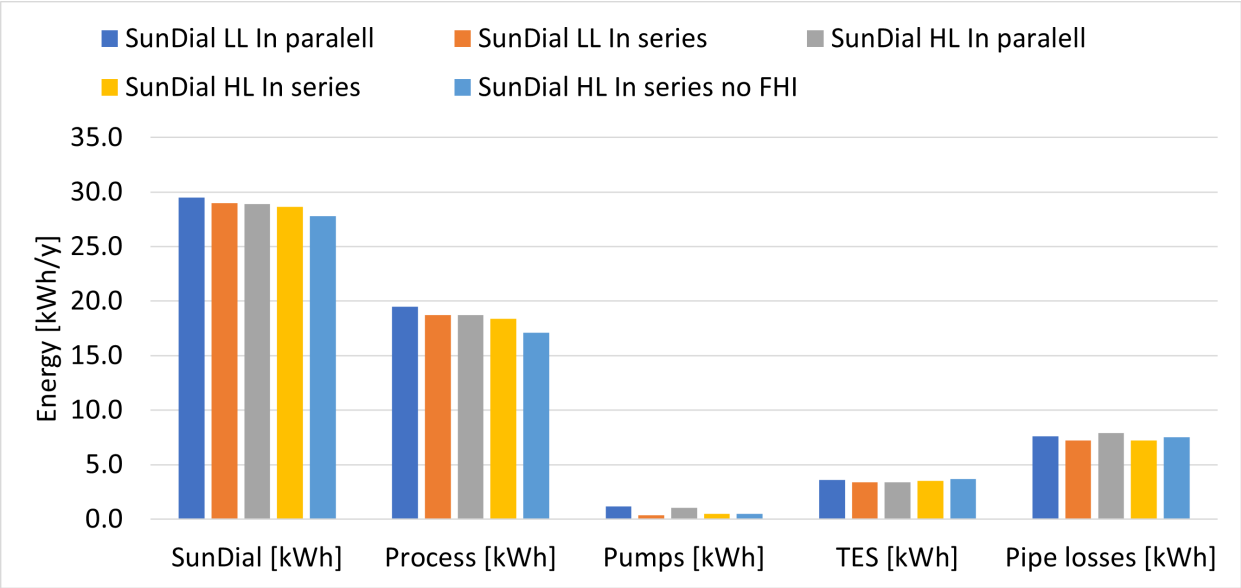

Figure 3.58: Annual energy results in MWh for SunDial with the TES connected in parallel or series.

The TES thermal losses are similar for both configurations.

Therefore, if instead considering only the energy supply to the process, the pumping energy is subtracted, the results for the SunDial- LL are 18.3 kWh/y for both configurations and in the SunDial-HL the series is higher with 17.9 kWh/y than the parallel 17.7 kWh/y. The results obtained in the annual simulation reaffirm the decision to select the series configuration for the ASTEP system in Section 3.2.2. Because the performance in terms of energy, if we discount the enthalpy added by the pumps, is the same or even higher in the series layout. Furthermore, the series configuration implies a simpler system with a reduction of the total components required and, therefore a lower cost.

Regarding the results obtained with the FHI, this produces more energy than a regular strategy that uses only one HX at a high temperature. The Sundial heat production is 1 MWh/year higher due to higher efficiency caused by lower inlet temperatures in the SunDial. The thermal losses in the piping and the TES are lower due to the lower temperatures in the system. All this translates into a higher amount of energy sent to the process.

3.4 Findings

This section has presented the model that is custom-built for the ASTEP system. The first part of the chapter focused on a dynamic model that has played a crucial role in the system's control strategy formulation and in determining the parameters of the Proportional-Integral controller. A comprehensive comparison between two potential configurations of thermal energy storage systems was carried out. Additionally, the model has been instrumental in the exploration of the dynamic behaviors exhibited by the ASTEP system, including its start-up

and shutdown sequences and responses to varying weather conditions, such as cloudy days. Several key concerns specific to the ASTEP system were addressed throughout this chapter. These included the impact of thermal inertia in the pipes and the implementation of the defocus controller, both of which have notable implications for the system's performance and control. The main findings can be summarized in the next points:

- The series connection of TES is the preferred choice for the ASTEP system, aligning well with the objectives of achieving a cost-effective and straightforward solution due to the fewer components and the simple control system.
- While the series configuration stands out in control performance and stability under varying irradiance conditions, the parallel configuration may find advantages in scenarios where rapid startup times are critical, depending on the specific application and system requirements.
- The control strategy proves to be effective in managing the transition between the different modes of operation and in supplying heat to two different process industries at medium temperatures and high latitudes.
- The ASTEP system demonstrates robustness in mitigating the impact of cloud cover by compensating for the absence of solar heat with charge storage in phase change material storage in both factories.
- Accounting for the thermal inertia of the pipe network in the system is crucial, as it can significantly affect energy production, particularly in scenarios with lower irradiance. The ASTEP system exhibits an 18 % deviation in the energy delivered to the process between simulations with and without the thermal capacitance model for the pipes.
- The defocus controller for the SunDial platform demands greater sensitivity than commercial parabolic trough collectors. However, this precision can be achieved through a closed-loop strategy based on an algorithm and active drives.

In the second part, a simplified model was developed to conduct annual simulations. The results indicate that the parallel configuration generates more energy but also consumes more pumping energy. After considering the net energy supply minus pumping energy, it becomes apparent that the series configuration yields equal or even better results, aligning with the decision to select this configuration for ASTEP. The implementation of flexible heat integration using two HXs operating at different temperature levels resulted in 7% higher energy production compared to regular integration with one HX. Ultimately, the ASTEP targets were not met due to higher thermal losses in the system, accounting for 35-40% of the solar energy produced by SunDial. These high thermal losses can be attributed to the small scale of the prototype and could potentially be improved by increasing collector size—an aspect which will be analyzed further in Chapter 5.

The in-series configuration was chosen for the ASTEP system because it offers a straightforward, simple, and robust solution. The different level strategy was selected as the control approach due to its higher efficiency. The next chapter will focus on designing an experimental facility and defining a set of experiments to demonstrate the performance of SunDials and the effectiveness of the control strategy.